

# Resource Allocation in Terrestrial and Non-terrestrial Networks for Sixth Generation Mobile Communications

August 2024

Go Otsuru

A Thesis for the Degree of Ph.D. in Engineering

**Resource Allocation in Terrestrial and  
Non-terrestrial Networks for Sixth  
Generation Mobile Communications**

August 2024

Graduate School of Science and Technology  
Keio University

Go Otsuru

# Abstract

As terrestrial networks (TNs) and non-terrestrial networks (NTNs) continue to evolve, there is a growing trend toward their integration in next-generation mobile communication systems. The integrated network promises enhanced connectivity that spans from the ground to the sky and even into space. To meet a large amount of traffic demand by a vast number of worldwide internet-of-things (IoT) devices connected to the network, it is crucial to increase system throughput to reduce a cost per bit especially under a condition of limited frequency resources. Multiple access (MA) schemes have been traditionally introduced to the TN and the NTN because a spectrum efficiency (SE) is improved through multiplexed signals in various domains. Thus, this thesis focuses on resource allocation schemes for TNs and NTNs and evaluates their performance in terms of throughputs and a number of accessible users.

Chapter 1 introduces the MA schemes, user scheduling schemes in the TN, and resource allocation schemes in the NTN and the motivation of the research.

In Chapter 2, the scheduling schemes in distributed antenna transmission (DAT) is investigated. In DAT, a proportional-fair (PF) scheduling shows higher system throughput and fairness among user equipments (UEs) than

---

a round-robin (RR) scheduling and a Max C/I scheduling. However, the scheduling schemes in DAT face a challenge related to computational complexity. This complexity arises because the feedback overhead at a central unit (CU) becomes immense due to a large number of transmission points (TPs). The proposed scheme is based on the RR scheduling that has lower computational complexity. An initial phase of a sequence of the RR scheduling is sequentially selected for each macro-cell to maximize the estimated system throughput. In the proposed RR scheduling, the inter-cell interference can be taken into account because the CU collects the initial phases of the macro-cells. Four criteria for the initial phase selection are proposed; a full search, a random selection, a maximum selection, and a selection with Gibbs sampling. Numerical results obtained through a computer simulation show that the maximum selection reaches the highest system throughput and effectively mitigates the inter-cell interference. However, intra-cell interference is not taken into account in this scheme. To overcome this problem, a UE set selection for the allocation sequence of the RR scheduling is also proposed. The UE sets that suffer from severe intra-cell interference are eliminated at the CU based on Q-values. Numerical results obtained through the computer simulation show the proposed RR scheduling is superior to a weighted-PF scheduling in restricted realms in terms of the computational complexity, the fairness among UEs, and the system throughput.

In Chapter 3, the resource allocation for a next-generation high throughput satellite (HTS) is investigated. The next-generation HTS is equipped with a digital channelizer that realizes flexible frequency resource sharing with adjacent beams. The allocation bandwidth for a current beam is influ-

---

enced by that for a preceding beam. Therefore, the frequency resource allocation problem is modeled as a beam-indexes-series finite Markov decision process (MDP) in this dissertation. The problem is solved with a Q-learning algorithm. The proposed scheme can reduce the computational complexity through sufficient amount of prior training. The proposed scheme introduces multiple evaluation functions; a system throughput maximization, the number of allocated UEs maximization, and a combined evaluation function. Numerical results through the computer simulation show the proposed frequency resource allocation scheme with the Q-learning achieves sub-optimum solution.

Chapter 4 summarizes the results of each chapter and concludes this dissertation.

# Contents

<b>Abstract</b>	<b>i</b>
<b>Contents</b>	<b>vi</b>
<b>List of Figures</b>	<b>x</b>
<b>List of Tables</b>	<b>xi</b>
<b>List of Acronyms</b>	<b>xii</b>
<b>List of Notations</b>	<b>xv</b>
<b>1 General Introduction</b>	<b>1</b>
1.1 Multiple Access Technologies . . . . .	5
1.1.1 Frequency Division Multiple Access (FDMA) . . . . .	5
1.1.2 Time Division Multiple Access (TDMA) . . . . .	7
1.1.3 Code Division Multiple Access (CDMA) . . . . .	8
1.1.4 Orthogonal Frequency Division Multiple Access (OFDMA) . . . . .	10
1.2 Resource Allocation . . . . .	12
1.2.1 User Scheduling in Terrestrial Network . . . . .	12
1.2.2 Resource Allocation in Satellite System . . . . .	17

---

1.3	Motivation of Research . . . . .	20
1.3.1	Overview of Chapter 2 . . . . .	24
1.3.2	Overview of Chapter 3 . . . . .	27
<b>2</b>	<b>Resource Allocation for Terrestrial Network</b>	<b>29</b>
2.1	Initial Phase Selection of RR Scheduling in Distributed Antenna Transmission . . . . .	29
2.1.1	Introduction . . . . .	29
2.1.2	System Description . . . . .	31
2.1.3	Proposed RR Scheduling . . . . .	35
2.1.4	Throughput Estimation . . . . .	36
2.1.5	Numerical Results . . . . .	40
2.1.6	Conclusions . . . . .	56
2.2	UE Set Selection for Allocation Sequence of RR Scheduling . . . . .	57
2.2.1	Introduction . . . . .	57
2.2.2	System Description . . . . .	59
2.2.3	Throughput Calculation . . . . .	63
2.2.4	Fairness Index . . . . .	63
2.2.5	Radio-Resource Scheduling . . . . .	64
2.2.6	Proposed RR Scheduling . . . . .	65
2.2.7	Numerical Results . . . . .	69
2.2.8	Conclusions . . . . .	81
2.3	Conclusions of Chapter 2 . . . . .	82
<b>3</b>	<b>Resource Allocation for Non-terrestrial Network</b>	<b>83</b>
3.1	Introduction . . . . .	83

---

3.2	Assumed Environment . . . . .	88
3.2.1	System Configuration . . . . .	88
3.2.2	System Model . . . . .	90
3.3	Allocation Scheme of Frequency Resources . . . . .	92
3.3.1	Resource Allocation of Links . . . . .	92
3.3.2	Resource Allocation of Beams . . . . .	95
3.4	Numerical Results . . . . .	101
3.4.1	Simulation Conditions . . . . .	101
3.4.2	Performance Evaluation for No. of allocated UEs and System Throughput Maximization . . . . .	102
3.4.3	Performance Evaluation for Combined Evaluation Func- tion . . . . .	107
3.5	Conclusions of Chapter 3 . . . . .	112
<b>4</b>	<b>Overall Conclusions</b>	<b>113</b>
4.1	User Scheduling in DAT for TN . . . . .	116
4.2	Frequency Resource Allocation in Next-generation HTS for NTN . . . . .	118
	<b>Acknowledgements</b>	<b>120</b>
	<b>List of Achievements</b>	<b>139</b>

# List of Figures

1.1	Requirements of beyond 5G/6G [2, 3]. . . . .	1
1.2	Non-terrestrial network [1]. . . . .	2
1.3	Frequency division multiple access (FDMA). . . . .	5
1.4	Time division multiple access (TDMA). . . . .	7
1.5	Code division multiple access (CDMA). . . . .	8
1.6	Orthogonal frequency division multiple access (OFDMA). . .	10
1.7	Delay profile of signals with multipath and multipath fading channel and its frequency response. . . . .	12
1.8	Max C/I scheduling. . . . .	14
1.9	Round-robin (RR) scheduling. . . . .	15
1.10	PF scheduling. . . . .	16
1.11	Motivation of research. . . . .	20
1.12	Assumed system in Chapter 2. . . . .	25
1.13	Assumed system in Chapter 3. . . . .	27
2.1	Cell model with DAT. . . . .	31
2.2	Signal and interference. . . . .	32
2.3	Order of sequential RR scheduling. . . . .	35

---

2.4	System throughput vs. no. of search iterations (single-user RR scheduling, $N_U = 3$ , inter-antenna distance 100 m). . . . .	42
2.5	System throughput vs. no. of search iterations (single-user RR scheduling, $N_U = 10$ , inter-antenna distance 100 m). . . . .	43
2.6	Average phase selection probability vs. relative throughput (single-user RR scheduling, $N_U = 10$ , 22 search iterations, inter-antenna distance 100 m). . . . .	43
2.7	CDF of throughput(single-user RR scheduling, $N_U = 10$ , 14 search iterations, inter-antenna distance 100 m). . . . .	45
2.8	CDF of difference between optimum and local optimum (single-user RR scheduling, $N_U = 3$ , inter-antenna distance 100 m). . . . .	45
2.9	System throughput vs. no. of users (single-user RR scheduling, 14 search iterations, inter-antenna distance 100 m). . . . .	46
2.10	System throughput vs. inter-antenna distance (single-user RR scheduling, $N_U = 10$ , 14 search iterations). . . . .	47
2.11	System throughput vs. no. of search iterations (2-user RR scheduling, $N_U = 3$ , inter-antenna distance 100 m). . . . .	49
2.12	System throughput vs. no. of search iterations (2-user RR scheduling, $N_U = 10$ , inter-antenna distance 100 m). . . . .	49
2.13	Average phase selection probability vs. relative throughput (single-user RR scheduling, $N_U = 10$ , 22 search iterations, inter-antenna distance 100 m). . . . .	51
2.14	Comparison with $\varepsilon$ -greedy scheme. . . . .	51
2.15	CDF of throughput(2-user RR scheduling, $N_U = 10$ , 14 search iterations, inter-antenna distance 100 m). . . . .	53

---

2.16 CDF of difference between optimum and local optimum (2-user RR scheduling, $N_U = 3$ , inter-antenna distance 100 m).	53
2.17 System throughput vs. no. of users (2-user RR scheduling, 14 search iterations, inter-antenna distance 100 m).	54
2.18 System throughput vs. inter-antenna distance (2-user RR scheduling, $N_U = 10$ , 14 search iterations).	55
2.19 Cell model.	59
2.20 Overview of cell model.	60
2.21 Multi-user MIMO systems in DAT ( $N_S = 2$ ).	61
2.22 UE set elimination with reinforcement learning.	68
2.23 System throughput vs. FI ( $N_U=5$ , inter-antenna distance 100 m).	72
2.24 System throughput vs. FI ( $N_U=10$ , inter-antenna distance 100 m).	72
2.25 Best and worst user throughput ( $x_E = 0.1$ , $w_1 - w_2 = 0.2$ , inter-antenna distance 100 m).	74
2.26 2nd best and 2nd worst user throughput ( $x_E = 0.1$ , $w_1 - w_2 = 0.2$ , inter-antenna distance 100 m).	74
2.27 Best and worst user throughput ( $x_E = 0.6$ , $w_1 - w_2 = 0.1$ , inter-antenna distance 100 m).	76
2.28 4th best and 4th worst user throughput ( $x_E = 0.6$ , $w_1 - w_2 = 0.1$ , inter-antenna distance 100 m).	76
2.29 System throughput vs. FI ( $N_U=10$ , inter-antenna distance 50 m).	78

---

2.30	System throughput vs. FI ( $N_U=10$ , inter-antenna distance 100 m).	78
2.31	System throughput vs. FI ( $N_U=10$ , inter-antenna distance 150 m).	80
2.32	System throughput vs. FI ( $N_U=10$ , inter-antenna distance 200 m).	80
3.1	Overview of assumed SATCOM environment.	88
3.2	Frequency bandwidth allocated to HTS multi-beam.	90
3.3	Example of link allocation.	92
3.4	Dynamic programming table for link allocation.	94
3.5	Update flow of Q-table for beam $b$ .	97
3.6	Average System throughput vs. number of episodes.	104
3.7	Probability of reaching maximum throughput vs. number of episodes.	104
3.8	Average number of allocated UEs vs. number of episodes.	106
3.9	Probability of reaching maximum number of allocated UEs vs. number of episodes.	106
3.10	Average system throughput vs. FI.	109
3.11	Average system throughput vs. FI ( $(A_{TH}, A_{UE}) = (0.003, 1)$ ).	109
3.12	Convergence performance analysis.	111
3.13	Distribution of evaluation function value to full search.	111

# List of Tables

1.1	Outline of the proposals for Chapter 2. . . . .	24
1.2	Outline of the proposals for Chapter 3. . . . .	24
2.1	UE allocation sequence. . . . .	36
2.2	Simulation conditions. . . . .	39
2.3	Simulation Conditions. . . . .	69
3.1	Simulation parameters . . . . .	101
3.2	SE according to MODCOD in DVB-S2X [96] . . . . .	102

# List of Acronyms

<b>B5G</b>	beyond 5G
<b>TN</b>	terrestrial network
<b>NTN</b>	non-terrestrial network
<b>3GPP</b>	third generation partnership project
<b>NR</b>	new radio
<b>RAN</b>	radio access network
<b>HAPS</b>	high altitude platform station
<b>LEO</b>	low earth orbiting
<b>GEO</b>	geosynchronous earth orbiting
<b>IoT</b>	internet-of-things
<b>AI</b>	artificial intelligence
<b>MA</b>	multiple access
<b>FDMA</b>	frequency division multiple access
<b>BPF</b>	band path filter
<b>TDMA</b>	time division multiple access
<b>ISI</b>	inter-symbol interference
<b>GT</b>	guard time
<b>GS</b>	ground station
<b>CDMA</b>	code division multiple access

---

**SSMA** spread spectrum multiple access

**OFDMA** orthogonal frequency division multiple access

**OFDM** orthogonal frequency division multiplexing

**RB** resource block

**LTE** long term evolution

**RR** round-robin

**PF** proportional-fair

**UE** user equipment

**FSS** fixed satellite service

**LOS** line-of-sight

**MSS** mobile satellite service

**DVB-S2** digital video broadcasting for satellite second generation

**ACM** adaptive coding and modulation

**CNR** carrier-to-noise ratio

**DBF** digital beamforming

**NOC** network operation center

**MT** mobile terminal

**DAT** distributed antenna transmission

**CU** central unit

**CSI** channel state information

**TP** transmission point

**HTS** high throughput satellite

**MDP** Markov decision process

**FI** fairness index

**CDAT** cooperative distributed antenna transmission

---

**CCI** co-channel interference

**MIMO** multi-user multi-input multi-output

**BF** block diagonalization

**GW** gateway

**DP** dynamic programming

**AWGN** additive white Gaussian noise

**RMS** root-mean-square

**CDF** cumulative distribution function

**DRL** deep reinforcement learning

**UAV** unmanned aerial vehicle

**TDD** time division duplex

**NOMA** non-orthogonal multiple access

**RL** reinforcement learning

**NLOS** non-line-of-sight

**SATCOM** satellite communication

**SIA** satellite industry association

**SE** spectral efficiency

**DEMUX** demultiplexer

**MUX** multiplexer

**ADC** analog-to-digital converter

**DAC** digital-to-analog converter

**MODCOD** modulation and coding methodology

**NP-hardness** non-deterministic polynomial-time hardness

# List of Notations

$f_c$	Carrier frequency
$f_d$	Frequency of desired signal
$f_1$	Frequency close to desired signal
$f_2$	Frequency close to desired signal
$f_{sc}$	Subcarrier separation
$T$	Symbol Duration
$N_{sc}$	Number of subcarriers
$i_{max}$	Allocated UE in max-C/I scheduling
$i_{PF}$	Allocated UE in PF scheduling
$R_i$	Instantaneous capacity for $i$ -th UE
$\bar{R}_i$	Average throughput for $i$ -th UE
$[\ ]$	Logarithmic notation
$L_d$	Free space propagation loss
$\lambda$	Wavelength for carrier frequency
$d$	Distance from satellite to UE
$A_{0.01}$	Rain attenuation
$\gamma_R$	Specific attenuation coefficient
$L_E$	Effective path length
$N_A$	Number of TPs in each macro cell
$N_U$	Number of UEs in a macro cell
$N_S$	Number of UEs allocated to a RB
$\binom{N_U}{N_S}$	Number of UE combinations
$n$	$n$ -th UE in macro cell
$m$	$m$ -th TP in macro cell
$r$	$r$ -th RB in timeslot
$l$	$l$ -th subcarrier in RB
$c$	$c$ -th macro cell
$P_{nm}^{rc}$	Receive signal power between $m$ -th TP and $n$ -th UE on $l$ -th subcarrier in $r$ -th RB at $c$ -th macro cell
$m_n^{rc}$	Index of selected TP associated to $n$ -th UE in $r$ -th RB at $c$ -th macro cell

---

$x_n^{rlc}$	Transmit signal to $n$ -th UE on $l$ -th subcarrier in $r$ -th RB at $c$ -th macro cell
$k_n^{rlc}$	Constellation point index of $x_n^{rlc}$
$K_n^{rc}$	Modulation order for $n$ -th UE in $r$ -th RB at $c$ -th macro cell
$y_n^{rlc}$	receive signal for $n$ -th UE on $l$ -th subcarrier in $r$ -th RB at $c$ -th macro cell
$h_{nm}^{rlc}$	Channel response between $m$ -th TP and $n$ -th UE on $l$ -th subcarrier in $r$ -th RB at $c$ -th macro cell
$z_n^{rlc}$	Additive white Gaussian noise for $n$ -th UE on $l$ -th subcarrier in $r$ -th RB at $c$ -th macro cell
$\{\mu^{rc}\}$	Set of $N_S$ UE indexes allocated to $r$ -th RB at $c$ -th macro cell
$\delta_c$	Initial phase at $c$ -th macro cell
$\hat{T}_n^{rlc}$	Tentative throughput for $n$ -th UE on $l$ -th subcarrier in $r$ -th RB at $c$ -th macro cell
$\hat{T}_{sum}^{rc}$	Sum of tentative throughput over subcarriers and allocated UEs in $r$ -th RB at $c$ -th macro cell
$\{l^r\}$	Set of subcarrier indexes in $r$ -th RB
$T_n^{rlc}(\delta, m_n^r)$	Throughput for $n$ -th UE in $l$ -th subcarrier of $r$ -th RB corresponding at $c$ -th macro cell to initial phase of $\delta$
$\eta_n^{rl}$	Sum of noise and interference from outer macro cells to $n$ -th UE in $l$ -th subcarrier of $r$ -th RB.
$T^{rc}$	Sum of throughput over subcarriers in $r$ -th RB at $c$ -th macro cell
$T^c$	Throughput at $c$ -th macro cell
$T$	System throughput
$\bar{T}_n^{rlc}(\delta, m_n^r)$	Expected throughput for $n$ -th UE on $l$ -th subcarrier in $r$ -th RB at $c$ -th macro cell corresponding to initial phase of $\delta$
$\bar{T}^c$	Expected throughput at $c$ -th macro cell
$\bar{T}$	Expected throughput corresponding to initial phases
$\{\delta_c\}$	Set of initial phases at $c$ -th macro cell
$\delta_c^{(t)}$	Phase selected in $c$ -th macro cell at $t$ -th time index
$P(\hat{\delta}_c)$	Probability of selecting phase, $\hat{\delta}_c$ , at $c$ -th macro cell
$K$	Temperature coefficient
$R$	Distance from an UE to a TP
$\mathbf{H}_{nm}^{rlc}$	Channel response vector with size of $1 \times N_S$ between TPs of $m^{rc}$ -th TP set and $n$ -th UE
$\mathbf{W}_{nm}^{rlc}$	Pre-coding vector with size of $N_S \times 1$ between TPs

---

	in $m^{rc}$ -th TP set index and $n$ -th UE
FI	Fairness index
$f^{rc}$	PF metric in $r$ -th RB at $c$ -th macro cell
$C_n$	Average user throughput for $n$ -th UE
$\tilde{T}^{rc}$	Estimated throughput UE over subcarriers in $r$ -th RB at $c$ -th macro cell
$\alpha$	Learning rate
$\gamma$	Discount rate
$s_t^r$	State in the $r$ -th RB at $t$ -th timeslot
$a_t^r$	Action in the $r$ -th RB at $t$ -th timeslot
$Q_t(s_{t+1}^r, a_t^r)$	Q-value for state $s_t^r$ and action $a_t^r$
$R_{t+1}^r$	Reward value for transition to state $s_{t+1}^r$
$L_{LOS}$	Average propagation loss for LOS conditions
$L_{NLOS}$	Average propagation loss for NLOS conditions
$N_{RB}$	Number of RBs
$P_{LOS}$	LOS possibility
$x_E$	Ratio of eliminated UE sets in allocation sequence
$W$	Frequency bandwidth
$B$	Number of beams
$N_b$	Number of UEs in beam $b$
$a_b$	Frequency bandwidth allocated to beam $b$
$q_{u_b}^{TH}$	Request throughput of UE $u_b$ in beam $b$
$q_{u_b}^{BW}$	Request bandwidth of UE $u_b$ in beam $b$
$\eta_{u_b}$	Spectral efficiency for $u_b$
$x_{u_b}$	Allocation coefficient for UE $u_b$
$v_{u_b}$	Valuation coefficient for UE $u_b$
$V[u_b, a_b]$	Maximum total value up to UE $u_b$ for allocated bandwidth $a_b$
$\mathbf{x}_{a_b}^{opt}$	Optimal combination of the allocated UEs under the allocated bandwidth $a_b$
$I$	Frequency interval of digital channelizer
$s_b$	State of for beam $b$
$Q(s_b, a_b)$	Q-value for state $s_b$ and action $a_b$
$r_b$	Immediate reward for beam $b$
$\Phi_{TH}$	Policy that maximizes system throughput
$\Phi_{UE}$	Policy that maximizes number of allocated UEs
$\Phi_{CMB}$	Policy that maximizes combined evaluation function

# Chapter 1

## General Introduction

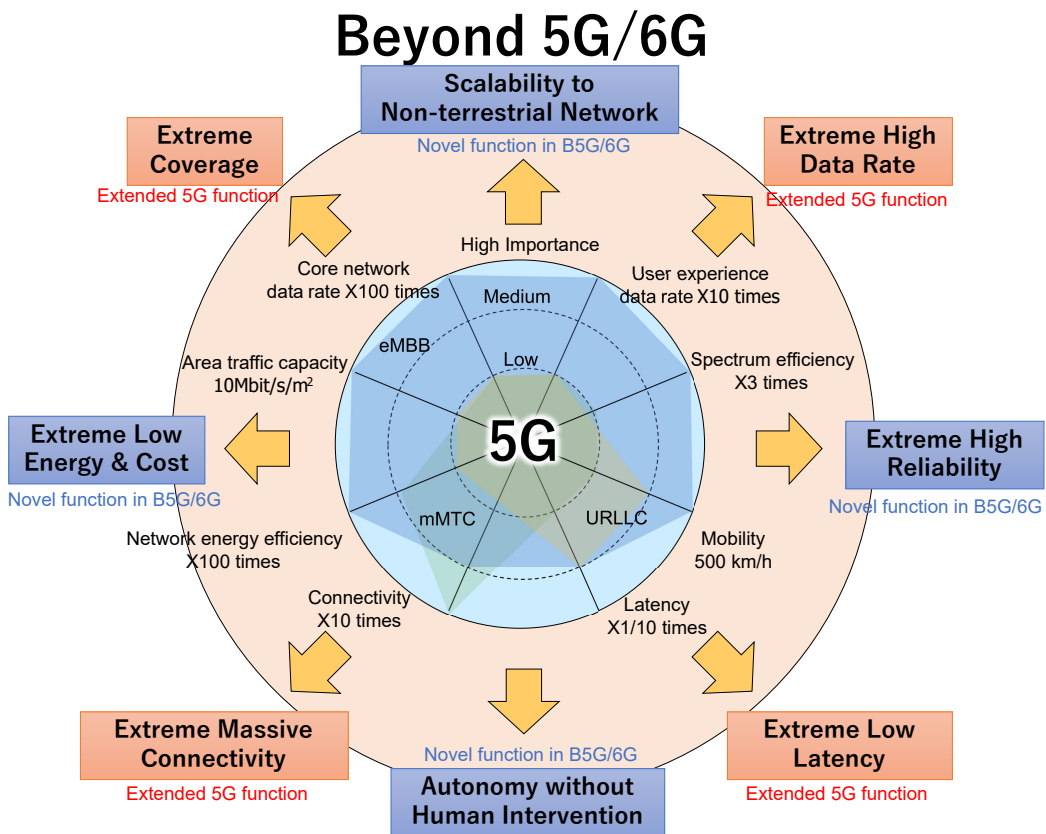


Figure 1.1: Requirements of beyond 5G/6G [2, 3].

Beyond 5G (B5G)/6G is a next-generation information and communica-

tion infrastructure and is expected to be an open platform that can grow sustainably in response to increasingly diverse use cases in the future [1]. The requirements of 6G are shown in Figure 1.1 [2, 3]. In addition to the advancement of characteristic features in 5G such as low latency, wide coverage, high connectivity, and high data rate, new features in 6G are expected to be created [1–3]. Not only humans but also a huge amount of things are connected on the network, and it is essential to reduce the unit price per bit and power consumption in order to cope with the traffic that is expected to increase in the future with limited resources. In addition, a communication path with high security and redundancy even in an emergency situation is immediately constructed by autonomous network control and device-to-device communication.

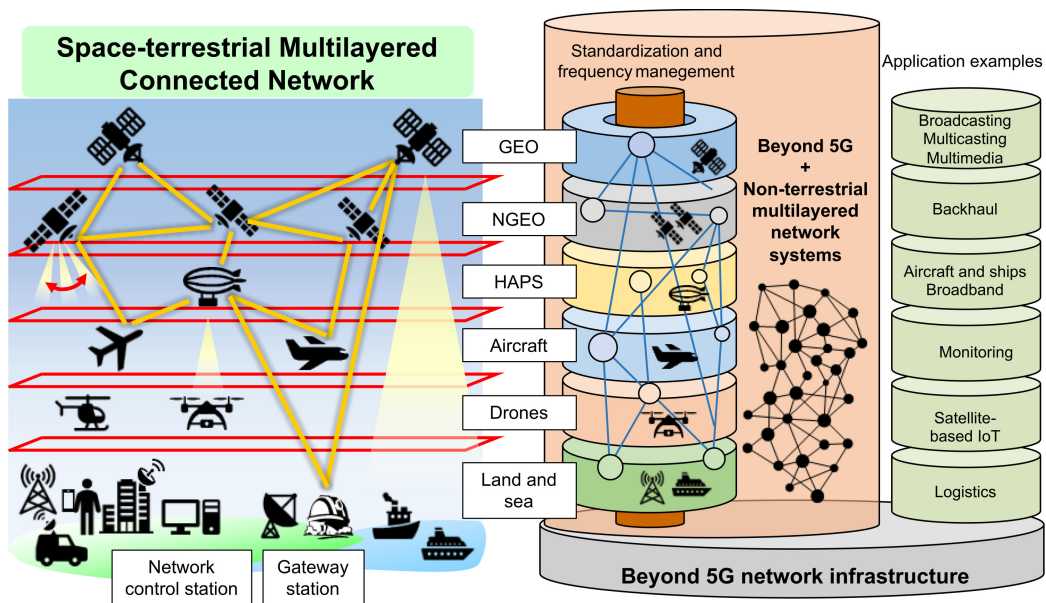


Figure 1.2: Non-terrestrial network [1].

Integration of a terrestrial network (TN) and a non-terrestrial network

---

(NTN), which have separately evolved up to now, is one of the significant requirements of 6G in order to realize flexible systems where people and devices can communicate each other wherever they are on the ground, in the sea, in the air, and even in space. The concept of the NTN is shown in Fig. 1.2 [1]. Third Generation Partnership Project (3GPP), a standardization project for a mobile communication system, had started to study the roles, deployment scenarios, and channel models for the NTN in a new radio (NR) system in the context of integration of the TN and the NTN in TR 38.811 of Release 15 [4,5]. Afterwards, the minimum requirement of enabling NR support for NTN was clarified in TR 38.821 of Release 16 [6]. This includes a NTN-based NT-RAN (radio access network) architecture, Layer 1 issues defined in OSI reference model, radio protocols, and interface protocols. In Release 17, in addition to high altitude platform systems (HAPSs), the necessities of low earth orbiting (LEO) satellites and geosynchronous earth orbiting (GEO) satellites were emphasized and the normative specifications including the NTN were released.

The integration of the TN and the NTN proceeds, as demands for better communication extends beyond the ground to the sky above. For example, the Japanese government proposed the concept of Society 5.0 in the 5th Science and Technology Basic Plan [7,8]. Society 5.0 is defined as “A human-centered society that balances economic advancement with the resolution of social problems by a system that highly integrates cyberspace and physical spaces.” The huge amount of information from internet-of-things (IoT) devices in physical spaces are analysed with artificial intelligence (AI) in cyberspace, and the results of the analysis are fed back to the physical spaces to

---

bring novel value to industry and society. The sensors distributed everywhere in physical spaces are required to upload high-precision and high-sampling data to a cloud server because more realistic information reflections from physical spaces to cyberspace are essential for the accurate simulation/emulation in cyberspace [9, 10].

---

## 1.1 Multiple Access Technologies

In this section, multiple access (MA) schemes are described, which are introduced to wireless communication systems in terrestrial and non-terrestrial network to achieve higher system throughput. Moreover, the necessity for resource allocation technologies have been increased as the complicated and flexible MA schemes emerge [11]. MA schemes are inevitable for maximizing the system throughput by multiplexing signals without interference.

### 1.1.1 Frequency Division Multiple Access (FDMA)

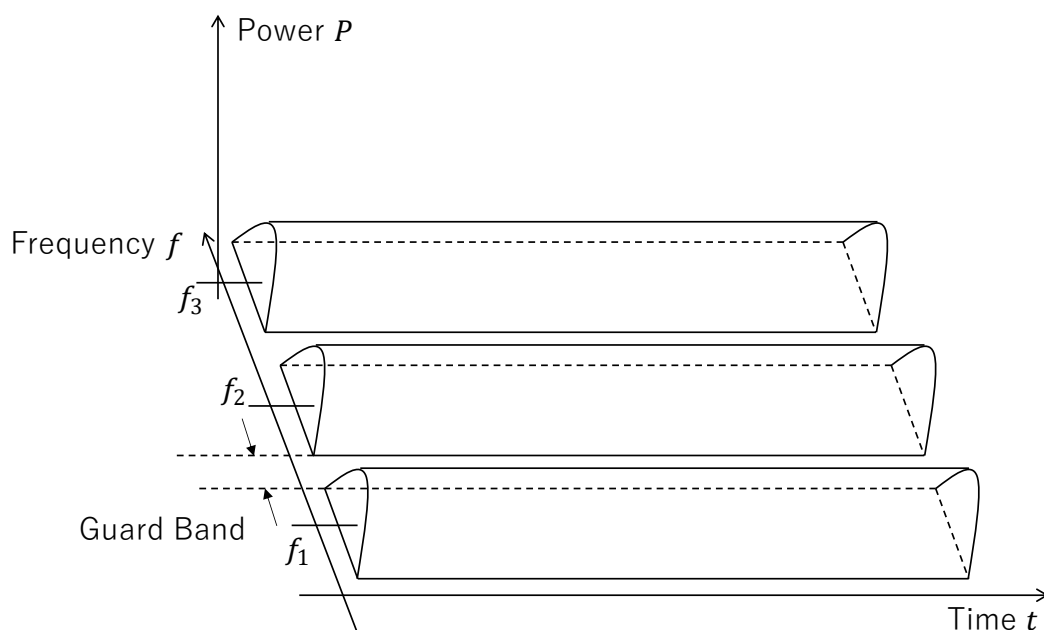


Figure 1.3: Frequency division multiple access (FDMA).

Frequency division multiple access (FDMA) is a well-known and typical scheme as a conventional one. The signals are upconverted to different channels upon modulation so that they do not interfere with each other. The

---

modulated signal upconverted to carrier frequency  $f_c$  has power spectrum spread around  $f_c$ . The width of the spectrum is called occupied bandwidth. The occupied bandwidth is depend on the transmission rate, and wider bandwidth enables higher rate communication.

The principle of FDMA is shown in Fig. 1.3. Each channel is allocated over frequency axis in order to make no overlap to adjacent channels. Assignment in frequency axis is easily changed by using another carrier frequency. At a receiver side, desired signal is extracted and demodulated by adopting the band path filter (BPF) whose center frequency of the pass band is coordinated to the center frequency of the carrier. The interval of the carrier frequencies is called channel separation, and the separation between the adjacent channels is called a guard band. In order to efficiently utilize the frequency bandwidth, the channel separation should be set to the occupied bandwidth. However, the out-of-band radiation owing to the roll-off rate of the filter requires the guard band between channels, which reduces the spectrum efficiency.

FDMA is a widely used scheme in satellite communication systems because of the ease in the configuration and the control of links. However, there is a problem of FDMA in the satellite communication. In FDMA, many signals with different center frequencies are amplified simultaneously in the a satellite transponder. When signals with two different carrier frequencies,  $f_1$  and  $f_2$ , that are close to that of the desired signal with the frequency  $f_d$  are input to the satellite transponder, third order intermodulation distortion occurs at the frequencies,  $2f_1 - f_2$  and  $2f_2 - f_1$ , by the non-linearity of an radio circuit amplifier. These interferences are difficult to remove by

---

the BPF if they are close to the frequency of the desired signal. In order to alleviate the interference of the third intermodulation distortion, the input signal should be fully backoffed to reduce the influence of the non-linearity of the satellite transponder or the carrier frequency allocated to signals should be considered.

### 1.1.2 Time Division Multiple Access (TDMA)

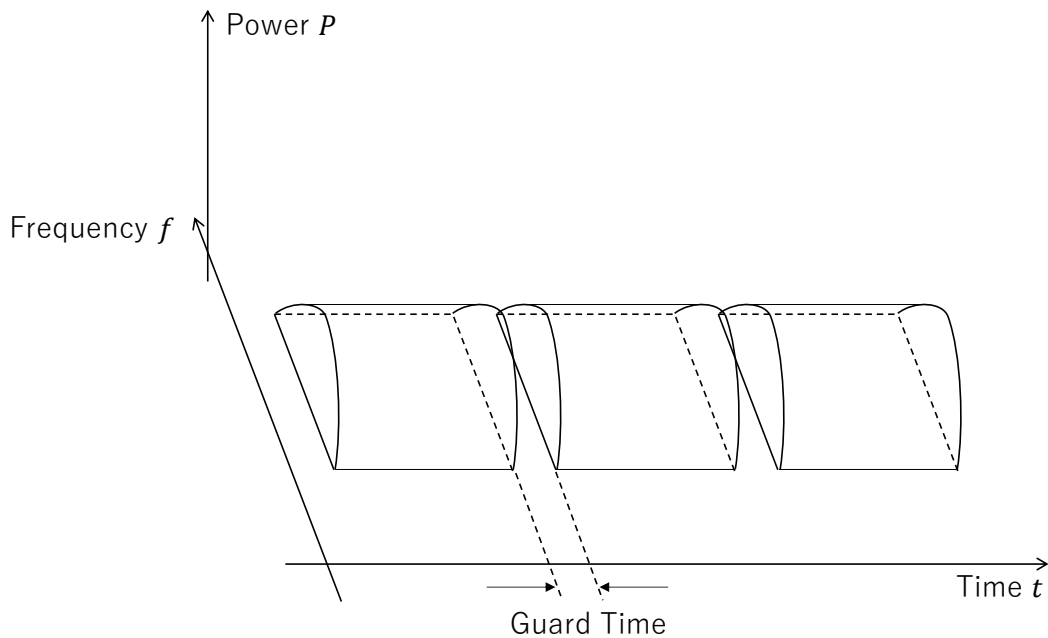


Figure 1.4: Time division multiple access (TDMA).

Time division multiple access (TDMA) emerged as digital processing technologies evolves. Compared to FDMA, TDMA is a scheme suitable for digital modulation and can reduce the complexity of transmitters and receivers. In TDMA, digital signals on multiple channels are transmitted by dividing into time slots on the time axis. In order to prevent inter-symbol interferences (ISIs), a signal distortion caused by the overlap of signals in

---

the adjacent time slots, a guard time (GT) is introduced between the signals as shown in Fig. 1.4. The GT with a longer time interval improves symbol robustness while the transmission efficiency of actual data is reduced. It is important to optimize the length of the GT.

TDMA is also adopted in satellite communication systems. The delays in NTN systems depend on the geographic location of the ground station (GS) and the orbital position of the NTN nodes. In another words, the propagation distance is very long and constantly fluctuates especially in the non-geostationary satellite. TDMA frame is composed of a reference burst and multiple data bursts. The GSs refer to the reference burst for the satellite transponder to receive transmitted burst in the specific time slot.

### 1.1.3 Code Division Multiple Access (CDMA)

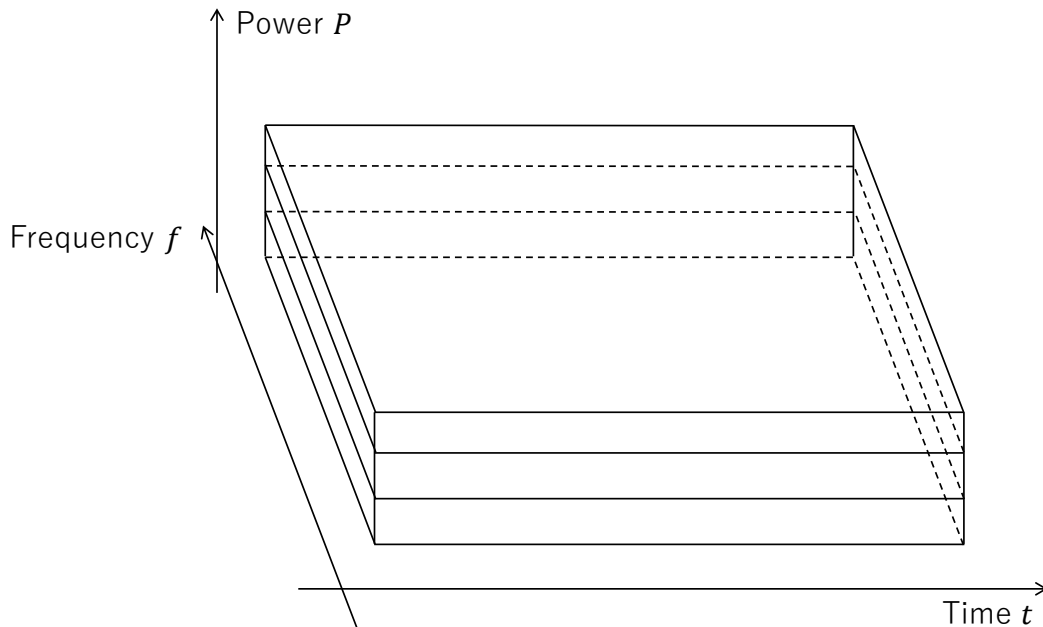


Figure 1.5: Code division multiple access (CDMA).

---

Code division multiple access (CDMA) realizes the multiplexing of multiple signals in spread code domain by different means from those of FDMA in frequency domain and TDMA in time domain. Spread spectrum communication is the fundamental scheme of CDMA. In the CDMA system, digitally modulated signals are spread and multiplexed by spreading codes that have a much wider bandwidth than the original signal. Spread spectrum communication systems are robust to noise and interference.

The specific signal can be demodulated from the multiplexed received signals with different spreading codes, which is the unique characteristic of CDMA. The multiplexing concept of CDMA is shown in Fig. 1.5. Unlike FDMA or TDMA that separates signals by frequency or time domains, the CDMA signals are transmitted in the same frequency and time slots.

Spread spectrum multiple access (SSMA) including CMDA as well as frequency hopping are used in the satellite communications. In order to spread or identify the GSs, spreading codes are used. The merits of SSMA in satellite communications are as follow;

- High non-disclosure and confidentiality
- Asynchronous random access
- High resistance to interference
- Compatibility with multibeam satellites and other NTN systems

On the other hand, the following demerits exist

- Non-linearity of satellite transponder

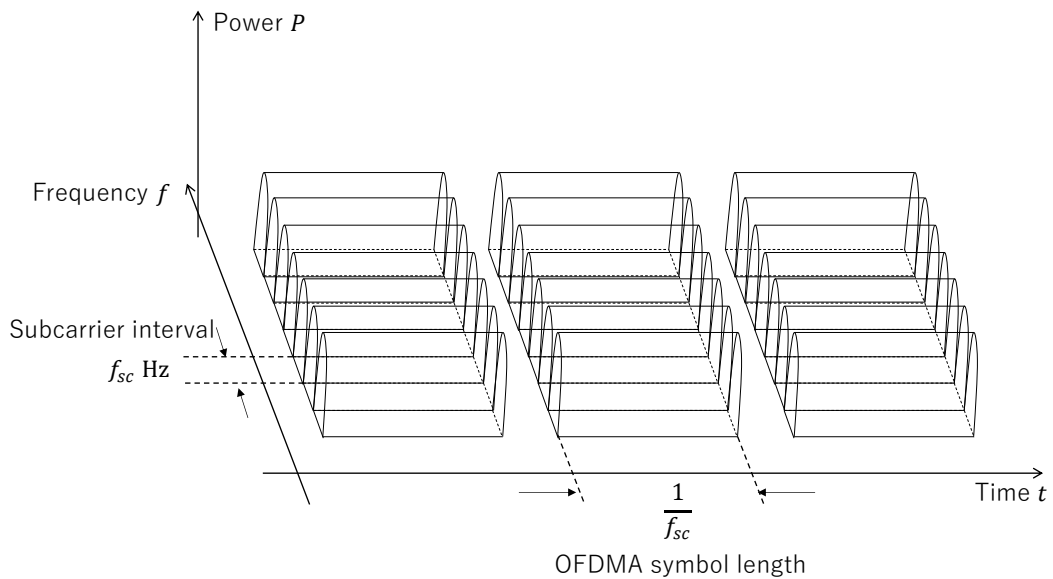


Figure 1.6: Orthogonal frequency division multiple access (OFDMA).

- Low spectrum efficiency compared to TDMA and FDMA
- Complicated device composition
- Hard carrier detection because of low power density of desired signal

#### 1.1.4 Orthogonal Frequency Division Multiple Access (OFDMA)

Orthogonal frequency division multiple access (OFDMA) utilizes orthogonal frequency division multiplexing (OFDM) that transmits multiple modulated signals on orthogonal carriers called subcarriers. The relation among carriers are based on the well-known orthogonality of the sine wave. Suppose that,  $T$  is the symbol duration and  $f_{sc}$  is the subcarrier separation, the following relations are hold;

---


$$\int_0^T \cos(2\pi m f_{sc} t) \cos(2\pi n f_{sc} t) dt = \begin{cases} \frac{T}{2} & (m = n) \\ 0 & (m \neq n) \end{cases}, \quad (1.1)$$

$$\int_0^T \sin(2\pi m f_{sc} t) \sin(2\pi n f_{sc} t) dt = \begin{cases} \frac{T}{2} & (m = n) \\ 0 & (m \neq n) \end{cases}, \quad (1.2)$$

$$\int_0^T \cos(2\pi m f_{sc} t) \sin(2\pi n f_{sc} t) dt = 0, \quad (1.3)$$

where  $m$  and  $n$  are integers and  $T = 1/f_{sc}$ . When the number of subcarriers is  $N_{sc}$ , the total frequency bandwidth of OFDM signal is  $N_{sc}f_{sc}$ .

In OFDMA, resource blocks (RBs) is the available unit of resource allocation. Users are assigned to each RB that consists of 12 subcarriers in a Long Term Evolution (LTE) system. In this way, the amount of user assignment information can be reduced.

---

## 1.2 Resource Allocation

The more complicated resource allocation scheme arises, the needs of the resource allocation and scheduling schemes are more significant. For the mobile communication systems in the TN, several resource allocation schemes in OFDMA such as max-C/I scheduling, round-robin (RR) scheduling, and proportional fair (PF) scheduling are introduced [12]. For the satellite system in the NTN, It is important to properly utilize the limited on-board satellite resources. Power allocation, digital beamforming (DBF), and beam hopping using DBF technique are described in this section. A digital channelizer that is expected to be used in high-throughput satellites is also introduced.

### 1.2.1 User Scheduling in Terrestrial Network

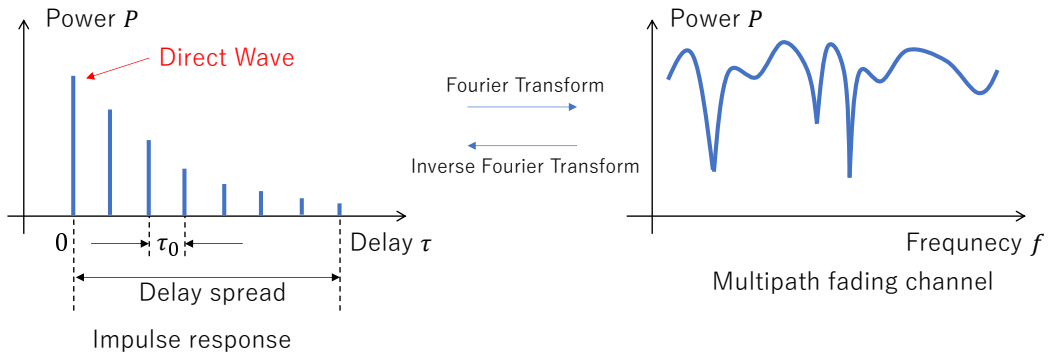


Figure 1.7: Delay profile of signals with multipath and multipath fading channel and its frequency response.

Multipath fading occurs when a transmitted signal reaches a receiver side through two or more paths with different delays. An example of the delay profile of a multipath channel and its corresponding frequency response is shown in Fig. 1.7. The multipath phenomenon arises due to the reflection,

---

diffraction, or scattering of the signals by surrounding objects such as buildings. A signal transmitted from a single source arrives at a receiver through different propagation paths. Consequently, the signals with different paths experience different propagation delays, propagation losses, and phase offsets at a receiver side.

- Signals with different delays can arise ISIs because the delayed waves can be received at a timing exceeding the symbol length including a guard interval.
- Phase offsets can cause constructive/in-phase or destructive/opposite-phase interference when signals through different paths are received.

OFDMA have longer symbol length than that of single-carrier modulation system and the longer symbol duration makes OFDM symbols more tolerant to ISI caused by delayed multipath signals. However, frequency selective fading caused by the multipath signals is inevitable, which means a user throughput greatly depends on assigned RBs. That is the resource allocation problem in OFDMA.

### 1.2.1.1 Max C/I Scheduling

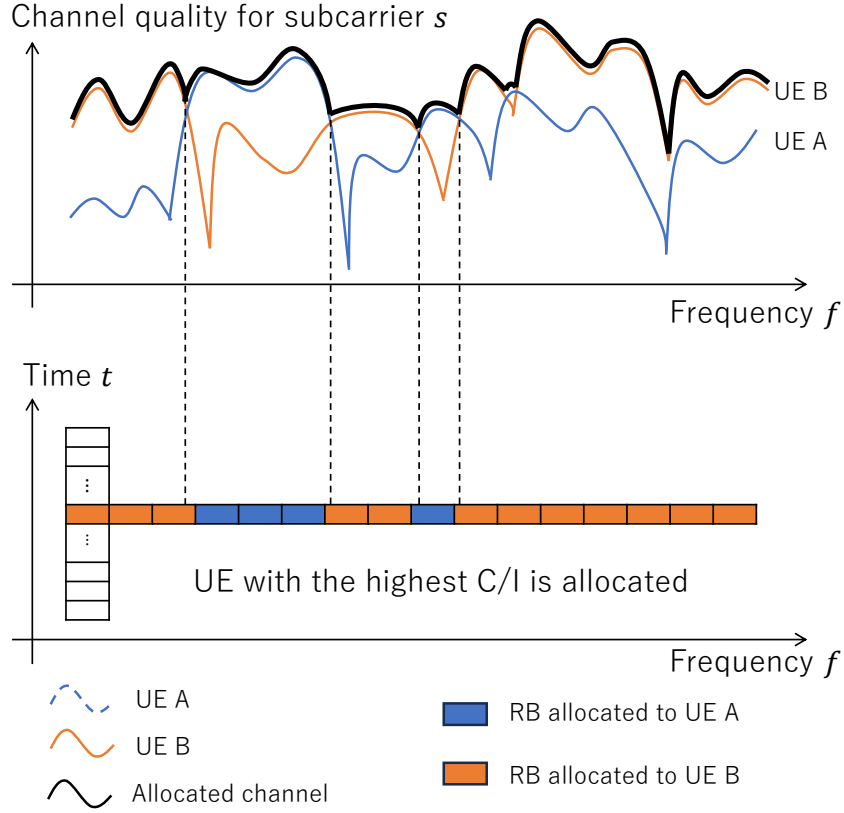


Figure 1.8: Max C/I scheduling.

In max-C/I scheduling, a user equipment (UE) that achieves the highest throughput are allocated to each RB. The allocated UE is specified as

$$i_{max} = \arg \max_i R_i \quad (1.4)$$

where  $R_i$  is the instantaneous throughput of the  $i$ -th UE. The other UEs without the highest throughput are not allocated and the cumulative throughputs of UEs are not taken into account as shown in Fig. 1.8. Therefore, max-C/I scheduling compromises the fairness among UEs.

---

### 1.2.1.2 Round-Robin Scheduling

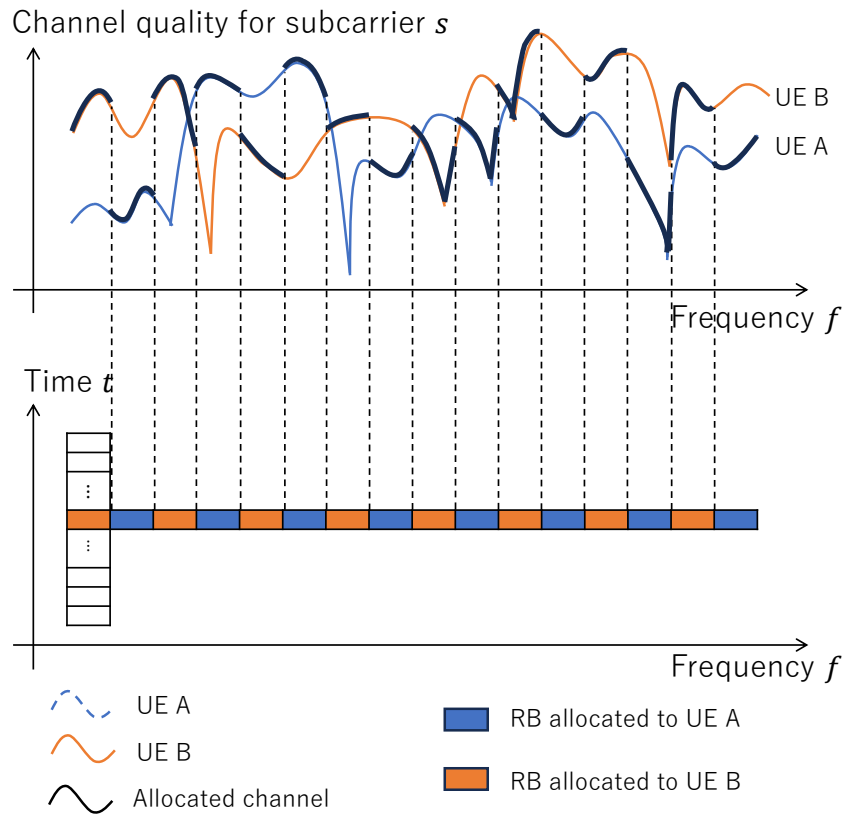


Figure 1.9: Round-robin (RR) scheduling.

RR scheduling allocates UEs sequentially to RBs without taking channel states into account as shown in Fig. 1.9. Therefore, the system throughput is lower than the other scheduling schemes while the fairness among UEs is better than that of max-C/I scheduling though it is not as good as PF scheduling. PF metric is calculated to each UE on each RB in PF scheduling. RR scheduling demands lower complexity as compared with PF scheduling.

### 1.2.1.3 Proportional Fair Scheduling

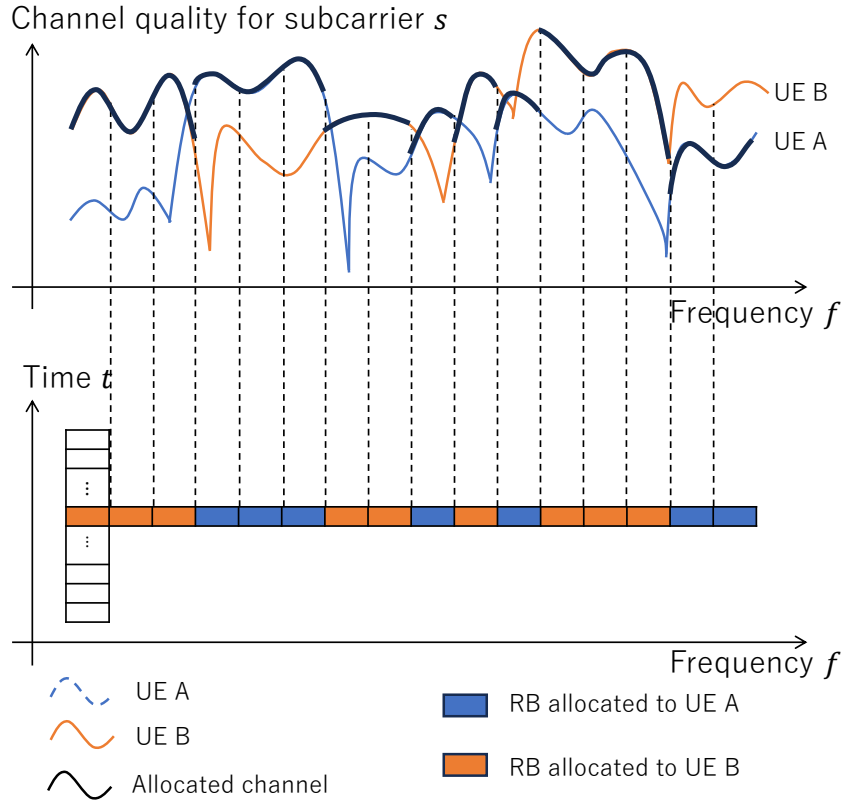


Figure 1.10: PF scheduling.

In PF scheduling, the UE allocated to a RB is given as

$$i_{PF} = \arg \max_i \frac{R_i}{\bar{R}_i}, \quad (1.5)$$

where  $R_i$  is the instantaneous throughput for the  $i$ -th UE and  $\bar{R}_i$  is the average throughput for the  $i$ -th UE. PF scheduling allocates UEs that achieve higher instantaneous throughput on the concerning RB or low average throughput as shown in Fig. 1.10. In this way, the fairness among UEs are maintained in PF scheduling.

---

### 1.2.2 Resource Allocation in Satellite System

Unlike the resource allocation for the terrestrial network explained in Section 1.2.1, a propagation in a fixed satellite service (FSS) environment can be treated as the free space propagation model in a line-of-sight (LOS) environment. The free space propagation loss,  $L_d$ , is given as

$$[L_d] = 10 \log \left( \frac{4\pi d}{\lambda} \right)^2, \quad (1.6)$$

where  $[ ]$  means the Logarithmic notation,  $d$  is the distance from a satellite to an UE, and  $\lambda$  is a wavelength for a carrier frequency. For a mobile satellite service (MSS), received signal power fluctuates due to shadowing and multipath fading in addition to the free space propagation loss. The received signal power fluctuates due to surrounding reflectors and scatterers of a receiver such as trees and buildings. They cause the multiple signals with different delays. The macro-scale variation of the channel is caused by shadowing, the micro-scale variation of the channel is caused by multipath fading.

Rain attenuation in higher carrier frequencies used in HTS systems such as Ka/Q/V/W-bands is much larger than that in lower carrier frequencies such as C/Ku-bands [13]. A rain attenuation estimation method is recommended in ITU-R P618-12 [14]. The rain attenuation  $A_{0.01}$  is calculated as

$$[A_{0.01}] = \gamma_R \times L_E, \quad (1.7)$$

where  $\gamma_R$  is a specific attenuation coefficient and  $L_E$  is effective path length. In order to adapt the fluctuating loss of radio links due to the surrounding

---

environment and the climate, the Digital Video Broadcasting for Satellite Second Generation (DVB-S2) and the extension of DVB-S2, DVB-S2X, standard are implemented. They use an adaptive coding and modulation (ACM). The radio link information is included in the physical layer of DVB-S2X and the appropriate ACM schemes are selected. It enhances the spectrum efficiency in a higher carrier-to-noise ratio (CNR) condition and provides robust communication in a lower CNR condition.

The resource allocation in the satellite system is restrained by the limited amount of on-board power because the satellites in an orbit can only be supplied by solar paddles. The optimum power allocation to beams can improve the system throughput through ACM.

Digital beamforming (DBF) technologies widely used in mobile communication systems is also promising in the satellite communication system [17–19]. The shape and the position of the beams can be controlled by a network operation center (NOC) that plans satellite operation. Wasteful resources can be reduced by the beams following to the positions of mobile terminals (MTs) such as airplanes and ships. Additional beams can also be formed to support traffic in the areas with concentrated traffic demands if the bandwidth of the fixed beams is not large enough.

Beam hopping is a technique of efficiently allocating satellite power with DBF [20, 21]. When a large number of active beams, such as 100 or 1000 beams for HTSs, are formed with DBF, a huge amount of power is required. Therefore, on-board power is saved by switching the active beams in a TDMA or a multi-frequency TDMA manner.

A digital channelizer realizes flexibility in a frequency domain [22–24]. It

---

is possible to map desired signals to an arbitrary sub-channels in the satellite transponder. It is expected to improve the spectrum efficiency for user links by flexible frequency resource allocation according to a traffic demand for each beam.

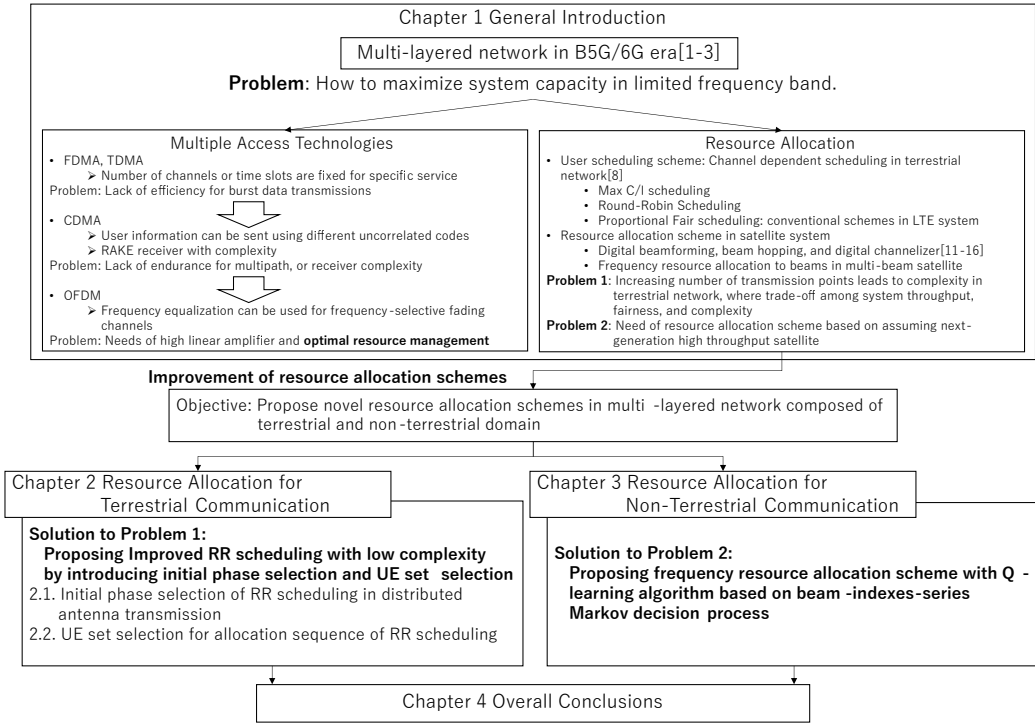


Figure 1.11: Motivation of research.

### 1.3 Motivation of Research

Efficient resource allocation utilizes limited resources such as allocation power or flexible bandwidth in the next-generation communication systems including the TN and the NTN. It may be possible to achieve better quality and larger capacity through the effective use of channels that suffer from frequency selectivity or surrounding environment. In the dissertation, the resource allocation schemes for the TN and the NTN are proposed, respectively, and they are based on interference avoidance in the assumed systems. It is possible to apply each resource allocation scheme independently to each system when the two systems utilize different frequency bandwidths. However,

---

it is inevitable to take the interference between the TN and the NTN system when they share the spectrum. The spectrum sharing between the different systems are out of the target of the dissertation. In Section 4, we describe the challenges and future prospects as to the multi-layered spectrum sharing. The equalization of communication opportunities through scheduling leads to better fairness among UEs. However, these objective functions are hard to maximize simultaneously and there is a trade-off relationship in maximizing these respective objective functions such as the bit rate, the system throughput, the fairness among UEs, and the computational complexity. In order to efficiently handle increasing traffic, it is required to apply a resource allocation scheme that demands less computational complexity as much as possible.

In the TN, 28GHz, 3.7GHz, and 4.5GHz bands have been allocated in Japan for the 5G NR in 3GPP. Such higher frequency bands makes the path loss larger than the other bands assigned for the LTE. Distributed antenna transmission (DAT) that is a promising system in the next-generation TN can resolve the problem of larger path loss in high-frequency bands by distributed antennas [25, 26]. Radio resource allocation in the DAT has a challenge in terms of the computational complexity because the centralized information at a central unit (CU) and the feedback overhead including channel state information (CSI) is huge due to many distributed transmission points (TPs) [27–29].

In the NTN, high throughput satellites (HTSs) have been paid attention because they have the potential to significantly reduce the cost per bit by increasing the throughput of each communication satellite. In a satel-

---

lite communication system using the HTS, a wide bandwidth above the Ka band is usually utilized. Extremely dense frequency reuse is realized by sharp multi-beams. The multiple gateway ground stations are simultaneously used for expanding the capacity of the feeder link. In the next generation of the HTS, in addition to the extension of existing functions, site diversity for selecting appropriate feeder links is realized as an emerging technology [30,31]. Furthermore, flexible frequency allocation with digital channelizers will be implemented for leveraging weather and traffic condition fluctuation prediction with AI technology. In prior research frequency flexibility were enabled by digital channelization on next-generation HTS systems and optimization problems in the time domain were modeled in [32]. Furthermore, the authors in [32, 33] focused on optimizing the amount of throughput and the number of control instances. However, optimization focuses on a beam index sequence by a channelizer. Then, no simultaneous optimization including fairness among UEs are carried out.

The overall structure of this dissertation is presented in Fig. 1.11. In Chapter 2, an improved RR scheduling scheme for the DAT, which maintains the system throughput and fairness among UEs, is introduced to reduce the computational complexity. The purpose, research issue, details, and its achievement of the proposed RR scheduling presented in Chapter 2 are summarized in Table 1.1. In Section 2.1, the initial phase selection of the RR scheduling in DAT is proposed. The initial phases for the RR scheduling sequence of the macro-cells controlled by the same CU are sequentially selected to maximize the system throughput. The inter-cell interference from adjacent cells can be estimated because the initial phases are selected in turn

---

and the control information for initial phases are shared among the macro-cells connected to the same CU. In Section 2.2, the proposed RR scheduling is further improved. Some UE sets with the lower tentative throughput are eliminated from the RR scheduling sequence. That is because those UE sets suffer from large intra-cell interference due to close UE positions. Moreover, the UE set selection can reduce the computational complexity in the initial phase selection because the candidate of the initial phases are limited by shortening the RR scheduling sequences.

In Chapter 3, a frequency resource allocation scheme for the HTS with the digital channelizer is proposed. The purpose, research issue, details, and its achievement of HTS resource allocation presented in Chapter 3 are summarized in Table 1.2. In Section 3.1, the flexible frequency resource allocation by the digital channelizer between adjacent beams is focused, and the process of determining the allocation frequency bandwidth for beams in the order of beam sequence is presented. Since the allocation bandwidth for the preceding beam determines the bandwidth to be assigned to the current beam and the allocated bandwidth depends on the configurable frequency interval of the channelizer. The frequency resource allocation to the beams is then modeled as a finite Markov decision process (MDP). In this dissertation, the numbers of allocated beam indexes is treated as a beam-index-series problem. In Section 3.2, the beam-index-series finite MDP is solved with a Q-learning algorithm. The proposed frequency resource allocation scheme adopts an evaluation function to balance the system throughput and the fairness among UEs. A sub-optimum solution of the evaluation function realizes the relationship of the throughput and the fairness and it is close to

Table 1.1: Outline of the proposals for Chapter 2.

Chapter 2	Purpose	Reduce the scheduling complexity for the DAT.
	Research issue	Radio-resource scheduling in DAT among multiple transmission points (TPs) with lower computational complexity is a challenge to solve.
	Proposed scheme	Determine the initial phase for the RR scheduling sequence on a macro-cell-by-macro-cell and select the UE set combinations in the RR scheduling sequence.
	Achievement	The proposed RR scheduling has reduced the computational complexity for the resource allocation in the OFDMA communication system while the deterioration of the system throughput and the fairness among UEs has been suppressed.

Table 1.2: Outline of the proposals for Chapter 3.

Chapter 3	Purpose	Develop the frequency resource allocation scheme of the beams for the next-generation HTS with the digital channelizer.
	Research issue	The resource allocation scheme with digital channelizer is required to balance the trade-off between the system throughput and the fairness among the UEs.
	Proposed scheme	Allocate the frequency resources to the beams for the next-generation HTS. It is modeled as the beam-index-series Markov decision process and solves the resource allocation problem with the Q-learning algorithm.
	Achievement	The proposed resource allocation scheme with the Q-learning algorithm is able to coordinate the trade-off between the system throughput and the fairness among UEs.

the optimum. It can also significantly reduce the computational complexity though enough amount of prior training is required to be carried out.

### 1.3.1 Overview of Chapter 2

The scheduling schemes such as the Max-C/I scheduling, the PF scheduling, and the RR scheduling for the DAT have been compared in [34]. The PF scheduling shows superior performance in terms of the system throughput and the fairness index (FI). However, it is shown that the system through-

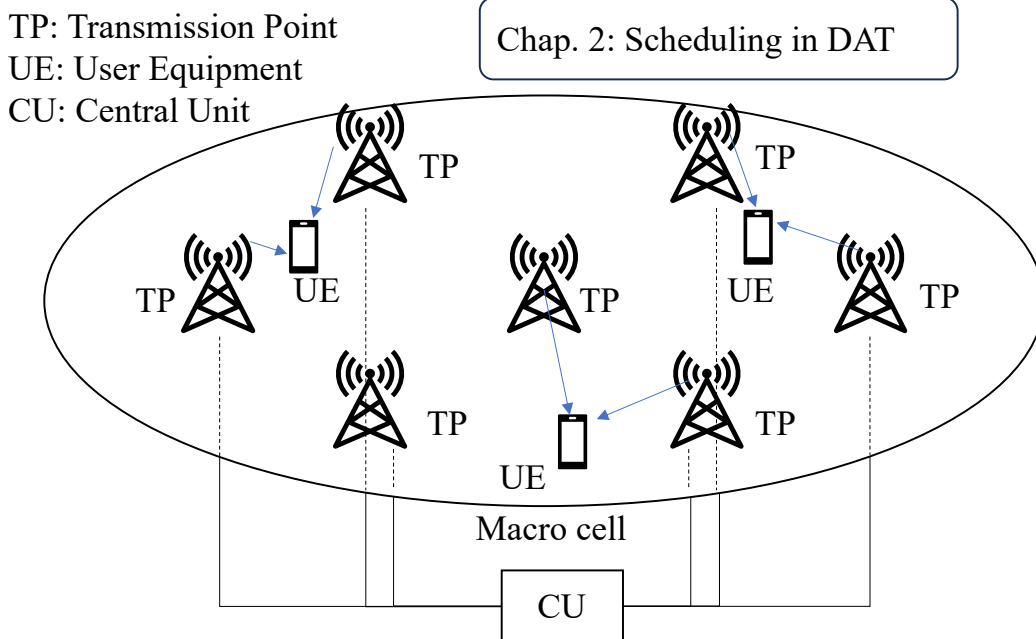


Figure 1.12: Assumed system in Chapter 2.

put and the user fairness of the RR scheduling are close to those of the PF scheduling and the RR scheduling demands lower computational complexity. On the other hand, the user fairness of the Max-C/I scheduling has resulted in significant performance deterioration. In [34–42], cooperative DAT (CDAT) with multi-user spatial multiplexing has been proposed to maximize the system throughput and to decrease the co-channel interference (CCI) especially for the cell-edge users. However, none of those prior research applied the improved RR scheduling to the DAT.

The assumed system of the DAT in Chapter 2 is shown in Fig. 1.12 [43, 44]. The multiple TP in multiple macro-cells are connected to the CU. The multi-user multi-input multi-output (MIMO) with the block diagonalization (BD) algorithm is introduced to the DAT to alleviate the intra-cell interference

---

because the multiple TPs are operated as the distributed MIMO [45].

In Section 2.1, initial phase selection for the RR scheduling has been proposed in the DAT. In the initial phase selection, the initial phases of the RR scheduling sequence of the targeted macro-cell are sequentially determined. The estimated throughput can be calculated by taking the inter-cell interference into account. This is possible since the allocation information in the adjacent macro-cells that are fixed at the previous scheduling time slot is collected by the CU. Three different initial phase selection algorithms based on the estimated throughput are introduced; the random selection, the maximum selection, and the selection with Gibbs sampling. The maximum selection effectively mitigates the inter-cell interference and shows the highest throughput.

In Section 2.2, UE sets selection has been introduced to reduce the intra-cell interference and the computational complexity. The intra-cell interference can be caused by the closer arrangement of UEs allocated to the same RB in the macro-cell. In the UE set selection, specific UE sets are eliminated from the RR scheduling sequence by the Q-learning algorithm because the sequences include UE combinations that cause large intra-cell interference. The computational complexity of the initial phase selections becomes lower because the number of the candidate initial phases decreases as the length of the RR scheduling sequences becomes shorter. Numerical results obtained through computer simulation show that under the some conditions the maximum selection is comparable to or outperforms the weighted PF scheduling in terms of the computational complexity, fairness, and throughput.

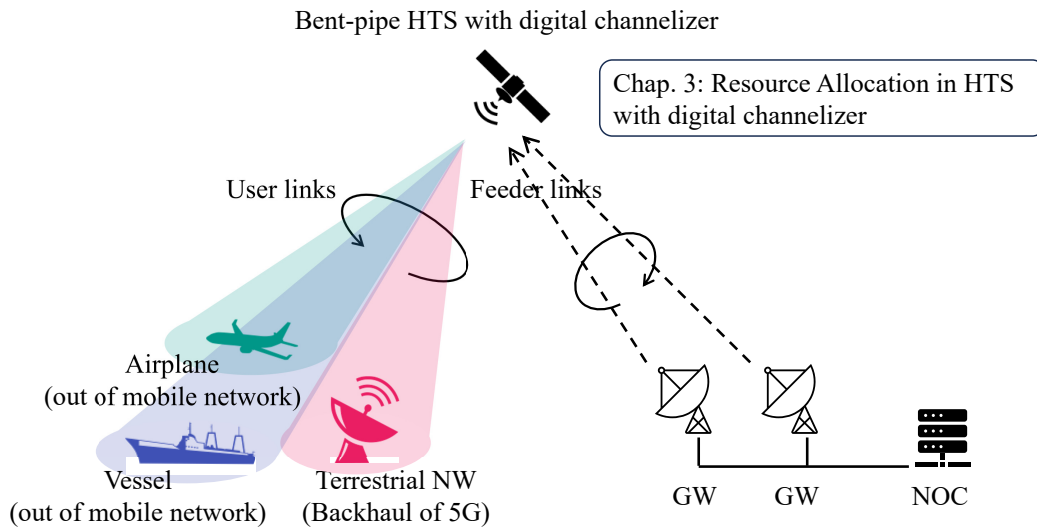


Figure 1.13: Assumed system in Chapter 3.

### 1.3.2 Overview of Chapter 3

The next-generation HTSs have hundreds of beams and the frequency band can be shared by adjacent beams because a digital channelizer realizes flexible resource allocation [47–52]. In prior research, frequency resource allocation schemes for the HTSs with the digital channelizer have been studied [32, 33, 53, 54]. In [53, 54], AI-based resource allocation schemes have been proposed. The authors focus on the frequency resource allocation, gain control, and power control. The authors in [32] have modeled the resource allocation as a time-series problem to reduce the amounts of satellite control and traffic loss. The frequency allocation to the current beam depends not only on previous allocation to the current beam but also on the frequency allocation to the preceding beam because the frequency bandwidth is shared by the adjacent beams. Moreover, the communication opportunity among UEs have not been included in the above researches. Therefore, it is necessary to

---

model the beam-index-series frequency allocation for the HTS with digital channelizer and to simultaneously optimize the system throughput and the fairness among UEs. The assumed system in Chapter 3 is shown in Fig. 1.13. A bent-pipe geostationary earth orbit (GEO) satellite establishes the forward link from gateways (GWs) to UEs.

In Section 3.1, frequency resource allocation is modeled as a beam-index-series finite Markov decision process. The state  $S$  is defined as a frequency resource allocation to the preceding beam and the action  $A$  is obtained by dividing the frequency bandwidth by the allocated frequency bandwidth to a beam. The number of actions is discretized per the configurable frequency interval of the digital channelizer. In Section 3.2, a resource allocation problem is solved by the Q-learning algorithm and the the system throughput is set as reward  $R$  for the action  $A$ . The system throughput is calculated through dynamic programming (DP). The policies of the resource allocation determined by a NOC are determined to maximize the number of allocated UEs, the system throughput, and a combined evaluation function composed of the system throughput and the number of the allocated UEs. The superiority of the proposed resource allocation scheme and the combined evaluation function are proved by numerical results obtained through computer simulation. The NOC is able to coordinate the trade-off between the system throughput and the fairness among UEs.

# Chapter 2

## Resource Allocation for Terrestrial Network

### 2.1 Initial Phase Selection of RR Scheduling in Distributed Antenna Transmission

#### 2.1.1 Introduction

Recently, smartphones and tablet computers are widely used all over the world. Therefore, the amount of mobile traffic has increased explosively [55]. In addition, the IoT applications have been paid a large attention [56]. The specifications in 5G are determined in order to provide reliable wireless connections to those devices [55]. The spectrum efficiency of the 5G system must be improved by at least three times as compared to that of the previous generation [57]. DAT have been investigated for achieving such high spectrum efficiency since it improves as the number of antennas increases [29, 46].

Moreover, channel conditions between UEs and base stations vary according to propagation environment. Therefore, spectrum efficiency also depends on the allocation of UEs and the selection of serving antennas [12]. In [58]

---

and [34,39,40] scheduling schemes for a DAT based cellular system have been investigated. The research in [58] has demonstrated a UE allocation scheme with a dedicated hardware. In this research, each antenna selects a UE that achieves the highest throughput. The iteration of UE selection enables the system throughput to be close to the optimum. In [34], Max-C/I scheduling, PF scheduling, and RR scheduling are compared. The RR scheduling is less complex, while it can achieve the equivalent throughput and fairness as compared to the PF scheduling. However, in this research no UE allocation sequence in RR scheduling is taken into account.

This section proposes a UE allocation scheme for the RR scheduling in the DAT. The proposed scheduling scheme aims to be implemented especially in a limited area such as the ones in factories [59,60]. Thus, for low complexity, the proposed scheme sequentially determines UE allocation over multiple cells with DAs and it only selects the phase of the predetermined UE allocation sequence in each macro cell. Four different phase selection criteria are compared in this section. This section evaluates the performance details of the proposed scheme and compares the tendencies of system throughputs in one user and two users allocation cases.

---

## 2.1.2 System Description

### 2.1.2.1 Cell Model

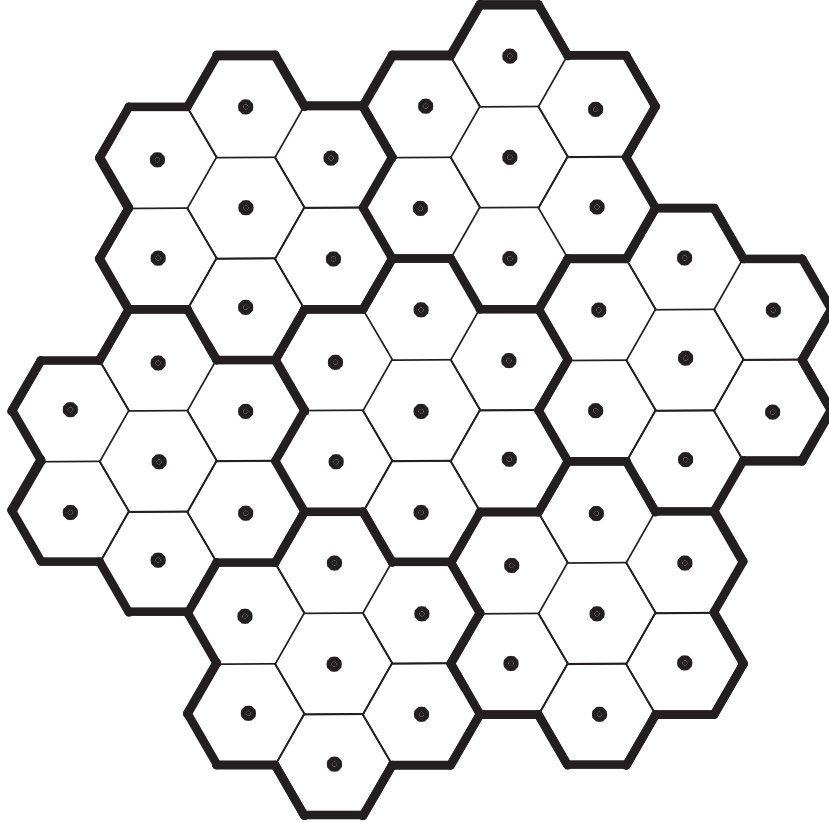


Figure 2.1: Cell model with DAT.

A hexagonal seven-cell model shown in Fig. 2.1 is assumed. One macro cell consists of seven micro cells and each DA is placed at the center of each micro cell. The number of DAs in each macro cell is  $N_A = 7$ . All DAs are connected to a CU. Interference only from adjacent macro cells is assumed to be known to the CU. Also, RR scheduling is adopted in an OFDM system for the allocation of UEs over RBs. Within the macro cell multiple UEs can be assigned to each RB and served by multiple DAs.

---

### 2.1.2.2 RR Scheduling

Suppose that the number of users in a macro cell is  $N_U$ , the number of users allocated to each RB is  $N_S$ , the total number of UE combinations is  $\binom{N_U}{N_S}$ , and the number of the DAs is  $N_A$ . The RR scheduling allocates UEs according to a UE allocation sequence with the length of  $\binom{N_U}{N_S}$ .

### 2.1.2.3 Antenna Selection

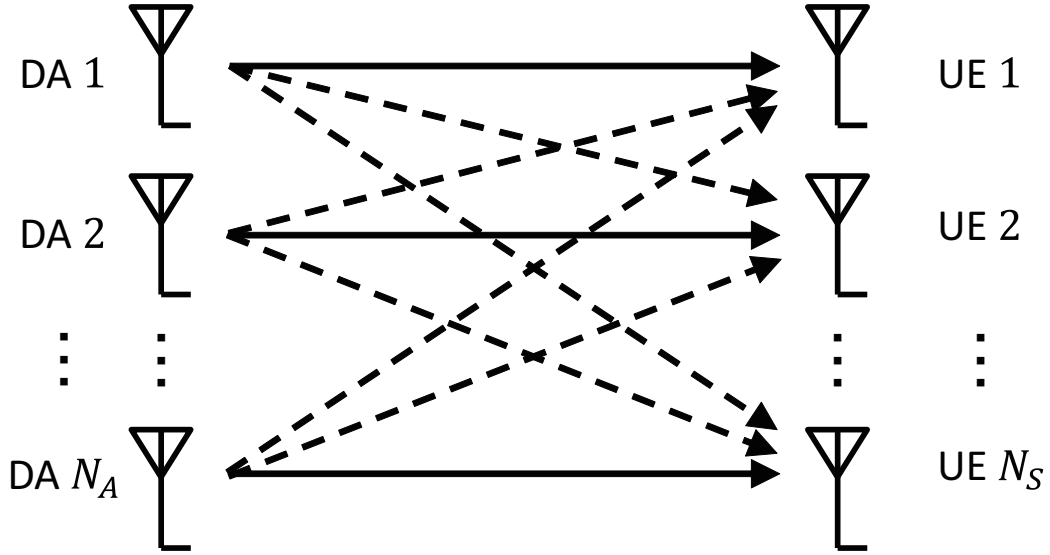


Figure 2.2: Signal and interference.

Each UE is connected by one of the DAs that can realize the highest throughput at each RB as shown in Fig. 2.2. This is represented by a coefficient,  $P_{nm}^r$ .  $P_{nm}^r$  for the  $m$ -th DA to the  $n$ -th UE in the  $r$ -th RB is given as

$$P_{nm}^r = \begin{cases} 1 & (m = m_n^r) \\ 0 & (m \neq m_n^r) \end{cases} \quad (2.1)$$

where  $m_n^r$  is the selected DA corresponding to the  $n$ -th UE in the  $r$ -th RB. Thus, the signal for the  $n$ -th UE in the  $r$ -th RB is transmitted only from the

---

$m_n^r$ -th antenna. The transmit signal to the  $n$ -th UE in the  $l$ -th subcarrier of the  $r$ -th RB is represented by  $x_n^{r,l}(k_n^{r,l})$ , where  $k_n^{r,l}$  ( $0 \leq k_n^{r,l} \leq K_n^r - 1$ ) is the constellation point index of the symbol and  $K_n^r$  is the modulation order for the  $n$ -th UE in the  $r$ -th RB.

Assuming that the RR scheduling with the phase of  $\delta$  is applied, the received signal for the  $\nu$ -th UE is given by

$$y_\nu^{r,l} = h_{\nu m_\nu}^{r,l} \sqrt{P_{\nu m_\nu}^r} x_\nu^{r,l}(k_n^{r,l}) + \sum_{m=1}^{N_A} \sum_{n \in \{\mu_\delta^r\}, n \neq \nu} h_{nm}^{r,l} \sqrt{P_{nm}^r} x_n^{r,l}(k_n^{r,l}) + z_\nu^{r,l} \quad (2.2)$$

where  $h_{\nu m_\nu}^{r,l}$  is the channel response between the  $m$ -th DA and the  $n$ -th UE,  $z_\nu^{r,l}$  is the additive white Gaussian noise (AWGN) with a mean of zero and a variance of  $\sigma^2$  on the  $l$ -th subcarrier of the  $r$ -th RB, and  $\{\mu_\delta^r\}$  is the set of  $N_S$  UE indexes allocated to the  $r$ -th RB based on the RR scheduling sequence with the initial phase of  $\delta$ . The details of the RR scheduling is explained in Section 2.2.

The throughput for the  $\nu$ -th UE in the  $l$ -th subcarrier of the  $r$ -th RB is calculated with as

$$\hat{T}_\nu^{r,l}(\delta, m_\nu^r) = \log_2 \left( 1 + \frac{P_{nm}^r}{\sum_{m=1}^{N_A} \sum_{n \in \{\mu_\delta^r\}, n \neq \nu} P_{nm}^r + \sigma^2} \right) \quad (2.3)$$

This is the tentative throughput for antenna allocation without taking inter-cell interference into account as it is determined after the allocation of DAs to UEs in the adjacent cells. The sum of the throughputs over the subcarriers and the allocated UEs in the  $r$ -th RB,  $\hat{T}_{sum}^r(\delta, m_1^r, \dots, m_{N_S}^r)$ , is then given

---

by

$$\hat{T}_{sum}^r(\delta, m_1^r, \dots, m_{N_S}^r) = \sum_{l \in \{l^r\}} \sum_{n \in \{\mu_{\delta}^r\}} \hat{T}_n^{r,l}(\delta, m_n^r) \quad (2.4)$$

where  $\{l^r\}$  is the set of subcarrier indexes in the  $r$ -th RB. The DAs are selected for  $N_S$  UEs to maximize the total throughput,  $\hat{T}_{sum}^r(\delta, m_1^r, \dots, m_{N_S}^r)$ .

This is described as

$$\{m_1^r, \dots, m_{N_S}^r\} = \arg \max_{\hat{m}_1^r, \dots, \hat{m}_{N_S}^r} T_{sum}^r(\delta, \hat{m}_1^r, \dots, \hat{m}_{N_S}^r) \quad (2.5)$$

where  $\hat{m}_n^r$  is the antenna index allocated to the  $n$ -th UE in the  $r$ -th RB.

#### 2.1.2.4 Throughput Calculation

Different from the tentative throughput, interference from other macro cells is included in the evaluation of the system throughput. The throughput for the  $\nu$ -th UE in the  $l$ -th subcarrier of the  $r$ -th RB corresponding to the phase of  $\delta$ ,  $T_{\nu}^{r,l}(\delta, m_{\nu}^r)$ , is given by

$$T_{\nu}^{r,l}(\delta, m_{\nu}^r) = \log_2 \left( 1 + \frac{P_{nm}^r}{\sum_{m=1}^{N_A} \sum_{n \in \{\mu_{\delta}^r\}, n \neq \nu} P_{nm}^r + \eta_{\nu}^{r,l^2}} \right) \quad (2.6)$$

where  $\eta_{\nu}^{r,l}$  is the sum of the noise and the interference from the outer macro cells to the  $\nu$ -th UE in the  $l$ -th subcarrier of the  $r$ -th RB. The total sum of the throughputs over the subcarriers and the allocated UEs in the  $r$ -th RB at the  $c$ -th macro cell,  $T_c(\delta_c)$ , is given by

$$T_c(\delta_c) = \sum_r \sum_{l \in \{l^r\}} \sum_{n \in \{\mu_{\delta_c}^r\}} T_n^{r,l}(\delta_c, m_n^r). \quad (2.7)$$

Therefore, the system throughput over seven macro cells normalized by the number of the macro cells and the subcarriers is given as

$$T = \frac{1}{7} \cdot \frac{1}{N_{SC}} \sum_{c=1}^7 T_c(\delta_c) \quad (2.8)$$

---

where  $N_{SC}$  is the number of the subcarriers.

### 2.1.3 Proposed RR Scheduling

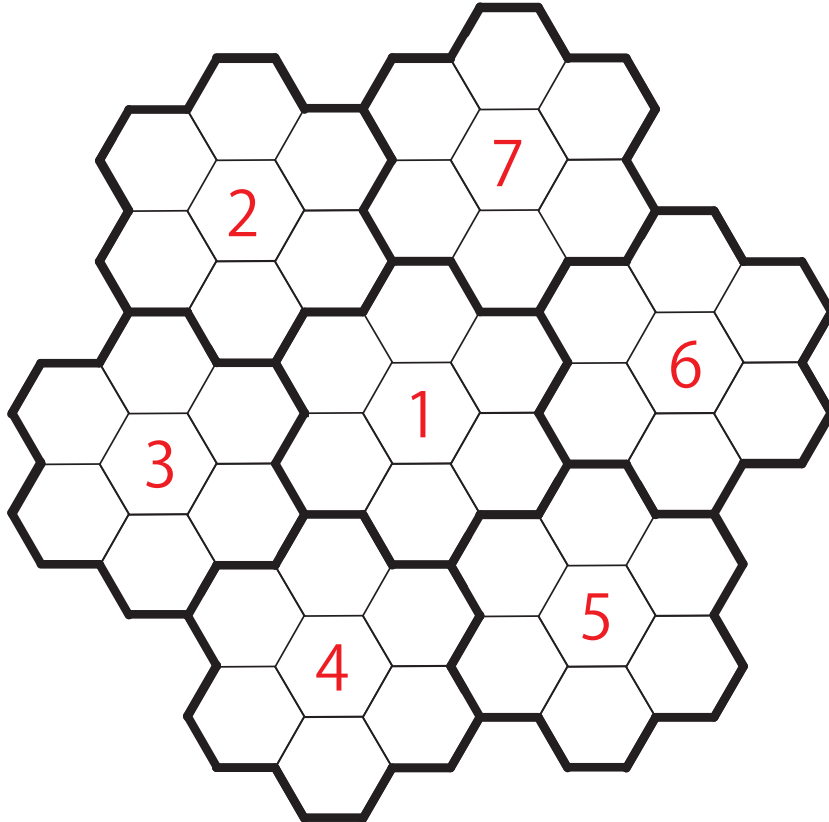


Figure 2.3: Order of sequential RR scheduling.

The proposed RR scheduling selects the phase of the UE allocation sequence. The phase selection is carried out in each macro cell sequentially over multiple macro cells. The order of the sequential phase selection is shown in Fig. 2.3.

In order to improve the system throughput with the proposed RR scheduling, the initial phase is determined in one of the seven macro cells at each timeslot. The initial phases of seven macro cells are then renewed over seven

---

timeslots and the interval of seven timeslots is here called as a period. For all the RBs during each timeslot, UEs are allocated based on the sequence with the initial phase. An example of the UE allocation sequence is presented in Table 2.1. The row indicates the initial phase index of the UE allocation sequence and the column indicates the allocation index of the UE allocated to the RBs. The length of the column is  $N_S$  because the number of the UEs allocated to one RB is represented as  $N_S$ . Therefore, the cell in the  $x$ -th row and the  $y$ -th column represents the  $x$ -th UE index allocated to the first RB at the initial phase  $y$ . The initial phases are selected according to the estimated system throughput and the set of UEs with the indexes contained in the row of the selected initial phase are assigned to the first RB. The set of UEs with the indexes contained in the next row are assigned to the second RB and the allocation is repeated. The allocation of the set of UEs returns to the top if it reaches the bottom of the table.

Table 2.1: UE allocation sequence.

Phase	UE allocated to RB			
	UE 1	UE 2	...	UE $N_S$
0	1	2	...	$N_S$
1	1	2	...	$N_S + 1$
$\vdots$	$\vdots$	$\vdots$	$\ddots$	$\vdots$
$\binom{N_U}{N_S} - 1$	$N_U - N_S + 1$	$N_U - N_S + 2$	...	$N_U$

#### 2.1.4 Throughput Estimation

Suppose that the expected throughput for the  $\nu$ -th UE in the  $l$ -th subcarrier of the  $r$ -th RB corresponding to the initial phase,  $\delta$ , is represented as  $\bar{T}_\nu^{rl}(\delta, m_\nu^r)$ . The total sum of the expected throughput over all the UEs and

---

the subcarriers of the RBs for the  $c$ -th macro cell is calculated from Eq. (2.6)

and is given by

$$\bar{T}_c(\delta_c) = \sum_r \sum_{l \in \{l^r\}} \sum_{n \in \{\mu_{\delta_c}\}} \bar{T}_n^{r_l}(\delta_c, m_n^r). \quad (2.9)$$

The expected system throughput corresponding to the set of the initial phases,  $\{\delta_c\}$ , over the macro cells is then given by

$$\bar{T}(\delta_1, \dots, \delta_7) = \sum_{c=1}^7 \bar{T}_c(\delta_c). \quad (2.10)$$

In this section, four different criteria to the expected throughputs are applied in the initial phase selection.

#### 2.1.4.1 Full Search

Full search calculates all the combinations of the initial phases over the seven macro cells. Since the length of the UE allocation sequence is  $\binom{N_U}{N_S}$ , the number of combinations in seven macro cells is  $(\binom{N_U}{N_S})^7$ .

#### 2.1.4.2 Random Selection

Random selection selects the initial phases in all the macro cells randomly and sequentially. Therefore, no throughput is estimated over all the periods.

#### 2.1.4.3 Maximum Selection

For low complexity, the proposed scheme selects the phases of the UE allocation sequence over multiple macro cells sequentially and it is repeated iteratively. Suppose that  $t$  is the time index and  $\hat{\delta}_c^{(t)}$  is the phase selected in the  $c$ -th macro cell at the  $t$ -th time index, the sum of the tentative throughputs given by the selection of the initial phase at the  $c$ -th macro

---

cell,  $\bar{T}(\hat{\delta}_1^{(t)}, \dots, \hat{\delta}_{c-1}^{(t)}, \hat{\delta}_c, \hat{\delta}_{c+1}^{(t-1)}, \dots, \hat{\delta}_7^{(t-1)})$ , is calculated from Eq. (2.10) for all of  $\delta_c (0 \leq \delta_c \leq \binom{N_U}{N_S} - 1)$ . The maximum selection selects the phase with the largest expected throughput. The maximum selection is defined as

$$\hat{\delta}_c^{(t)} = \arg \max_{\hat{\delta}_c} \bar{T}(\hat{\delta}_1^{(t)}, \dots, \hat{\delta}_{c-1}^{(t)}, \hat{\delta}_c, \hat{\delta}_{c+1}^{(t-1)}, \dots, \hat{\delta}_7^{(t-1)}). \quad (2.11)$$

Since this criterion selects the phase sequentially, the system throughput may fall into a local optimum. The throughput estimation is conducted  $7 \binom{N_U}{N_S}$  times at each period.

#### 2.1.4.4 Selection with Gibbs Sampling

The selection with Gibbs sampling uses the expected throughput,  $\bar{T}(\hat{\delta}_1^{(t)}, \dots, \hat{\delta}_{c-1}^{(t)}, \hat{\delta}_c, \hat{\delta}_{c+1}^{(t-1)}, \dots, \hat{\delta}_7^{(t-1)})$ , corresponding to the set of the phases,  $\{\delta_c\}$ . The probability of selecting the phase,  $\hat{\delta}_c$ , in the  $c$ -th macro cell is given by

$$P(\hat{\delta}_c) = \frac{\exp(\bar{T}(\hat{\delta}_1^{(t)}, \dots, \hat{\delta}_{c-1}^{(t)}, \hat{\delta}_c, \hat{\delta}_{c+1}^{(t-1)}, \dots, \hat{\delta}_7^{(t-1)})/K)}{\sum_{\hat{\delta}_c=0}^{\binom{N_U}{N_S}-1} \exp(\bar{T}(\hat{\delta}_1^{(t)}, \dots, \hat{\delta}_{c-1}^{(t)}, \hat{\delta}_c, \hat{\delta}_{c+1}^{(t-1)}, \dots, \hat{\delta}_7^{(t-1)})/K)} \quad (2.12)$$

where  $K$  is the temperature coefficient. The denominator is the sum of the exponentials of the estimated throughputs for each selected initial phase, and the numerator is the exponential of the estimated throughput for a particular initial phase  $\hat{\delta}_c$  selected. Therefore, the probability of selecting the initial phase is higher as the estimated throughput of the initial phase is larger. Unlike the maximum selection, the selection with Gibbs sampling results in the avoidance of a local optimum because other than the initial phase with the highest estimated throughput is stochastically selected. If  $K$  is large, this

Table 2.2: Simulation conditions.

Cell layout	Hexagonal 7-cell model
Inter-antenna distance	50, 100, 150, 200 m
Minimum distance between UE and DA	5 m
Height of antennas	10 m
Height of UEs	1.5 m
System bandwidth	4.32 MHz
RB bandwidth	180 kHz
Number of RBs	24
Number of subcarriers per RB	12
Transmit power	30 dBm
Distance dependent path loss	$140.7 + 36.7 \log_{10}(R)$ dB $R$ :Distance (km)
Shadowing standard deviation	8 dB
Channel model	Intersite cell: One-path Rician From outer cell: Six-path Rayleigh
Receiver noise density	-174 dB/Hz
Allocation	Single-user allocation 2-user allocation
Number of UEs per macro cell	3, 5, 10, 15, 20
Temperature coefficient $K$	100, 1000, 10000

criterion tends to perform as random selection. If  $K$  is small, this criterion works similarly as maximum selection. The throughput estimation is carried out  $7 \binom{N_U}{N_S}$  times at each period.

The advantage of applying Gibbs sampling is that there is a certain probability that the search result may escape from a local optimum even if the search falls into it and the set of the phases approaches the global optimum.

---

## 2.1.5 Numerical Results

### 2.1.5.1 Simulation conditions

The hexagonal 7-cell model is assumed as a cell layout. The inter-antenna distance is selected from 50, 100, 150, or 200 meters as 256QAM signals with less than 50 MHz bandwidth can be transported over a LAN cable by up to 200 meters [63]. The height of the DAs is 10 meters and the height of the UEs is 1.5 meters. The system bandwidth is 4.32 MHz and the RB bandwidth is 180 kHz. The number of RBs is 24 and the number of subcarriers per RB is 12. The transmit power per a antenna is set to 30dBm. The decay coefficient of the propagation loss is 36.7. The shadowing deviation is 8dB. An one-path Rician fading channel model is assumed for intra cell and a six-path Rayleigh fading channel with an exponential decay profile is assumed for interference from outer cells. The root-mean-square (RMS) delay spread is set to 1  $\mu$ s. The receiver noise density is set to -174 dB/Hz. A single-user allocation ( $N_S = 1$ ) and a 2-user allocation ( $N_S = 2$ ) are evaluated. The number of UEs per macro cell is 3, 5, 10, 15, or 20. The temperature coefficient,  $K$ , is set as 100, 1000, or 10000. The average system throughput per subcarrier per cell is evaluated for different phase selection criteria unless it is specified.

To measure the effect of temperature coefficient, the selection probability of the phase versus the estimated relative throughput is evaluated. The estimated relative throughput with the initial phase,  $\hat{\delta}_c$ , in the  $c$ -th macro cell is given by

$$R(\hat{\delta}_c) = \frac{\bar{T}(\hat{\delta}_1^{(t)}, \dots, \hat{\delta}_{c-1}^{(t)}, \hat{\delta}_c, \hat{\delta}_{c+1}^{(t-1)}, \dots, \hat{\delta}_7^{(t-1)})/K}{\sum_{\hat{\delta}_c=0}^{\binom{N_U}{N_S}-1} \bar{T}(\hat{\delta}_1^{(t)}, \dots, \hat{\delta}_{c-1}^{(t)}, \hat{\delta}_c, \hat{\delta}_{c+1}^{(t-1)}, \dots, \hat{\delta}_7^{(t-1)})/K}. \quad (2.13)$$

---

### 2.1.5.2 Single-User RR Scheduling

In single-user RR scheduling, the system throughput characteristics versus the number of search iterations are presented in Figs. 2.4 and 2.5. The number of UEs are 3 or 10 and the inter-antenna distance is 100 meters. The system throughput for the full search is included in Fig. 2.4. The maximum selection achieves the largest throughput except the full search. The system throughput for the maximum selection reaches 99% of that for the optimum system throughput even the number of search iterations is small. This implies that not many local optimums exist in the search space. Therefore, the system throughput for the Gibbs sampling with the smaller temperature parameters is larger. The system throughput of the random selection is equivalent with those of the Gibbs sampling with  $K = 100$  and  $K = 1000$ . The average phase selection probability in the Gibbs sampling versus the estimated relative throughput is presented in Fig. 2.6. The number of UEs is 10, the inter-antenna distance is 100 meters, and the number of search iterations is 22. In single-user RR scheduling, the number of combinations for the initial phases is equivalent to the number of UEs and each criterion for the phase selection picks up the initial phases from the candidates of the initial phases. The Gibbs sampling with  $K = 1000$  or  $K = 10000$  selects the initial phase almost randomly while the Gibbs sampling with  $K = 100$  tends to select the initial phases with higher throughputs.

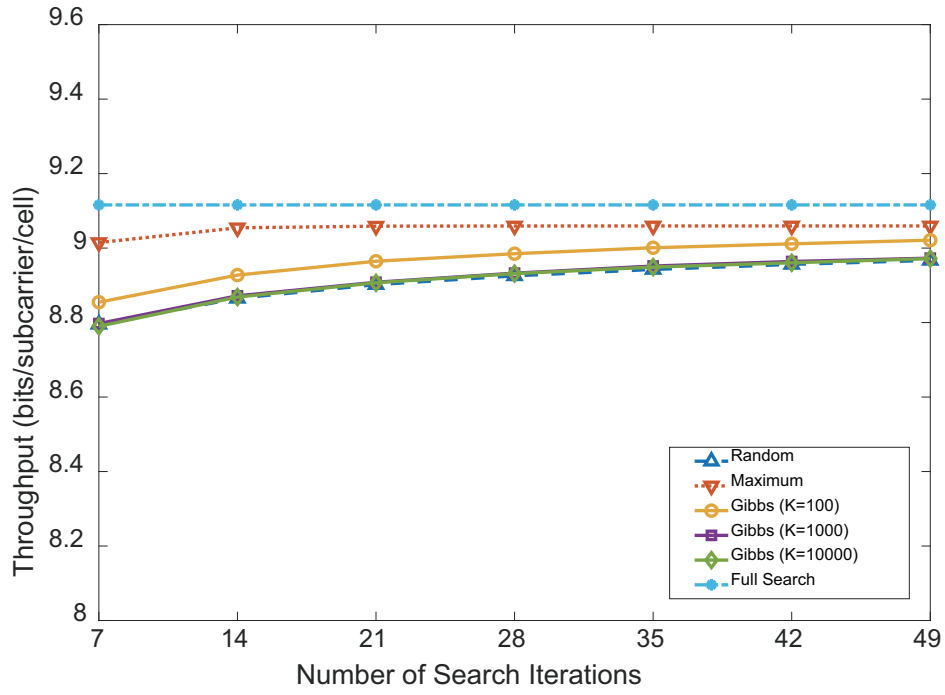


Figure 2.4: System throughput vs. no. of search iterations (single-user RR scheduling,  $N_U = 3$ , inter-antenna distance 100 m).

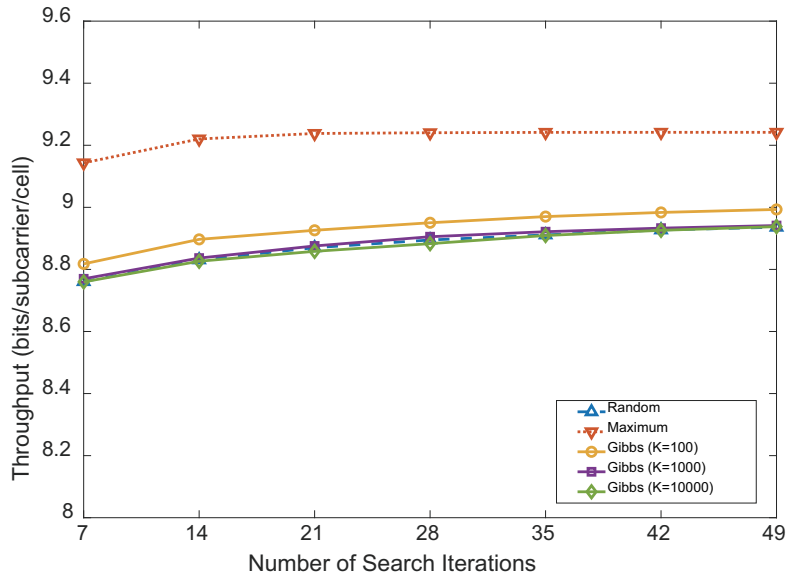


Figure 2.5: System throughput vs. no. of search iterations (single-user RR scheduling,  $N_U = 10$ , inter-antenna distance 100 m).

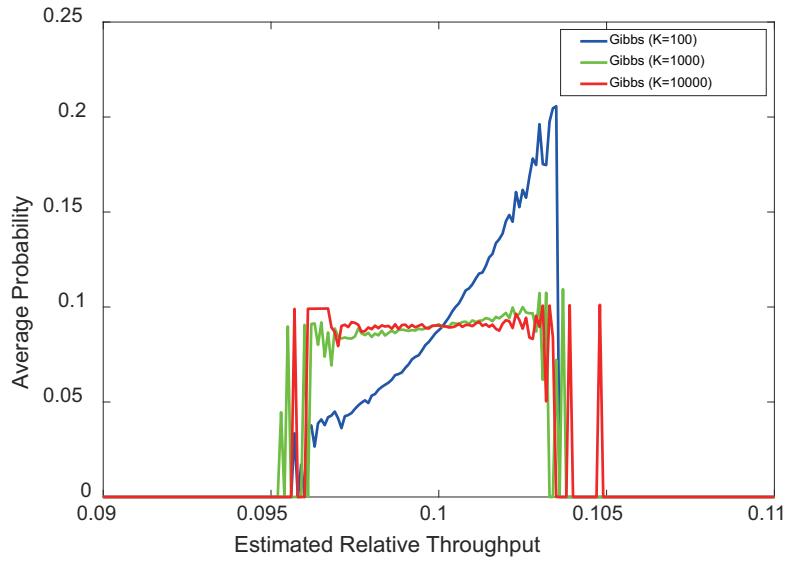


Figure 2.6: Average phase selection probability vs. relative throughput (single-user RR scheduling,  $N_U = 10$ , 22 search iterations, inter-antenna distance 100 m).

---

The cumulative distribution function (CDF) of the throughput is shown in Fig. 2.7. The figure indicates that the maximum selection is also superior to the other criteria in terms of 5%-CDF throughput. Maximum selection achieves higher throughput than the others criteria including the selection with Gibbs sampling. Gibbs sampling is able to escape from a local optimum and the selection with Gibbs sampling tends to indicate superior performance. However, in the assumed system, the local optimum rarely exists and the throughput difference between the optimum and the local optimum is small. The ratio of the local optimums is 0.62 % among all the combinations. The CDF of the throughput difference between the optimum when  $N_U = 3$  and the local optimum is shown in Fig. 2.8. The search result hardly falls into the local optimum and the throughput difference is small even if the search falls into it. Consequently, maximum selection outperforms the other criteria.

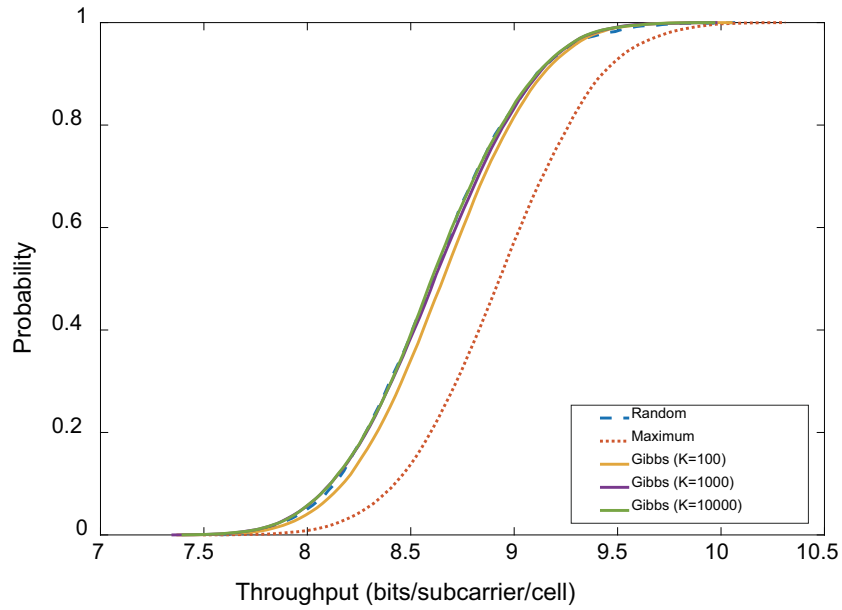


Figure 2.7: CDF of throughput(single-user RR scheduling,  $N_U = 10$ , 14 search iterations, inter-antenna distance 100 m).

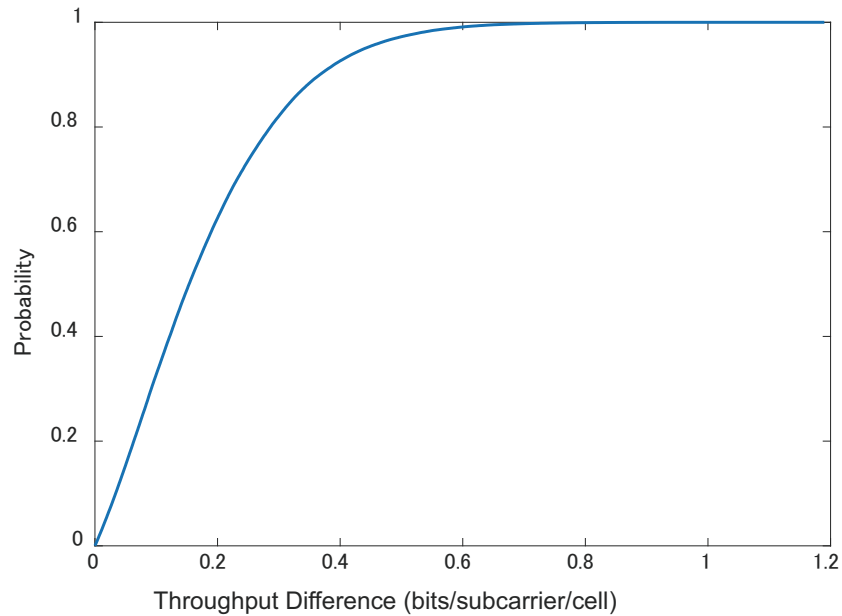


Figure 2.8: CDF of difference between optimum and local optimum (single-user RR scheduling,  $N_U = 3$ , inter-antenna distance 100 m).

In single-user RR scheduling, the system throughput characteristics versus the number of users are shown in Fig. 2.9. The number of search iterations is 14 and the inter-antenna distance is 100 meters. If the number of UEs increases from 3 to 15, the system throughput increases. If the number of UEs increases from 15 to 20, the system throughput deteriorates. The reason is that the allocated UEs over all the RBs includes more versatile combinations if the number of UEs increases. Therefore, it is harder to assign better combinations of the UEs over the macro cells just by selecting the initial phase of the sequences.

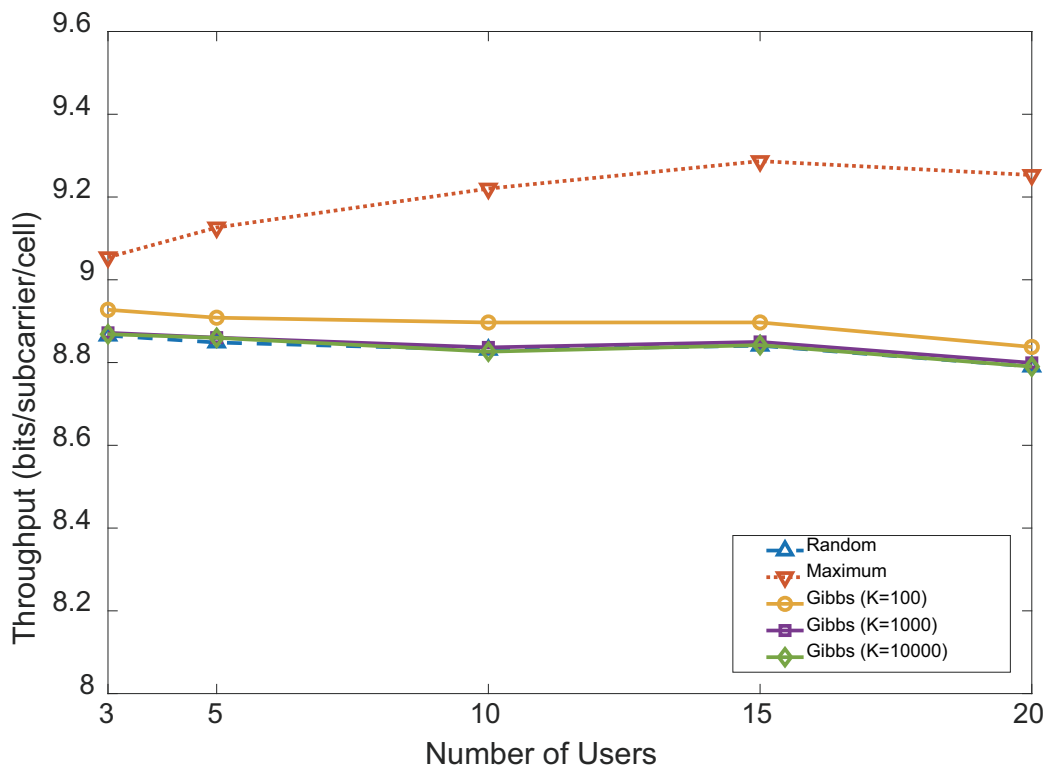


Figure 2.9: System throughput vs. no. of users (single-user RR scheduling, 14 search iterations, inter-antenna distance 100 m).

The system throughput versus the inter-antenna distance is shown in Fig. 2.10. The number of UEs is 10 and the number of search iterations is 14. If the inter-antenna distance is larger, the system throughput is improved. This is because the interference from the outer macro cells decreases owing to the propagation loss. When the inter-antenna distance changes from 150 meters to 200 meters, almost the same system throughput is maintained. Thus, the inter-cell interference is not significant if the inter-antenna distance is larger. However, the distance between the DA and the UE also increases and the received signal power reduces. Thus, less improvement in the system throughput is observed.

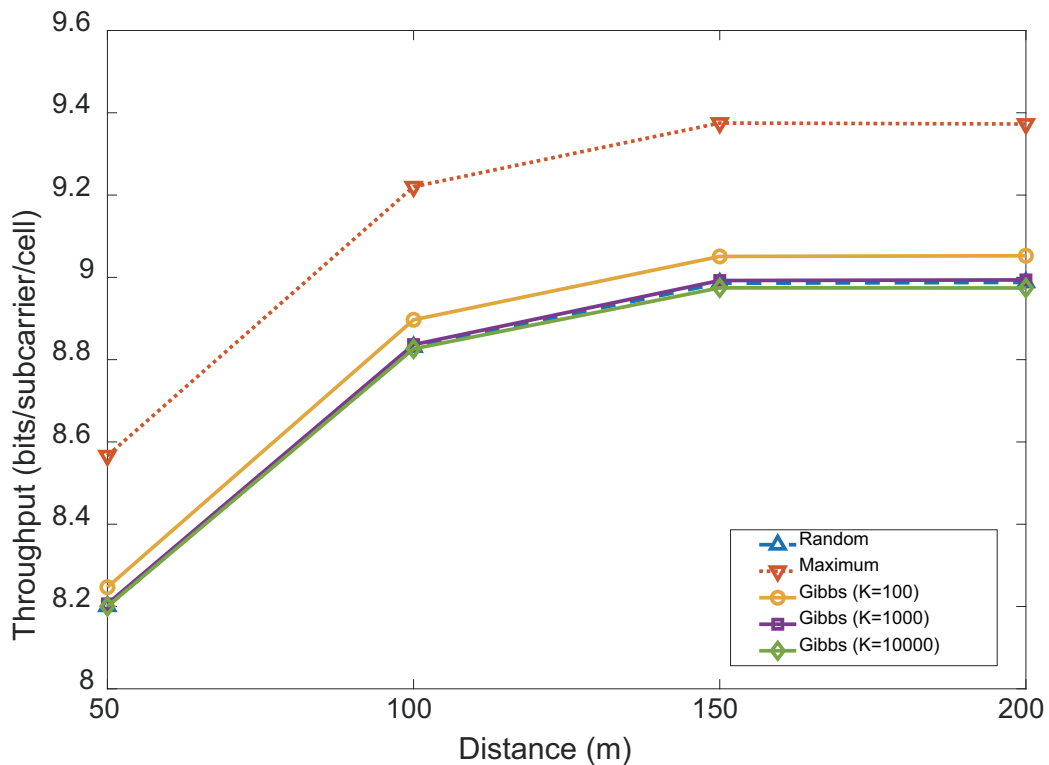


Figure 2.10: System throughput vs. inter-antenna distance (single-user RR scheduling,  $N_U = 10$ , 14 search iterations).

---

### 2.1.5.3 2-User RR Scheduling

In 2-user RR scheduling, the system throughput versus the number of search iterations is shown in Figs. 2.11 and 2.12. The number of UEs is 3 or 10 and the inter-antenna distance is 100 meters. The same as the system throughput in single-user RR scheduling the maximum selection indicates the largest throughput and it reaches 99.5% of that for the full search as shown in Fig. 2.11. In terms of the system throughput with the Gibbs sampling the same tendencies can be observed with those in single-user RR scheduling. The system throughput for the Gibbs sampling with the smaller temperature parameter is larger.

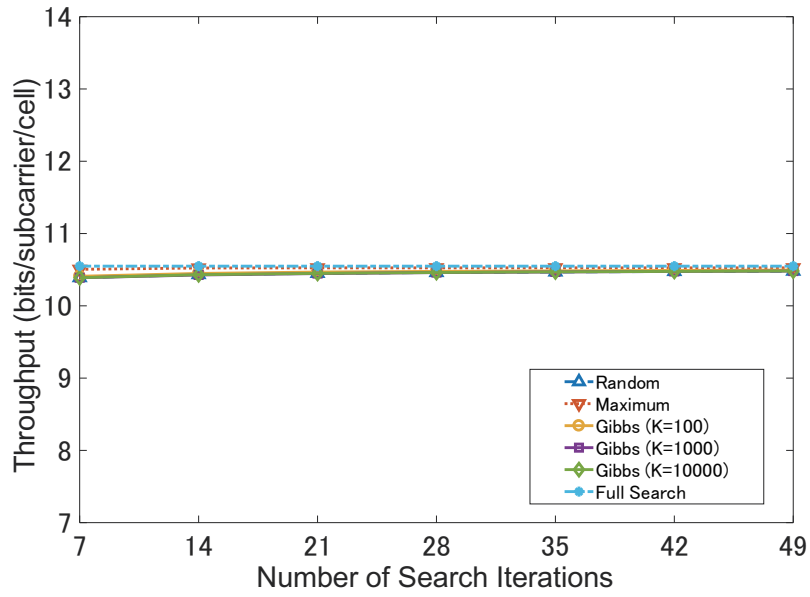


Figure 2.11: System throughput vs. no. of search iterations (2-user RR scheduling,  $N_U = 3$ , inter-antenna distance 100 m).

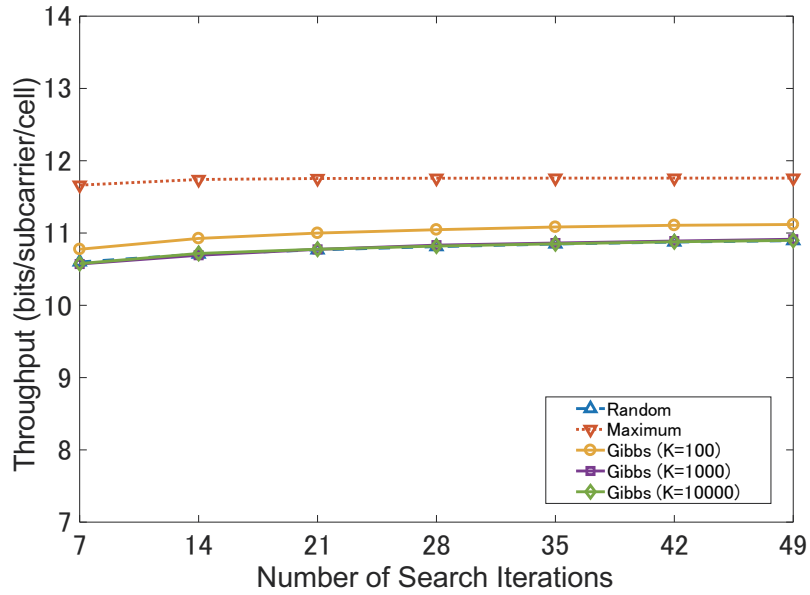


Figure 2.12: System throughput vs. no. of search iterations (2-user RR scheduling,  $N_U = 10$ , inter-antenna distance 100 m).

---

The average phase selection probability in the Gibbs sampling versus the estimated relative throughput is presented in Fig. 2.13. The number of UEs is 10, the inter-antenna distance is 100 meters, and the number of search iterations is 22. In 2-user RR scheduling, the number of combinations for the initial phases is  $\binom{10}{2}$  and each criterion for the phase selection picks up the initial phases from the candidates of the initial phases. The Gibbs sampling with  $K = 1000$  or  $K = 10000$  selects the initial phase almost randomly while the Gibbs sampling with  $K = 100$  tends to select the initial phases with higher throughputs. The convergence performance of the criterion for the initial phase selection is shown in Fig. 2.14. The selection of the initial phase in each macro cell exhibits a marked enhancement in terms of the throughput during the initial period except for the random selection and the selection with Gibbs sampling in large temperature coefficient  $K$ . The selections with the high randomness are treated as the conventional RR scheduling scheme because of the lack of the performance improvement. Moreover, an  $\varepsilon$ -greedy scheme is implemented in Fig. 2.14 and the parameter that represents the probability of selecting other than the initial phase with the largest estimated throughput,  $\varepsilon$ , is set to 0.5, 0.1, and 0.01. As the probability of selecting the initial phase with the largest estimated throughput increases, the throughput with the  $\varepsilon$ -greedy scheme approaches that of the maximum selection. The result emphasizes that there are almost no local solutions and the optimal solution can be reached by the maximum selection.

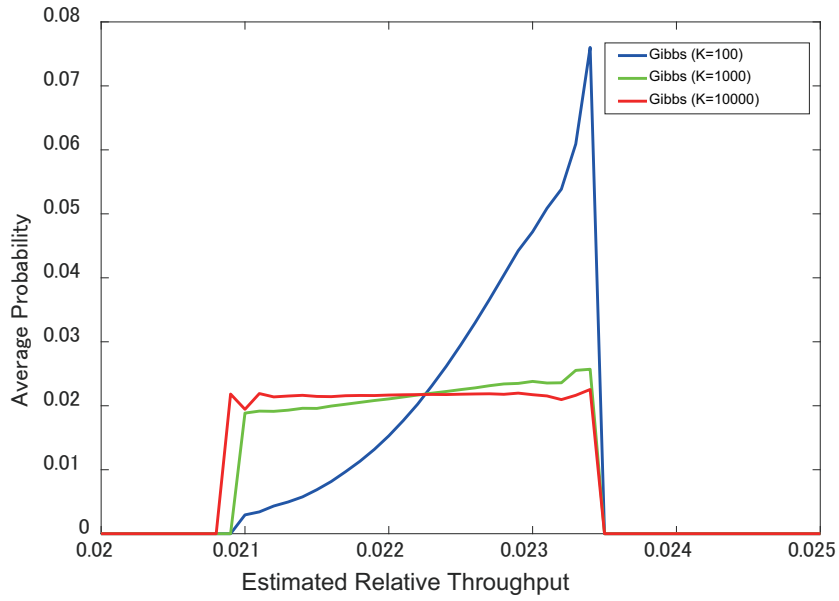


Figure 2.13: Average phase selection probability vs. relative throughput (single-user RR scheduling,  $N_U = 10$ , 22 search iterations, inter-antenna distance 100 m).

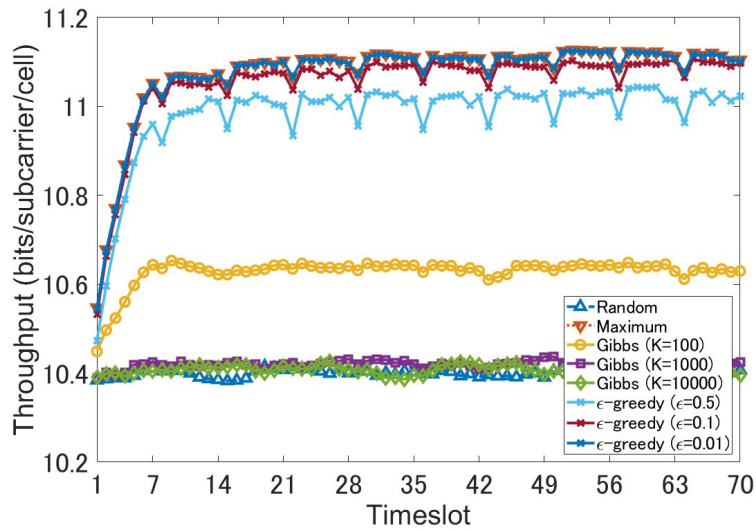


Figure 2.14: Comparison with  $\epsilon$ -greedy scheme.

---

The CDF of the throughput is shown in Fig. 2.15. The figure indicates that the maximum selection is also superior to the other criteria in terms of 5%-CDF throughput. Maximum selection achieves higher throughput than the others criteria including the selection with Gibbs sampling. Gibbs sampling is able to escape from a local optimum and the selection with Gibbs sampling tends to indicate superior performance. However, in the assumed system, the local optimum rarely exists and the throughput difference between the optimum and the local optimum is small. The ratio of the local optimums is 0.50 % among all the combinations. The CDF of the throughput difference between the optimum and the local optimum when  $N_U = 3$  is shown in Fig. 2.16. The search result hardly falls into the local optimum and the throughput difference is small even if the search falls into it. Consequently, maximum selection outperforms the other criteria.

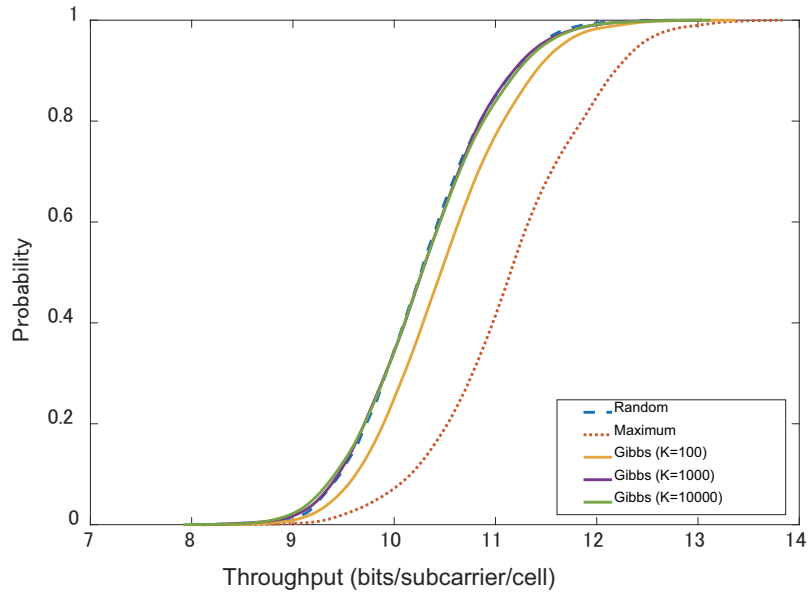


Figure 2.15: CDF of throughput(2-user RR scheduling,  $N_U = 10$ , 14 search iterations, inter-antenna distance 100 m).

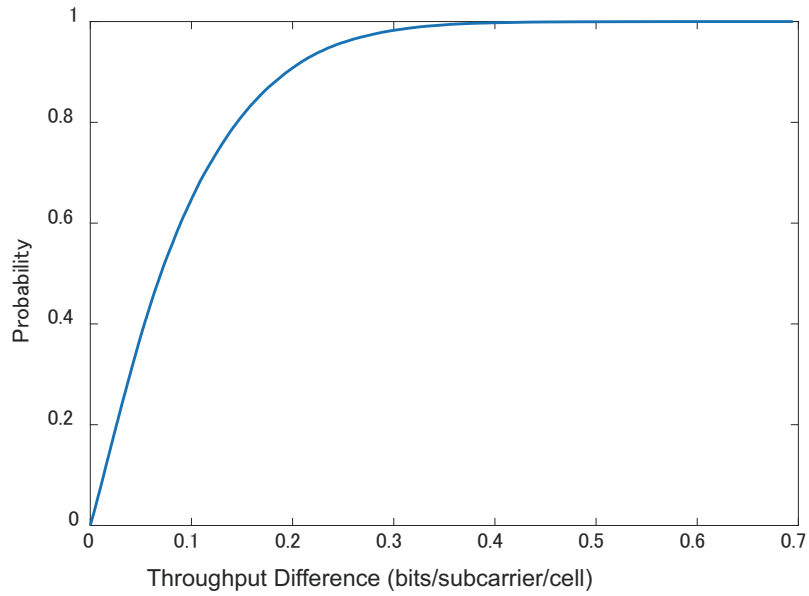


Figure 2.16: CDF of difference between optimum and local optimum (2-user RR scheduling,  $N_U = 3$ , inter-antenna distance 100 m).

In 2-user RR scheduling, the system throughput versus the number of UEs are presented in Fig. 2.17. The number of the search iterations is 14 and the inter-antenna distance is 100 meters. Different from those in single-user RR scheduling, the system throughput increases as the number of UEs grows. This is because of the UE allocation sequence given in Table. 2.1. In 2-user RR scheduling, the same UE index is allocated as UE 1 consecutively. Therefore, by selecting the initial phase of the sequence, the same UE can be allocated to the consecutive RBs and it is more possible to find better combinations of UEs over the macro cells and all the RBs.

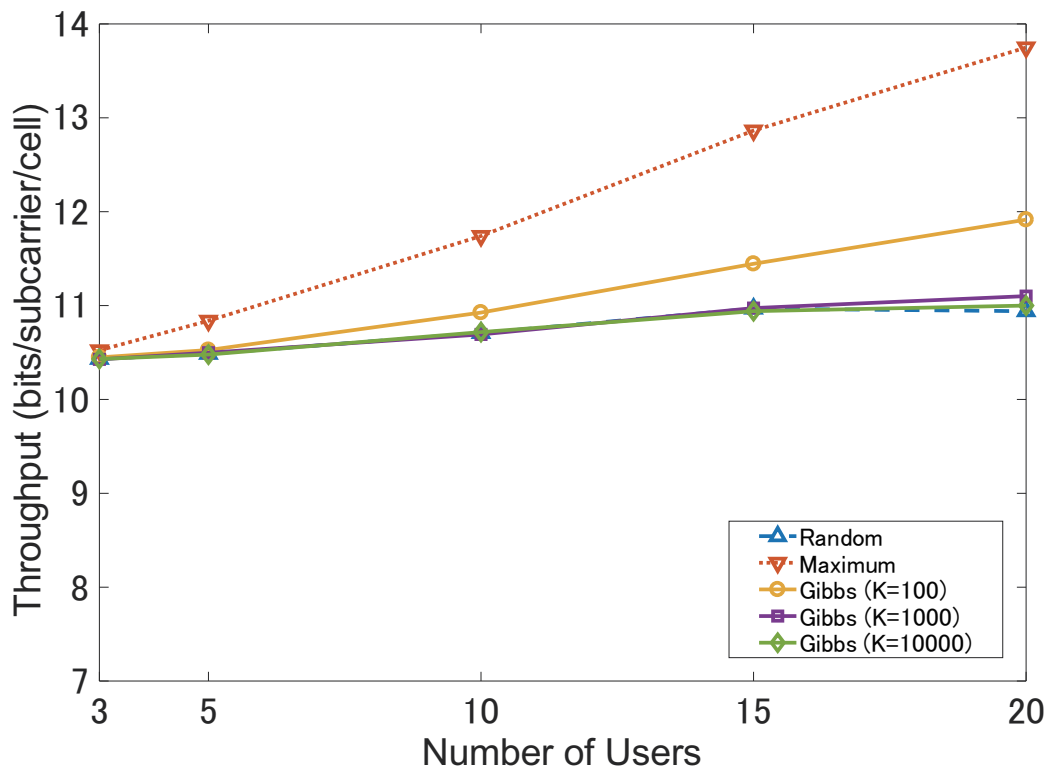


Figure 2.17: System throughput vs. no. of users (2-user RR scheduling, 14 search iterations, inter-antenna distance 100 m).

The system throughput versus the inter-antenna distance is shown in Fig. 2.18. The number of UEs is 10 and the number of the search iterations is 14. If the inter-antenna distance is longer, the system throughput improves. The reason is that the interference from other macro cells decreases owing to the propagation loss as the inter-antenna distance is long. Different from those in single-user RR scheduling, when the inter-antenna distance changes from 150 meters to 200 meters, the system throughput still increases. In 2-user RR scheduling, the intra-cell interference among the DAs as well as inter-cell interference reduces if the inter-antenna distance increases and the system throughput improves.

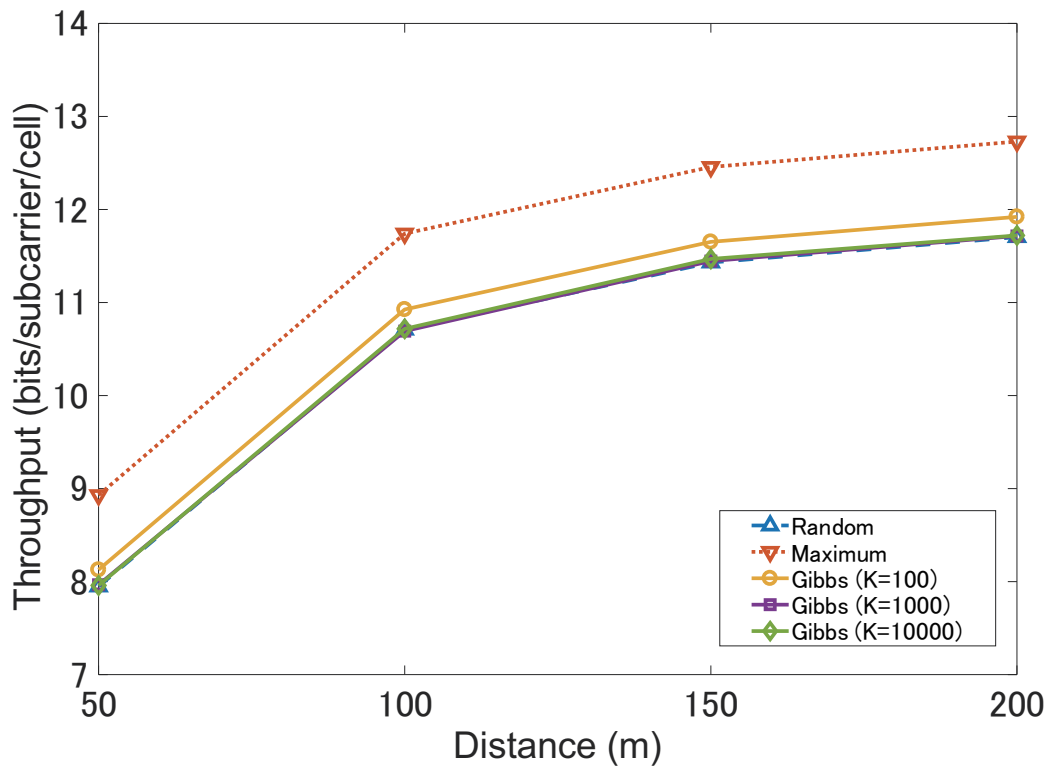


Figure 2.18: System throughput vs. inter-antenna distance (2-user RR scheduling,  $N_U = 10$ , 14 search iterations).

---

### 2.1.6 Conclusions

In this section, the UE allocation scheme for the RR scheduling is proposed. The proposed scheme selects the initial phases of the UE allocation sequence over the macro cells sequentially. Four different phase selection criteria are compared in this section. It has been shown through the numerical results that the maximum selection achieves the largest throughputs and it reaches over 99% of that for the optimum selection when the number of UEs is three. In single-user RR scheduling, the proposed scheme achieves the largest throughput when the number of UEs is about 15 while the different tendencies are observed in 2-user RR scheduling. The system throughput improves as the inter-antenna distance increases especially in 2-user RR scheduling.

---

## 2.2 UE Set Selection for Allocation Sequence of RR Scheduling

### 2.2.1 Introduction

Recently, many IoT applications have been launched and the amount of mobile traffic has increased explosively [57]. DAT has been studied as one form of the 5G mobile communication deployment and can resolve the problem of larger path loss in high frequency bands. Radio-resource scheduling in DAT among multiple TPs with lower computational complexity is the challenge to solve under a trade-off between system throughput and fairness among users [12].

To accomplish higher system throughput and to mitigate CCI especially for cell-edge users, CDAT using multi-user spatial multiplexing has been proposed [34–37,39,41,42]. The combination of CDAT, UE classification, UE clustering, and cluster-antenna association is investigated as evolved CDAT in [36,37]. Fractional frequency reuse (FFR) is adopted in [36] to mitigate inter-cell interference of cell edge UEs. In [34], Max C/I scheduling, PF scheduling, and RR scheduling in CDAT are compared. In spite of the low complexity of RR scheduling, the system throughput and the fairness were close to those of PF scheduling. On the other hand, coordinated radio-resource scheduling with a global scheduler has been introduced in [41,42]. The global scheduler computes a PF metric for each combination of UEs while local schedulers determine the association between TPs and UEs.

However, those researches for UE allocation apply no scheduling criterion for RR scheduling in DAT. In order to mitigate inter-cell interference, the

---

initial phase selection of UE allocation sequences for RR scheduling in DAT has been proposed in section 2.1 [61,62]. The problem of the scheme in section 2.1 is that no fairness among UEs was taken into account even though the system throughput was improved. It is necessary that the system throughput is enlarged while user fairness is maintained.

The researches on the resource allocation with reinforcement learning have been flourishing because it can be applied to a system that is difficult to be modelled. For example, in [64], in order to utilize the limited backhaul capacity of millimeter-wave communication, the blockage patterns of channel states can be captured and predicted with deep reinforcement learning (DRL). In [65,66], the authors have applied the DRL to high mobilities, such as trains or unmanned aerial vehicles (UAVs), which cause unpredicted and fluctuating links. They support the time division duplex (TDD) configuration in real-time and adaptively change the ratio of TDD uplink/downlink. As the integrated access and the backhaul architecture could be huge and time-varying, the DRL have been introduced in [67] to the problem in which the optimal solution that maximizes the sum rate of all UEs is intractable to find. In [68,69], the aggregate network capacity employing the beamforming and non-orthogonal multiple access (NOMA) have been maximized by utilizing three reinforcement learning (RL) methods. The authors in [70,71] approximate a traditional iterative power allocation algorithms that require high computational complexity with the DRL algorithm with low computational complexity. The RL on the resource allocation is promising and have the feasibility of spectrum efficiency improvement. However, to the best of our knowledge, the RL has not been adapted to the RR scheduling

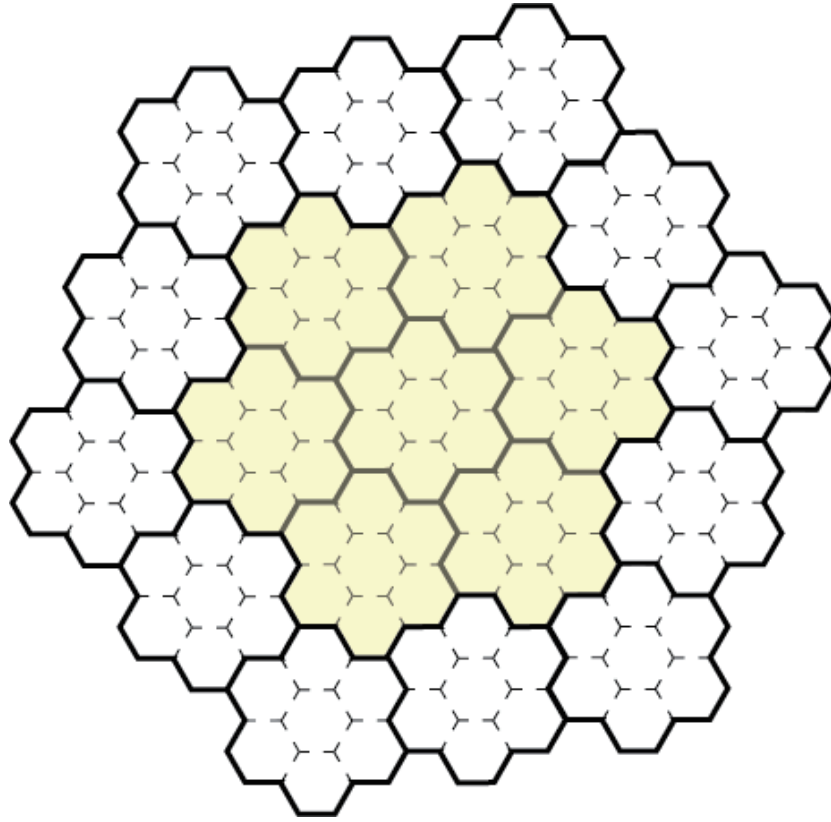


Figure 2.19: Cell model.

in DAT. In this section, RR scheduling with RL is proposed to realize the efficient UE allocation sequence of the RR scheduling for DAT with a BD algorithm [72]. The proposed RR scheduling is compared to the weighted PF scheduling in terms of the computational complexity, fairness, and the system throughput [73].

## 2.2.2 System Description

### 2.2.2.1 Cell Model

A cell model shown in Fig. 2.19 is assumed. One macro cell consists of hexagonal seven micro cells. A distributed antenna called a TP is located

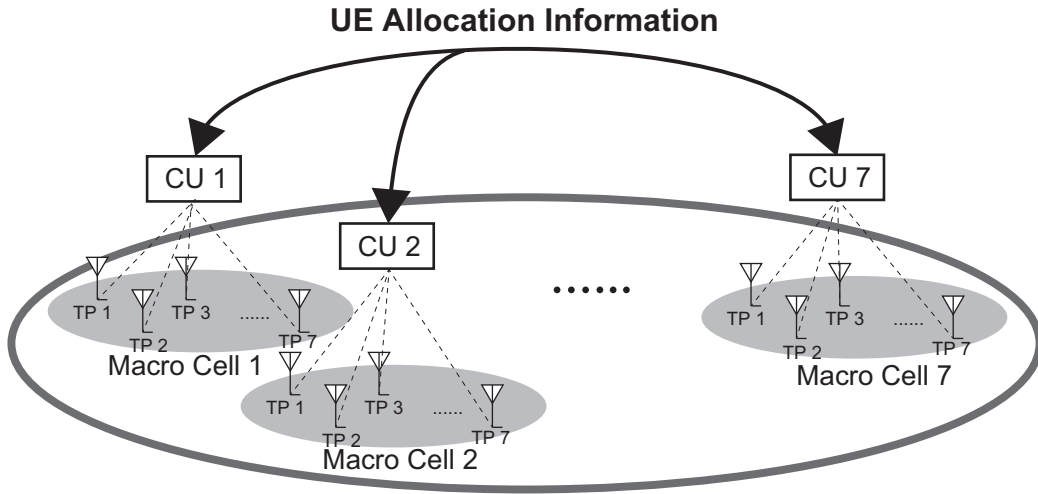


Figure 2.20: Overview of cell model.

at the center of each micro cell. The number of TPs in each macro cell is  $N_A = 7$ . All TPs are controlled by the same CU. CCI is caused by reusing the same frequency channel in the other macro cells. The colored macro cells in Fig. 2.19 exchange UE allocation information as shown in Fig. 2.20 and the system throughput is evaluated over the colored seven macro cells in this section. Moreover, radio-resource scheduling for the allocation of UEs over RBs is adopted for OFDM signal transmission. Multiple UEs can be assigned to each RB and served by TPs within a macro cell. Suppose that the number of UEs in a macro cell is  $N_U$  and the maximum number of UEs allocated to each RB is  $N_S$ .

### 2.2.2.2 Antenna Selection

Multi-user MIMO with the BD algorithm is introduced to the DAT and the system throughput calculation at the antenna selection [72]. As shown in Fig. 2.21  $N_S$  TPs are selected from  $N_A$  TPs and signals for  $N_S$  single antenna

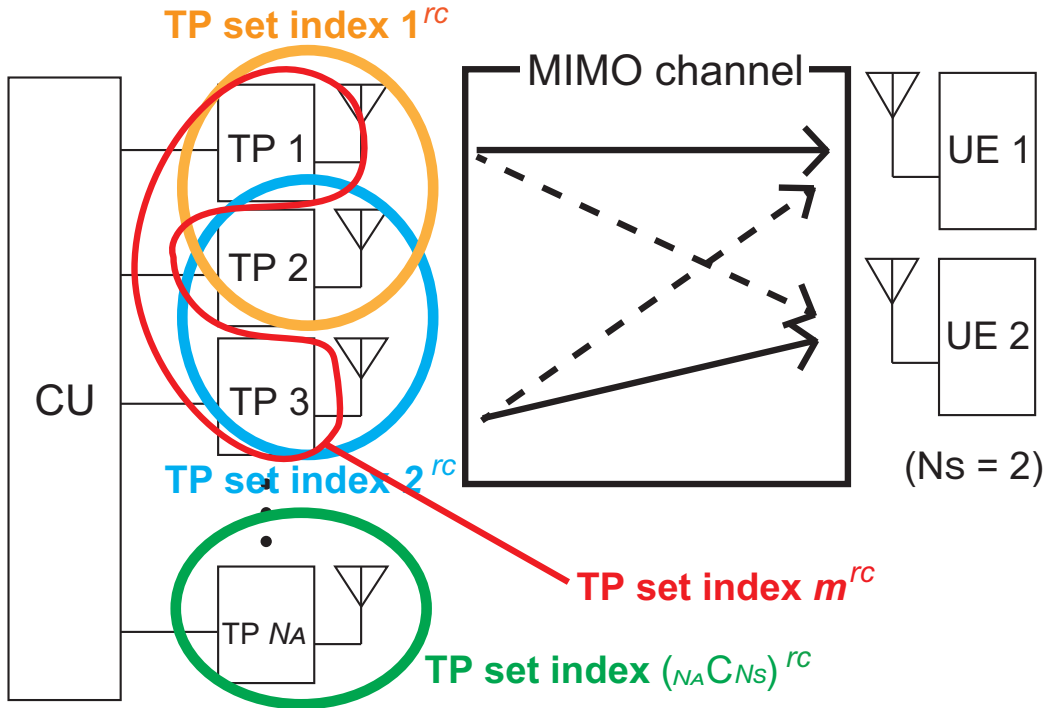


Figure 2.21: Multi-user MIMO systems in DAT ( $N_S = 2$ ).

UEs are spatially multiplexed. The TPs to support UEs should be selected at the initial stage of radio-resource scheduling. Each UE is connected to one of TPs that can achieve the highest estimated throughput. The estimated throughput takes no inter-cell interference into account because which TPs in adjacent macro cells cause CCI to UEs may change all the time. The TP is selected exclusively so that  $N_S$  TPs are connected to  $N_S$  UEs. Suppose that  $m^{rc}$  is the TP set index of the TPs associated in the  $r$ -th RB at the  $c$ -th macro cell as shown in Fig. 2.21. The number of TP set indexes is  $\binom{N_A}{N_S}$ . The signals for the  $n$ -th UE in the  $r$ -th RB is transmitted only from the TPs of the  $m^{rc}$ -th TP set and the transmit signals from the other TPs are regarded as intra-cell interference. The transmit signals are pre-coded with the BD

---

algorithm so that only a desired signal reach each UE. The transmit signal to the  $n$ -th UE on the  $l$ -th subcarrier in the  $r$ -th RB is represented by  $x_n^{r_l}$ . The received signal for the  $n$ -th UE at the  $c$ -th macro cell is given by

$$y_n^{r_l c} = \mathbf{H}_{nm^{rc}}^{r_l c} \mathbf{W}_{nm^{rc}}^{r_l c} x_n^{r_l c} + \sum_{\nu \in \{\mu^{rc}\}} \mathbf{H}_{nm^{rc}}^{r_l c} \mathbf{W}_{\nu m^{rc}}^{r_l c} x_\nu^{r_l c} + z_n^{r_l c} \quad (2.14)$$

where  $\mathbf{H}_{nm^{rc}}^{r_l c}$  is the channel response vector with a size of  $1 \times N_S$  between the TPs of the  $m^{rc}$ -th TP set and the  $n$ -th UE,  $\mathbf{W}_{nm^{rc}}^{r_l c}$  is the pre-coding vector with a size of  $N_S \times 1$  between the TPs in the  $m^{rc}$ -th TP set index and the  $n$ -th UE,  $\nu$  is the index of a UE that causes interference to the  $n$ -th UE,  $z_n^{r_l c}$  is the AWGN with a mean of zero and a variance of  $\sigma^2$  on the  $l$ -th subcarrier in the  $r$ -th RB, and  $\{\mu^{rc}\}$  is the set of  $N_S$  UE indexes allocated to the  $r$ -th RB at the  $c$ -th macro cell. The number of UE index sets,  $\{\mu^r\}$ , is  $\binom{N_U}{N_S}$ .

The throughput for the  $n$ -th UE on the  $l$ -th subcarrier in the  $r$ -th RB at the  $c$ -th macro cell is calculated as

$$\hat{T}_n^{r_l c}(m^{r_l c}) = \log_2 \left( 1 + \frac{P_{nm^{rc}}^{r_l c}}{\sum_{\nu \in \{\mu^{rc}\}} P_{\nu m^{rc}}^{r_l c} + \sigma^2} \right) \quad (2.15)$$

where the received signal power is represented as  $P_{nm^{r_l c}}^{r_l c} = |\mathbf{H}_{nm^{r_l c}}^{r_l c} \mathbf{W}_{nm^{r_l c}}^{r_l c}|^2$  for the  $\nu$ -th UE from the TPs of the  $m^{rc}$ -th TP set on the  $l$ -th subcarrier in the  $r$ -th RB at the  $c$ -th macro cell. This is the tentative throughput for TP association without taking inter-cell interference into account as it is determined after the association of TPs to UEs in the adjacent cells. The sum of the throughputs over subcarriers and the allocated UEs in the  $r$ -th RB,  $\hat{T}_{sum}^{rc}$ , is then given by

$$\hat{T}_{sum}^{rc}(m^{r_l c}) = \sum_{l \in \{l^r\}} \sum_{n \in \{\mu^{rc}\}} \hat{T}_n^{r_l c}(m^{r_l c}) \quad (2.16)$$

---

where  $\{l^r\}$  is the set of subcarrier indexes in the  $r$ -th RB. The TP set indexes are selected for  $\binom{N_U}{N_S}$  UE sets to maximize the total throughput,  $\hat{T}_{sum}^{rc}(m^{r1c})$ .

### 2.2.3 Throughput Calculation

Different from the tentative throughput, interference from the other macro cells is included in the system throughput calculation. The throughput for the  $n$ -th UE on the  $l$ -th subcarrier in the  $r$ -th RB at the  $c$ -th macro cell,  $T_n^{r1c}$ , is given by

$$T_n^{r1c}(m^{r1c}) = \log_2 \left( 1 + \frac{P_{nm^{r1c}}^{r1c}}{\sum_{\nu \in \{\mu^{rc}\}} P_{\nu m^{r1c}}^{r1c} + \eta_n^{r1c2}} \right) \quad (2.17)$$

where  $\eta_n^{r1c}$  is the sum of the noise and the interference from the outer macro cells to the  $n$ -th UE on the  $l$ -th subcarrier in the  $r$ -th RB. The total sum of the throughputs to the  $n$ -th UE over the subcarriers in the  $r$ -th RB at the  $c$ -th macro cell,  $T^{rc}$ , is given by

$$T^{rc}(n) = \sum_{l \in \{l^r\}} T_n^{r1c}(m^{r1c}). \quad (2.18)$$

Therefore, the system throughput over seven macro cells, RBs, and allocated UEs normalized by the numbers of the macro cells is given as

$$T = \frac{1}{7} \sum_{c=1}^7 \sum_r \sum_{n \in \{\mu^{rc}\}} T^{rc}(n) \quad (2.19)$$

where  $\{\mu^{rc}\}$  is the sets of UE indexes.

### 2.2.4 Fairness Index

The FI is calculated as [74]

$$FI = \frac{\sum_{c=1}^7 \sum_{n=1}^{N_U} \frac{1}{T_{ave}} \sum_{t=1}^{T_{ave}} T^c(n, t)}{7 \sum_{c=1}^7 N_U \sum_{n=1}^{N_U} \left( \frac{1}{T_{ave}} \sum_{t=1}^{T_{ave}} T^c(n, t) \right)^2} \quad (2.20)$$

---

where  $T^c(n, t)$  is the throughput for the  $n$ -th UE in the  $t$ -th timeslot at the  $c$ -th macro cell calculated from Eq. (2.18) over all the RBs and  $T_{ave}$  is the period for averaging the radio-resource scheduling.

## 2.2.5 Radio-Resource Scheduling

In this section, one subframe consists of multiple timeslots and one timeslot consists of 14 OFDM symbols. Because of TDD, a half of the symbols are allocated to downlink communication.

### 2.2.5.1 PF Scheduling

Weighted PF scheduling is applied in this section as a reference [73, 75]. In the  $r$ -th RB at the  $c$ -th macro cell for the set of  $N_S$  UE indexes, it maximizes the following metric,  $f^{rc}$ ;

$$f^{rc}(\mu^{rc}) = \prod_{n \in \{\mu^r\}} \left( 1 + \frac{(\tilde{T}^{rc}(n, t))^{w_1 - w_2}}{(C_n(t))^{w_2}} \right) \quad (2.21)$$

where  $\tilde{T}^{rc}(n, t)$  is the estimated throughput derived from Eq. (2.18) for the  $n$ -th UE set over the subcarriers in the  $r$ -th RB in the  $t$ -th timeslot at the  $c$ -th macro cell, and  $w_1$  and  $w_2$  are the weights for the weighted PF scheduling. A larger weight,  $w_1$ , as well as a smaller weight,  $w_2$ , tend to allocate a RB to UEs with larger estimated throughputs. The interference from outer macro cells are calculated on the basis of TPs that are associated to UEs in the preceding subframe and  $C_n(t)$  is the average user throughput for the  $n$ -th UE at the  $t$ -th timeslot. The PF metric is calculated at every subframe. The throughput estimation is conducted  $N_{RB} \cdot \binom{N_U}{N_S}$  times at each RB allocation.

---

### 2.2.5.2 RR Scheduling

The total number of UE combinations is  $\binom{N_U}{N_S}$ . The conventional RR scheduling allocates UEs according to a UE allocation sequences with the length of  $\binom{N_U}{N_S}$ .

## 2.2.6 Proposed RR Scheduling

### 2.2.6.1 Throughput Estimation

Suppose that the expected throughput for the  $n$ -th UE set on the  $l$ -th subcarrier in the  $r$ -th RB corresponding to the initial phase  $\delta_c$  for the  $c$ -th macro cell is represented as  $\bar{T}_n^{rlc}(\delta_c, m^{rc})$ . The total sum of the expected throughput over all the UEs and the subcarriers of the RBs for the  $c$ -th macro cell is calculated from Eq. (2.17) and is given by

$$\bar{T}^c(\delta_c) = \sum_r \sum_{l \in \{l^r\}} \sum_{n \in \{\mu_{\delta_c}\}} \bar{T}_n^{rlc}(\delta_c(m^{rc})) \quad (2.22)$$

where  $\delta_c$  is the initial phase for the  $c$ -th macro cell. The expected system throughput corresponding to the set of the initial phases,  $\{\delta_c\}$ , over the macro cells is then given by

$$\bar{T}(\delta_1, \dots, \delta_7) = \sum_{c=1}^7 \bar{T}^c(\delta_c). \quad (2.23)$$

### 2.2.6.2 Algorithms for Initial Phase Selection

In this section, two different initial phase selection algorithms based on the expected throughputs are applied in the initial phase selection proposed in section 2.1 [61, 62].

---

**Random Selection** Random selection selects the initial phases in all the macro cells randomly and sequentially. Therefore, no throughput is estimated over all the RB allocation.

**Maximum Selection** Maximum selection selects the initial phases of the UE allocation sequences sequentially over multiple macro cells and it is repeated iteratively. Suppose that  $t$  is the time index and  $\hat{\delta}_c^{(t)}$  is the candidate of the initial phase selected in the  $c$ -th macro cell at the  $t$ -th time index, the sum of the tentative throughputs given by the selected initial phases at the  $c$ -th macro cell,  $\bar{T}(\hat{\delta}_1^{(t)}, \dots, \hat{\delta}_{c-1}^{(t)}, \hat{\delta}_c, \hat{\delta}_{c+1}^{(t-1)}, \dots, \hat{\delta}_7^{(t-1)})$ , is calculated from Eq. (2.23) for all of  $\delta_c (0 \leq \delta_c \leq (1 - x_E) \binom{N_U}{N_S} - 1)$ . The maximum selection selects phase of the sequence with the largest expected throughput. The maximum selection is presented as

$$\hat{\delta}_c^{(t)} = \arg \max_{\hat{\delta}_c} \bar{T}(\hat{\delta}_1^{(t)}, \dots, \hat{\delta}_{c-1}^{(t)}, \hat{\delta}_c, \hat{\delta}_{c+1}^{(t-1)}, \dots, \hat{\delta}_7^{(t-1)}). \quad (2.24)$$

Since this criterion selects the initial phases sequentially, the system throughput may fall into a local optimum. The throughput estimation is conducted  $N_{RB} \cdot (1 - x_E) \cdot \binom{N_U}{N_S}$  times at each RB allocation.

### 2.2.6.3 UE Set Selection in RR Allocation Sequence with Reinforcement Learning

In the proposed scheduling, the RR allocation sequence is modified for each RB because the channel response in each RB is different according to the frequency selectivity of a fading channel. The expected throughput for each UE set in each RB is calculated from Eq. (2.17) with maximum selection because the initial phase selections with maximum selection are exhaustively

---

searched. In the proposed RR scheduling, the reinforcement learning is applied to the RR allocation sequence in order to eliminate UE combinations that suffer from larger interference. The CUs select the action  $a_t$  with the largest Q-value. In other words, the CUs eliminate the UE combinations under severe interference at every timeslot after the initial phase selection.

The RR allocation sequence in the  $r$ -th RB at the  $t$ -th timeslot is expressed as the state,  $s_t^r$ . The elimination of the specific UE combination in the  $r$ -th RB at the  $t$ -th timeslot is the possible action of CU, and it is denoted as  $a_t^r$ . The predicted Q-value for the next timeslot in the  $r$ -th RB at the  $t$ -th timeslot is given as  $Q_t(s_{t+1}^r, a_r)$ . The Q-value of the action,  $a_t^r$ , for the state,  $s_t^r$ , is given as

$$Q_t(s_t^r, a_t^r) \leftarrow (1 - \alpha)Q_t(s_t^r, a_t^r) + \alpha[R_{t+1}^r + \gamma \max_{a^r} Q_{t+1}(s_{t+1}^r, a^r)], \quad (2.25)$$

where  $\alpha$  is the learning rate that indicates the impact of the current and past learning,  $\gamma$  is the discount rate, and  $R_{t+1}^r$  is the reward value for transition to the state,  $s_{t+1}^r$ .  $R_{t+1}^r$  is calculated from the estimation throughput averaged over UE combinations in the allocation sequence except for the UE combination that is eliminated in the action,  $a_t^r$ .

The possible transition state at the  $t$ -th timeslot is shown in Fig. 2.22. Suppose that the length of the allocation sequence for the initial state,  $s_t^r$ , is  $L$ , the CU takes an action,  $a_t^r$ , which is the elimination of a UE set. The next state after the initial action is expressed as  $s_{t+1}^r$  whose length of an allocation sequence is  $L - 1$  and the reward for the initial action,  $R_{t+1}^r$ , is calculated from the remaining UE sets. The UE combination that results in the smallest system throughput is excluded according to the action,  $a_{t+1}^r$ , and

the reward,  $R_{t+2}^r$ , is derived from the state,  $s_{t+2}^r$ .  $R_{t+2}^r$  is the reward value for the transition to the state,  $s_{t+2}^r$ , at the  $t$ -th timeslot and corresponds to the average estimation throughput when the UE combination that realizes the smallest system throughput is excluded. The CU takes the action with the largest Q-value.

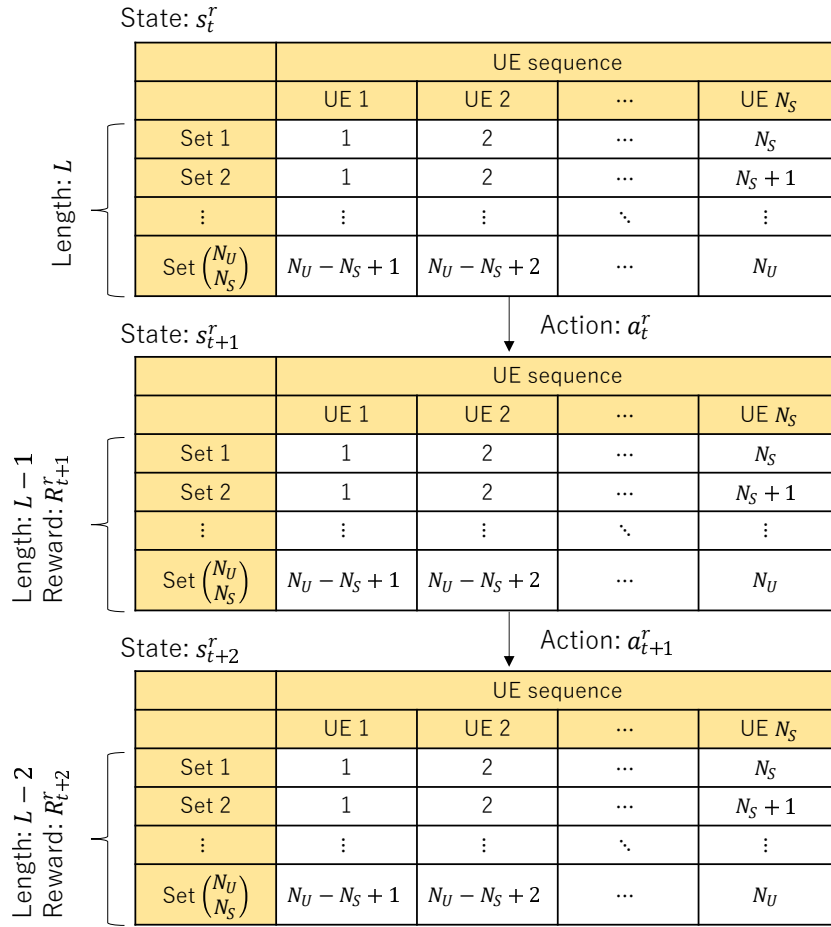


Figure 2.22: UE set elimination with reinforcement learning.

## 2.2.7 Numerical Results

### 2.2.7.1 Simulation Conditions

Table 2.3: Simulation Conditions.

Inter-antenna distance	50, 100, 150, 200 m
Minimum distance between UE and TP	5 m
Height of TP	10 m
Height of UE	1.5 m
Carrier frequency	4.65 GHz
System bandwidth	72 MHz
RB bandwidth	720 kHz
No. of RBs	100
No. of subcarriers per RB	12
Transmit power	30 dBm
LOS probability	$P_{LOS} = \min(\frac{18}{d}, 1)\{1 - \exp(-\frac{d}{d_{LOS}})\} + \exp(-\frac{d}{d_{LOS}})$ $d$ : Distance from an UE to a TP
Path loss	$L_{LOS} = 22.0 \log_{10}(d) + 28.0 + 20 \log_{10}(f_c)$ dB $L_{NLOS} = 36.7 \log_{10}(d) + 22.7 + 26 \log_{10}(f_c)$ dB $f_c$ : Carrier frequency
Shadowing standard deviation	4 dB
Channel model	LOS: Rician path + 15-path uniform Rayleigh ( $K$ -factor:10) NLOS: 16-path uniform Rayleigh
Receiver noise density	-174 dB/Hz
Noise figure	9 dB
Allocation	2-user allocation
No. of UEs per macro cell	5, 10, 15, 20
Temperature coefficient $K$	100, 1000, 10000
Ratio of eliminated UE sets in sequence	$0 \leq x_E \leq 0.8$
Weight for PF $w_1 - w_2$	$0 \leq w_1 - w_2 \leq 1.0$
Weight for PF $w_2$	1.0

---

The simulation conditions are shown in Table 2.3. The inter-antenna distance is selected from 50, 100, 150, or 200 meters. The height of the TPs is 10 meters and the height of the UEs is 1.5 meters. The carrier frequency is 4.65 GHz, the system bandwidth is 72 MHz, and the RB bandwidth is 720 kHz. The number of RBs is 100 and the number of subcarriers per RB is 12. The transmit power per antenna is set to 30dBm. The amounts of average propagation loss,  $L_{LOS}$  and  $L_{NLOS}$ , are different between LOS and non-line-of-sight (NLOS) conditions. In Section 2.1, the propagation environment was treated to be LOS when the UE that are emitting or receiving interference are located within the same macro cell. Conversely, the propagation environment was assumed to be NLOS when they are in different macro cells. This condition is unfair because UEs that are very close to each other are treated as NLOS environments if they are in the different cells. Therefore, in this section, the propagation environment is stochastically determined according to the distance between UEs. The LOS probability model and the path loss model are the same as those in [76, 77]. The shadowing deviation is 4dB. The first Rician fading path and following 15 uniform Rayleigh paths are assumed in the LOS condition and a 16-path uniform Rayleigh fading channel is assumed in the NLOS condition. The  $K$ -factor in the LOS model is 10. The receiver noise density is set to -174 dB/Hz and the noise figure is 9dB. Two user allocation ( $N_S = 2$ ) is assumed. The number of UEs per macro cell is 5 and 10 and the uniform user distribution is applied. The temperature coefficient,  $K$ , is set as 100, 1000, or 10000. The average system throughput per subcarrier per cell is evaluated for different phase selection criteria unless it is specified. The ratio of the eliminated UE allocation sequences,  $x_E$ , is

---

varied from 0.0 to 0.8. The weight for PF scheduling,  $w_2$ , is set to 1.0 while the weight,  $w_1 - w_2$  are varied from 0.0 to 1.0.

### **2.2.7.2 Effect of Number of UEs**

The system throughput versus FI is shown in Figs. 2.23 and 2.24. The number of UEs is 5 and 10. The ratio of eliminated UE sets in allocation sequences,  $x_E$ , is varied from 0.0 to 0.8. The inter-antenna distance is 100 meters. The curves in these figures show that the fairness of the weighted PF scheduling is superior to that of the proposed RR scheduling if the weight for PF is larger than 0.3. However, the performance of the proposed RR scheduling is as equivalent as that of the weighted PF scheduling in the lower estimated throughput region if the weight for PF is lower than 0.3. Especially maximum selection exceeds the weighted PF scheduling in terms of both of the fairness and the throughput. In addition to the improvement of the system performance, the computational complexity of the proposed RR scheduling is much lower than that of the weighted PF scheduling. Therefore, the cellular system operators can adopt the proposed RR scheduling when they do not overestimate the fairness among UEs, while they can adopt the PF scheduling when they provide a service that requires high degree of fairness, such as traffic whose QoS class identifier is classified to a guaranteed bit rate service. In addition, the conventional RR scheduling can be selected when the computational resources are strictly limited. The range of the system throughput is larger as the number of UEs increases. That is because the candidates of UE sets increase and the UE sets with lower inter-cell interference can be allocated.

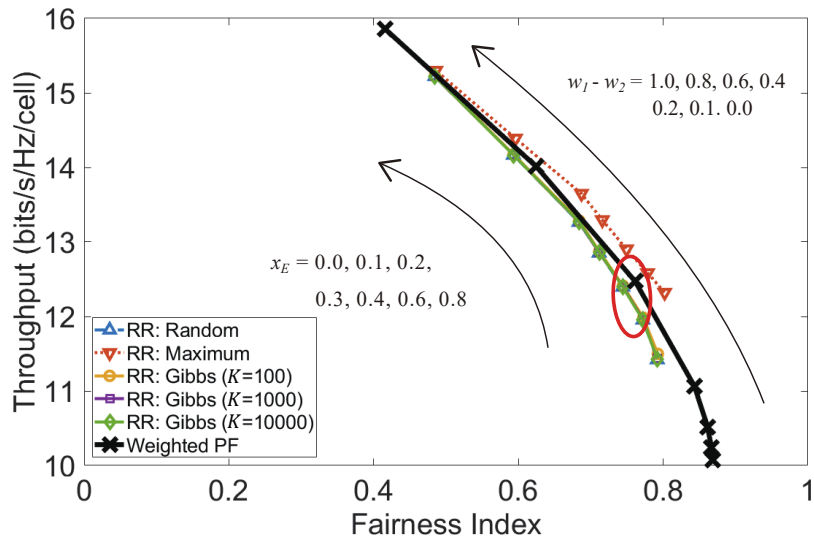


Figure 2.23: System throughput vs. FI ( $N_U=5$ , inter-antenna distance 100 m).

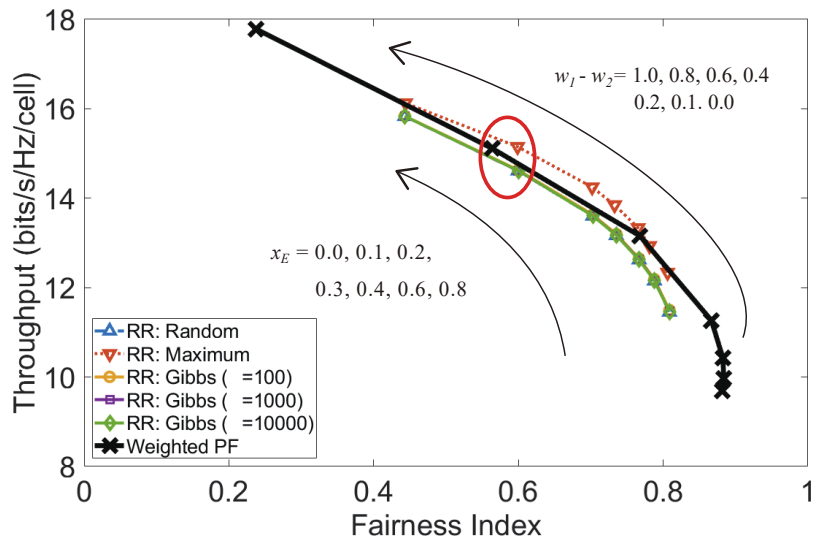


Figure 2.24: System throughput vs. FI ( $N_U=10$ , inter-antenna distance 100 m).

---

The CDF of user throughputs for  $N_U = 5$  is shown in Figs. 2.25 and 2.26. The points surrounded by the red circle in Fig. 2.23 are compared. The inter-antenna distance is 100 meters. The ratio of eliminated UE sets,  $x_E$ , is 0.1 and the computational complexity of the proposed RR scheduling is 90% of that of the PF scheduling. The weight for PF scheduling,  $w_1 - w_2$ , is 0.2. The CDF curves of the worst and best user throughputs are shown in Fig. 2.25 and those of the 2nd best and 2nd worst user throughputs are shown in Fig. 2.26. It is shown in Fig. 2.25 that the user throughput for the worst user is equivalent in the proposed RR scheduling and the weighted PF scheduling. The user throughput for the best user of the proposed RR scheduling ranges narrower than that of the weighted PF scheduling. It is also shown in Fig. 2.26 that the user throughput for the 2nd worst user of the maximum selection is as equal as that of the weighted PF scheduling. The user throughput for the 2nd best user of the maximum selection is better than that of the weighted PF scheduling.

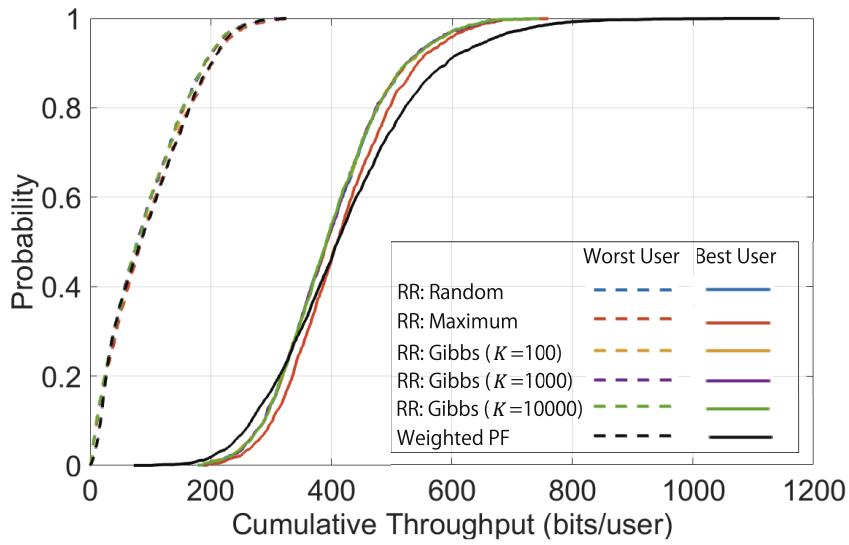


Figure 2.25: Best and worst user throughput ( $x_E = 0.1$ ,  $w_1 - w_2 = 0.2$ , inter-antenna distance 100 m).

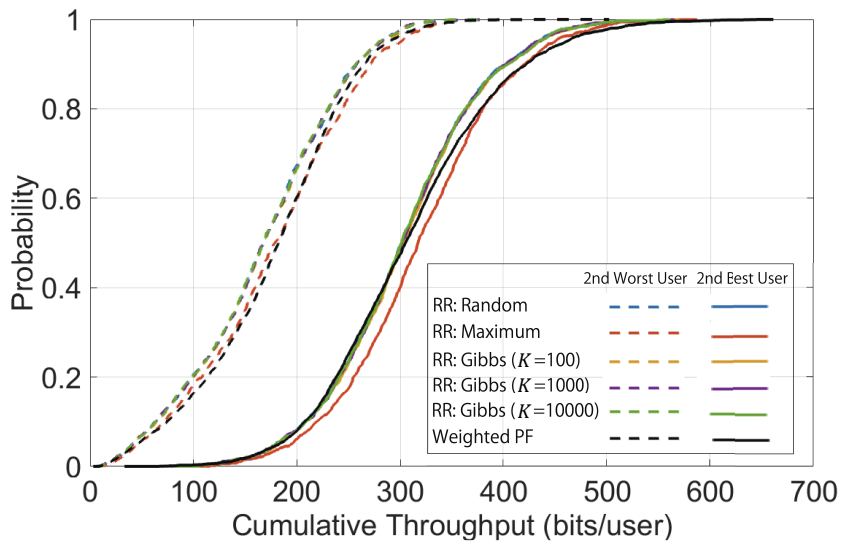


Figure 2.26: 2nd best and 2nd worst user throughput ( $x_E = 0.1$ ,  $w_1 - w_2 = 0.2$ , inter-antenna distance 100 m).

---

The CDF of user throughputs for  $N_U = 10$  is shown in Figs. 2.27 and 2.28. The points surrounded by the red circle in Fig. 2.24 are compared. The inter-antenna distance is 100 meters. The ratio of eliminated UE sets,  $x_E$ , is 0.6 and the computational complexity of the proposed RR scheduling is 40% of that of the PF scheduling. The weight for PF scheduling,  $w_1 - w_2$ , is 0.1. The CDF curves of the worst and best user throughputs are shown in Fig. 2.27 and those of the 4th best and 4th worst user throughputs are shown in Fig. 2.28. It is shown in Fig. 2.27 that the user throughputs for the best and worst user of the weighted PF scheduling exceed those of the proposed RR scheduling. However, the user throughput for the 4th best user of the proposed RR scheduling is much larger than that of the weighted PF scheduling.

The reason of the above explained tendencies is that the weighted PF scheduling tends to allocate to the worst user in order to take the fairness among UEs into account while the proposed RR scheduling allocate more to the next best and worst users according to the shortened RR sequences in which the UE sets with lower throughput are eliminated.

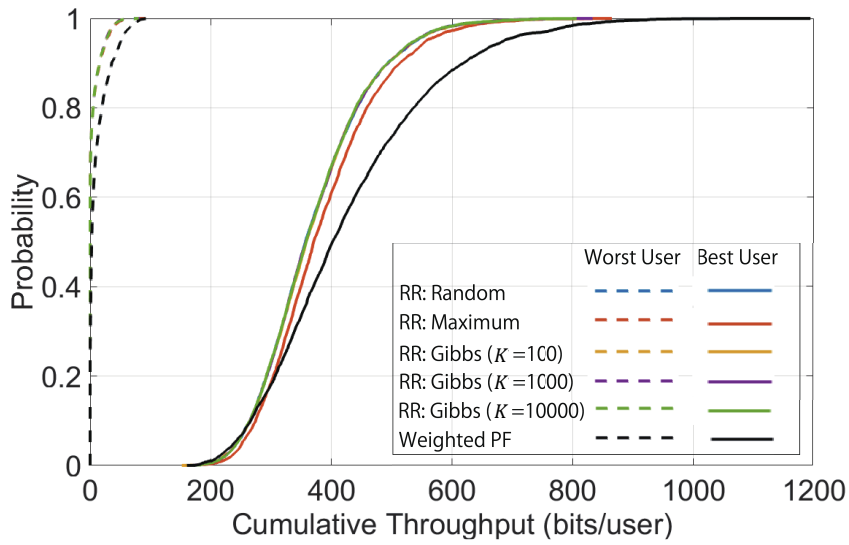


Figure 2.27: Best and worst user throughput ( $x_E = 0.6$ ,  $w_1 - w_2 = 0.1$ , inter-antenna distance 100 m).

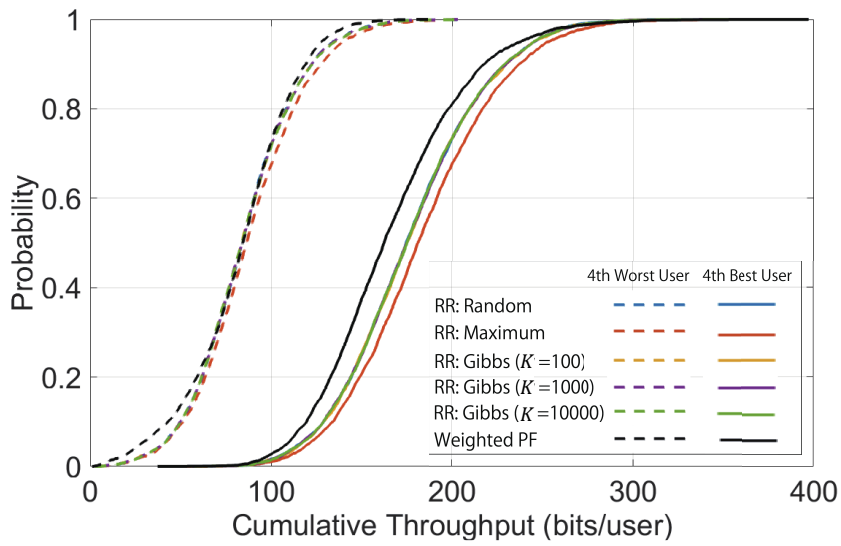


Figure 2.28: 4th best and 4th worst user throughput ( $x_E = 0.6$ ,  $w_1 - w_2 = 0.1$ , inter-antenna distance 100 m).

---

### 2.2.7.3 Effect of Inter-antenna Distance

The system throughput versus FI is shown in Figs. 2.29, 2.30, 2.31, and 2.32 for different inter-antenna distances. The inter-antenna distances are 50, 100, 150, and 200 meters, respectively. The number of UEs is 10. The ratio of eliminated UE sets in allocation sequences is varied from 0.0 to 0.8. Regardless of the inter-antenna distance, as the weight for PF scheduling and the ratio of eliminated UE sets in allocation sequences increases, the system throughput improves and the fairness deteriorates. This is because the inter-cell interference is significant if the inter-antenna distance is small. According to the increase of the inter-antenna distance, the fairness deteriorates and the system throughput improves. The increase in distance from TPs and cell-edge UEs leads to the larger difference of the throughput among UEs and deteriorates the fairness.

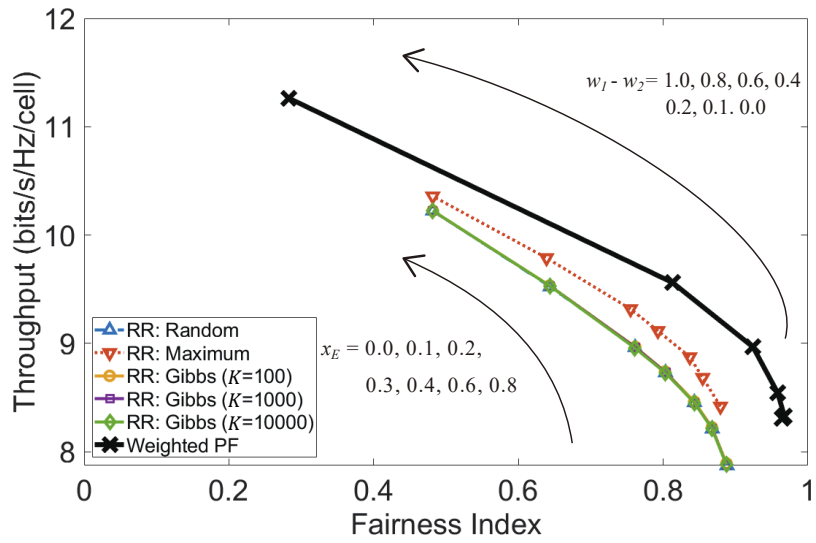


Figure 2.29: System throughput vs. FI ( $N_U=10$ , inter-antenna distance 50 m).

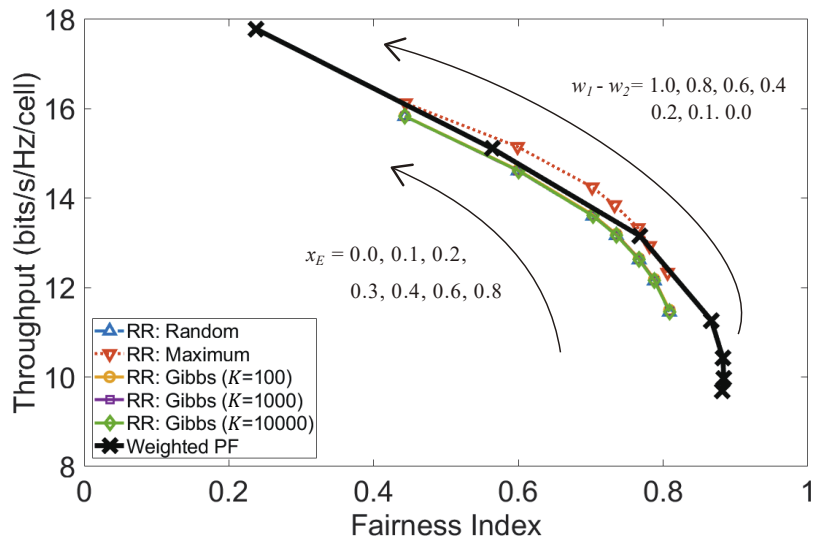


Figure 2.30: System throughput vs. FI ( $N_U=10$ , inter-antenna distance 100 m).

---

The performance of the weighted PF scheduling is superior to that of the proposed RR scheduling as shown in Fig. 2.29 when the inter-antenna distance is 50 meters. One of the proposed RR scheduling, the maximum selection, surpasses the weighted PF scheduling in terms of both of the fairness and the throughput in Fig. 2.30 if the weight for PF scheduling is lower than 0.3 and the inter-antenna distance is 100 meters. The other criterion of the proposed RR scheduling also realizes better performance than the weighted PF scheduling as shown in Figs. 2.31 and 2.32 as the inter-antenna distance increases to 150 and 200 meters. It is also the same reason that the weighted PF scheduling tends to allocate to the worst user in order to take the fairness among UEs into account while the proposed RR scheduling allocate more to the next best and worst users. This tendency is more significant as the range of the throughputs of UEs enlarges as the inter-antenna distance increases. The estimated throughput takes no inter-cell interference into account and is not accurate if the inter-antenna distance is small. That is why the weighted PF scheduling is superior to the proposed RR scheduling in Fig. 2.29.

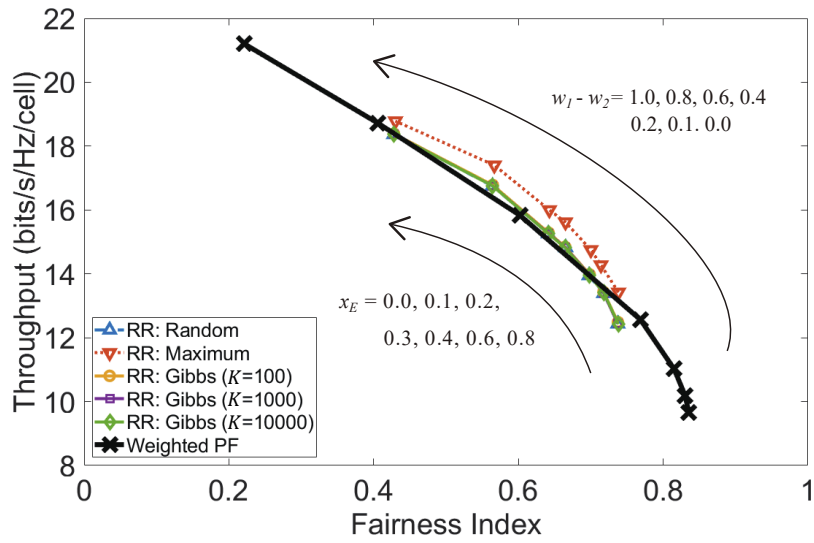


Figure 2.31: System throughput vs. FI ( $N_U=10$ , inter-antenna distance 150 m).

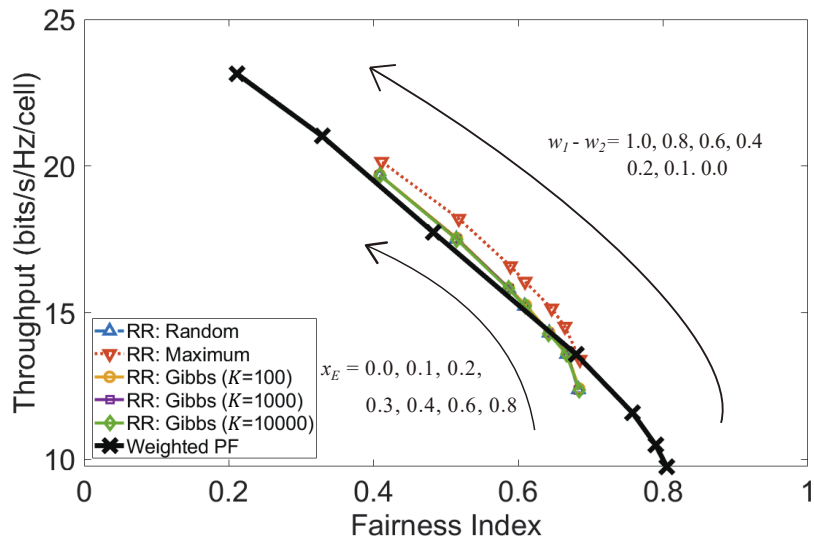


Figure 2.32: System throughput vs. FI ( $N_U=10$ , inter-antenna distance 200 m).

---

### 2.2.8 Conclusions

In this section, the proposed RR scheduling incorporated the initial phase selection and user set elimination in allocation sequence in DAT with BD pre-coding. In UE set elimination scheme, the UE sets that expect the lowest throughputs are eliminated. The initial phase selection criteria in RR scheduling are also applied on top of the proposed scheme; the maximum selection, the random selection, and the selection with Gibbs sampling. Here, the performance of the proposed RR scheduling depends on the cellular system environment such as the number of UEs, inter-antenna distance, and the parameters of the proposed scheme. The operators of the cellular system appropriately adopt the user scheduling scheme according not only to the cellular system environment and but also to their resource management policies. Numerical results obtained through computer simulation have shown that the proposed RR scheduling, especially maximum selection, is superior to the weighted PF scheduling in terms of the computational complexity, the fairness among UEs, and the throughput if the weight for PF scheduling is lower than 0.3 and the inter-antenna distance is larger than 100 meters. That is because the proposed RR scheduling mitigate intra-cell interference with MU-MIMO technology with BD algorithm and eliminates the UE sets with lower throughputs while the weighted PF scheduling takes the fairness of each UE separately.

---

## 2.3 Conclusions of Chapter 2

In chapter 2, the improved RR scheduling for the DAT has been proposed. In the proposed scheduling scheme, the key idea is the initial phase selection of the allocation sequence to decrease the inter-cell interference and the UE set selection of the allocation sequence to decrease the intra-cell interference. The computational complexity of the proposed RR scheduling is lower than that of the PF scheduling in terms of the number of times to calculate the estimated throughput. Numerical results show the proposed RR scheduling scheme that adopts the maximum selection and the UE set selection achieves higher performance than the weighted PF scheduling under the specific conditions.

# Chapter 3

## Resource Allocation for Non-terrestrial Network

### 3.1 Introduction

The escalating demands of satellite communications (SATCOM) underscore its vital role in today's world. The Satellite Industry Association (SIA) disclosed that the total revenue of the global space economy reached 386 billion dollars in 2021, with satellite services, ground equipment, satellite manufacturing, and the launch industry contributing 118 billion dollars, 142 billion dollars, 6.2 billion dollars, and 5.7 billion dollars, respectively [78]. To nurture this vast market's growth, enhancing affordability is key, which necessitates the reduction of cost per bps for end users by improving capacity improvement per satellite [79].

A traditional satellite has a single or a few beams that covers the wide geographical region in the C/Ku band. In the conventional SATCOM system, the system throughput is low because of the limited frequency band is used for the wide area. Meanwhile, the HTSs have multiple beams and each beam covers the limited narrow area and the frequency reuse is densely con-

---

ducted in the higher frequency band, i.e. Ka/Q/V/W band [80, 81]. HTSs realize the high capacity through the advanced digital signal processing and the broadband bandwidth [81]. Next-generation HTSs are expected to bring the lower cost per bit by digital processing technologies. They offer further advanced features such as adjustable bandwidth allocation to beams, variable beam shape, 100-1000 multi-beams, higher frequency band for wider frequency bandwidth, and site diversity technology [81–84].

Research interest in the HTSs has intensified in recent years due to the demands for high-rate communication, reduced launch costs, and improved performance of satellite equipment. This tendency in scholarly attention is evidenced by studies that have explored various aspects of resource allocation for the HTSs [85–87]. One notable study [85] highlights a resource allocation scheme based on digital beamforming (DBF) technology and the authors proposed a fusion control as to power resource allocation for satisfying the geographic distribution of traffic requirements. In [86, 87], the optimization problem for user-carrier assignment, beam hopping (BH) pattern, and illumination duration was modeled as a mixed integer linear programming problem for a HTS system utilizing a BH and a carrier aggregation (CA). A joint BH-CA scheme was proposed in order to realize an efficient joint beam illumination pattern for BH and an aggregation strategy for CA. The authors of [86] employ a beam pattern in which a set of two adjacent beams uses different polarization and the set covers the whole system bandwidth, which implies no illumination pattern is selected if the same polarization and frequency are assigned to the beams in the adjacent areas. In these researches [85, 86], the frequency bandwidth allocated to each beam is fixed.

---

The advent of the digital channelizer has brought flexible frequency resource allocation in HTSs [49, 51, 52]. To utilize the frequency flexibility of HTSs and enhance spectral efficiency (SE), the frequency resource allocation schemes are studied [32, 33, 53, 54, 88–92]. The authors in [53] have leveraged a multi-objective deep reinforcement learning to resolve time-frequency resource allocation issues. The study in [54] decomposes resource management into a two-stage machine learning approach, considering beam-domain resource configuration including power and gain control, and user-domain resource configuration focusing on bandwidth allocation with soft frequency reuse. In [32, 33], a beam cluster arrangement is designed, consisting of four beams with distinct frequencies and polarizations, and the satellite operation is planned in terms of the effectiveness of the frequency flexibility. In addition, the frequency resource allocation was modeled as a time-series problem to realize the effective assignment and reduce the number of control times. The authors of [88] have compared multiple algorithms for flexible payload architectures for dynamic resource management in terms of performance, complexity, and latency. However, the fairness among user equipments (UEs) are not considered in [32, 33, 53, 54, 88].

The study in [89] formulated an optimization problem and proposed both carrier and power assignment scheme for minimizing the sum of transmit power and allocated bandwidth for a next generation broadband geostationary earth orbit (GEO) satellite under the assumption that the atmospheric loss for the considered broadband frequency bandwidth is approximately similar. In [90, 91], a radio resource management scheme was proposed for the payload with bandwidth flexibility and the results show that the flexible

---

payload with the proposed management scheme is more efficient than the conventional payload in terms of the capacity and the fairness. However, the proposed scheme in [90] employs a simulated annealing and the amount of change in the number of chunks is limited to -1, 0, or 1. In [92], the authors proposed a channel capacity fairness carrier allocation (CCFCA) algorithm in order to ensure fairness and system communication capacity. The UEs with the larger difference between the required capacity and the actual capacity are assigned with priority in the algorithm. The algorithm is not optimized for the discrete beam allocation while it can be applied with the low complexity. The resource allocation scheme with the CCFCA algorithm is implemented as a reference scheme in this chapter.

In this chapter, we apply reinforcement learning to the frequency resource allocation problem concerning the beam-indexes-series Markov chain with the objective of achieving a balance between the system throughput and the fairness among UEs.

The contribution of the paper can be demarcated into two segments. First, the frequency resource allocation problem to beams is modeled not as a time-series finite Markov decision process (MDP) but as a beam-indexes-series finite MDP because the allocated bandwidth of the specific beam depends on that of the adjacent beams. A Q-learning algorithm is employed to maximize the total reward of the combinations of the allocated bandwidth to each beam. The immediate reward is calculated using a dynamic programming (DP) algorithm for optimal resource allocation of links formulated as a 0-1 knapsack problem. The evaluation values of the immediate reward are entirely distinct when the different policies of a network operation center

---

(NOC) are adopted even if the frequency resource allocation to all beams and links is conducted in the same manner. Therefore, the second contribution of the paper is to propose a combined evaluation function for realizing the balanced resource allocation in terms of the system throughput and the fairness among UEs.

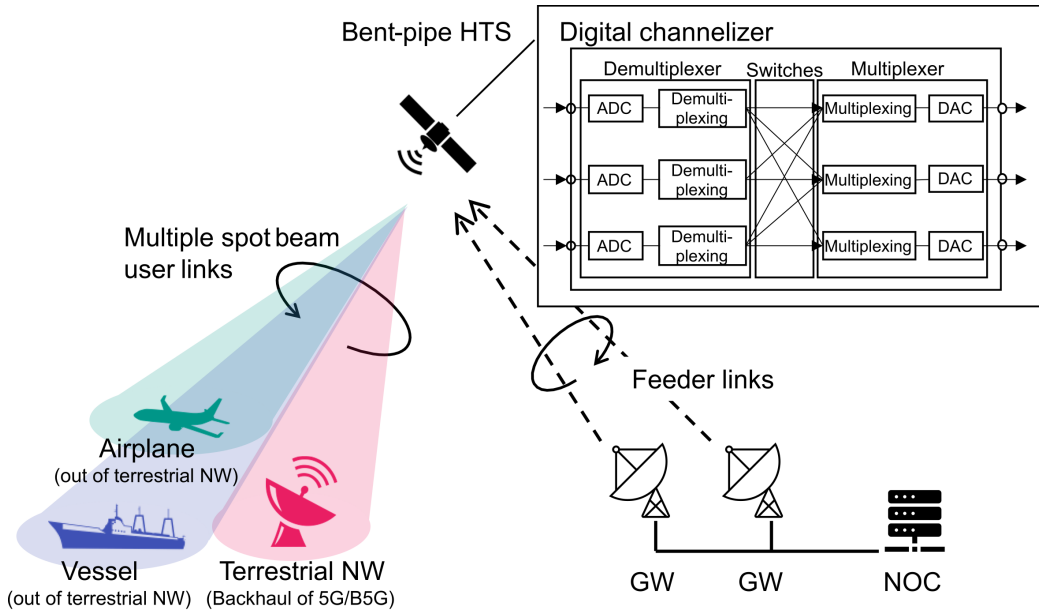


Figure 3.1: Overview of assumed SATCOM environment.

## 3.2 Assumed Environment

In this section, we delineate the configuration of the bent-pipe high throughput satellite in SATCOM, incorporating the digital channelizer. Subsequently, we introduce the system model.

### 3.2.1 System Configuration

The SATCOM environment is visualized in Figure 3.1. In our assumed system, a bent-pipe GEO satellite establishes forward links from GWs to UEs through multiple spot beams in user links and several beams in feeder links. The multi beams in the user links are fixed to the geographic locations and the fluctuating traffic demand is based on the region illuminated by each beam. The next-generation bent-pipe HTS incorporates a digital channelizer, facilitating adaptive frequency resource allocations and dynamic beam

---

assignments to cater to evolving traffic demands. In the assumed GEO SAT-COM environment, the propagation model is static because of the LOS environment and the frequency selective fading is not taken into account. The architecture of the digital channelizer encompasses demultiplexers (DEMUXs), switches, and multiplexers (MUXs) [49]. After conversion to digital signals via analog-to-digital converters (ADCs), uplink signals are demultiplexed in the DEMUXs. Each demultiplexed signal is switched to the desirable frequency, routed through the MUX, and subsequently processed by the digital-to-analog converter (DAC). The presence of the digital channelizer augments the SE, enabling individual traffic to be allocated to the preferred frequency, in case that there is no overlapping frequency resource in neighboring beams.

Regarding service typologies for NTN user UEs within feeder links, they are categorized into fixed satellite services and mobile satellite services, the latter of which includes aircraft and maritime vessels equipped with active phased array antennas. Each NTN UE is outfitted with modems compliant with the DVB-S2X standards, resulting in varied modulation and coding (MODCOD) schemes based on each UE environment.

Satellite resource operations, inclusive of resource allocations within the transponder on the GEO-HTS, are planned in the NOC. Satellite operators predict traffic demands and channel states based on UE location-specific environmental conditions, encompassing factors like rainfall, cloud cover, and path loss. Such predictive intelligence is input to the NOC and utilized for satellite operation plans. The next-generation HTS, equipped with its digital channelizer, employs the Ka-band multi-beam to enhance capacity. This facilitates support for diverse applications, including but not limited

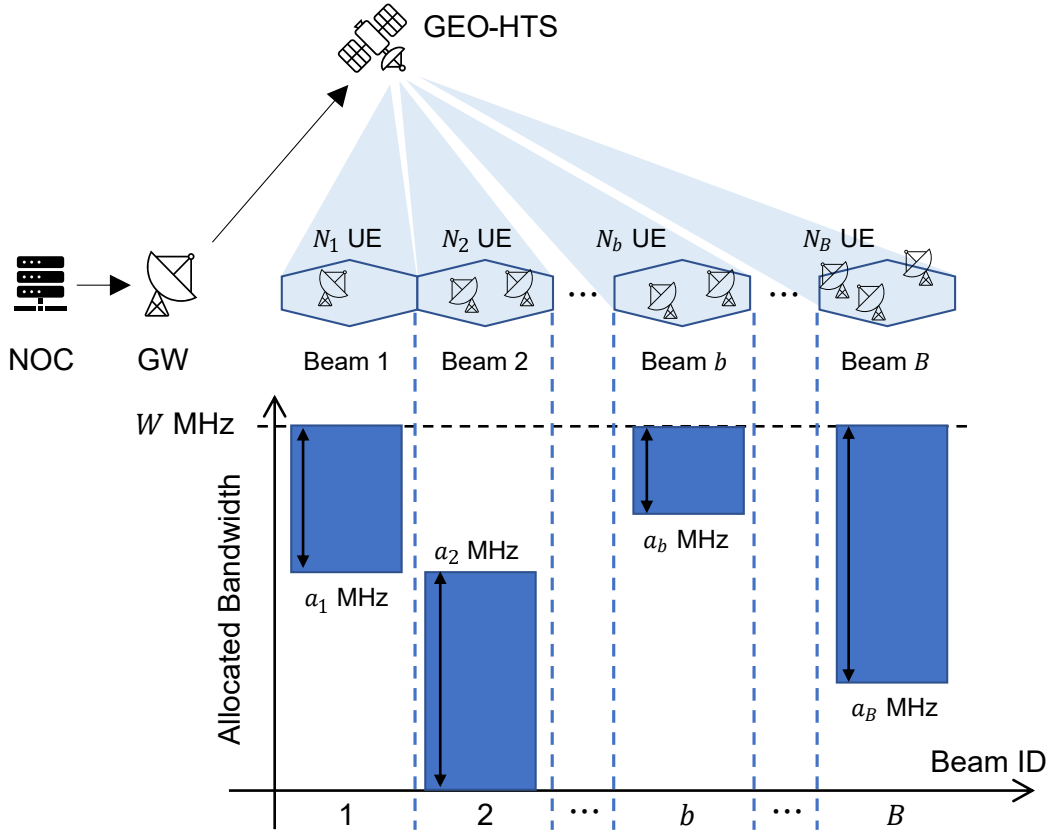


Figure 3.2: Frequency bandwidth allocated to HTS multi-beam.

to terrestrial network backhaul communication, aerial and maritime non-terrestrial communication, and emergent communication during disasters.

### 3.2.2 System Model

In the downlink of user links, the frequency bandwidth is denoted as  $W$  MHz. The number of beams is represented by  $B$  and the number of UEs in the beam  $b$  is given by  $N_b$  as shown in Fig. 3.2. The frequency bandwidth allocated to beam  $b$  is denoted by  $a_b$  MHz. The sum of the allocated frequency bandwidth in adjacent beams should not exceed the system bandwidth  $W$  MHz. It should be noted that a frequency reuse method for satellite systems

---

is described in TR 38.821 of Release 16 [93]. In the circularly polarized wave, a right-handed circularly polarized wave and a left-handed circularly polarized wave can be used selectively, and interference between the beams can be reduced considerably using different circularly polarized waves for the adjacent beam sequences. The constraint for resource allocation to beam  $b$ ,  $C1$ , is represented as follows:

$$C1 : \begin{cases} a_{b-1} + a_b \leq W & \text{for } b \geq 2, \\ a_b + a_{b+1} \leq W & \text{for } b \leq B - 1. \end{cases} \quad (3.1)$$

The request throughput of UE  $u_b$  in the beam  $b$  is represented as  $q_{u_b}^{TH}$  and is described by the relation  $q_{u_b}^{TH} = q_{u_b}^{BW} \eta_{u_b}$ , where  $q_{u_b}^{BW}$  signifies the requested frequency bandwidth, and  $\eta_{u_b}$  represents the throughput per hertz of UE  $u_b$ .

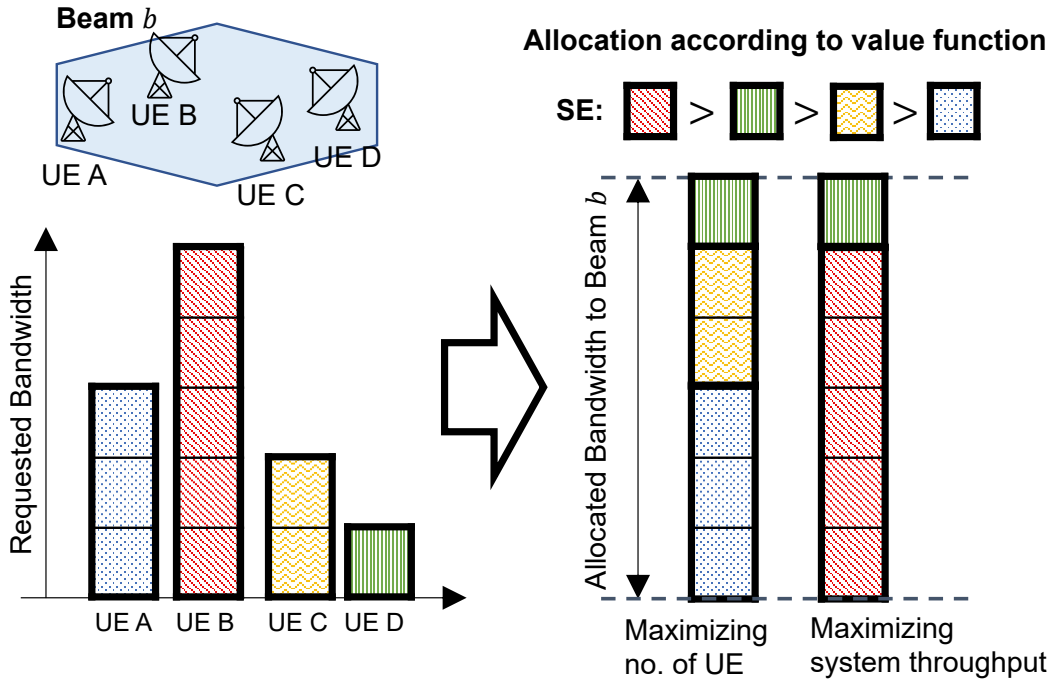


Figure 3.3: Example of link allocation.

### 3.3 Allocation Scheme of Frequency Resources

In this section, the allocation scheme of frequency resources is proposed. First, we propose the allocation scheme of frequency resource to links with DP. Second, the allocation scheme of frequency resources to beams with the Q-learning algorithm is proposed. In addition, an immediate reward maximization scheme, a full search scheme, and the CCFCA algorithm in [92] are explained for references.

#### 3.3.1 Resource Allocation of Links

As mentioned in the system configuration, even within the same beam  $b$ , different UEs adopt different MODCODs based on link states. The ideal bandwidth allocation for beam  $b$  depends on the evaluation criteria as illus-

---

trated in Fig. 3.3. To maximize the number of allocated UEs, it is preferable to allocate UEs requiring smaller frequency bandwidths. Conversely, to enhance system throughput, UEs with a higher SE should be prioritized.

Furthermore, under the condition of allocated bandwidth  $a_b$ , this frequency resource allocation quandary for UEs can be equated to a 0-1 knapsack problem, which belongs to non-deterministic polynomial-time hardness.

$$\begin{aligned}
 f(\mathbf{x}_b) &= \max \sum_{u_b=1}^{N_b} v_{u_b} x_{u_b}, & (3.2) \\
 \text{subject to } & \sum_{u_b=1}^{N_b} q_{u_b}^{BW} x_{u_b} \leq a_b, \\
 & x_{u_b} \in \{0, 1\}, \\
 & u_b \in \{1, \dots, N_b\},
 \end{aligned}$$

where  $x_{u_b}$  is the variable that represents whether the UE  $u_b$  is allocated to the link and can take 0 or 1. The set of feasible solution is the set of Boolean vectors  $\mathbf{x}_b = \{x_1, \dots, x_{N_b}\}$ . The characteristics of systems are influenced by the weight  $v_{u_b}$ . To maximize system throughput, it is set as  $v_{u_b} = q_{u_b}^{TH}$ , and to maximize the number of allocated UEs, it is set as  $v_{u_b} = 1$ . Taking into account all UE combinations leads to a complexity of  $O(2^{N_b})$ . Nevertheless, the 0-1 knapsack problem is known to have efficient solutions. For the target allocation problem, we adopt the DP [94,95]. The mathematical formulation for the knapsack problem by Bellman's principle of optimality is given as

$$f_{u_b}(nI) = \max(v_{u_b} + f_{u_b-1}(nI - q_{u_b}^{BW}), f_{u_b-1}(nI)), \quad (3.3)$$

where  $u_b \in \{1, \dots, N_b\}$  is the UE index,  $n \in \{0, \dots, \frac{W}{I}\}$  is the resource index,  $I$  represents the frequency interval of the digital channelizer, and

		Allocated bandwidth to beam $b$ [MHz]				
		0	...	$nI$	...	$a_b$
UE index for beam $b$	1	$f_1(0)$	...	$f_1(nI)$	...	$f_1(a_b)$
	$\vdots$	$\vdots$	$\ddots$	$\vdots$	$\ddots$	$\vdots$
	$u_b$	$f_{u_b}(0)$	...	$f_{u_b}(nI) = \max(v_{u_b} + f_{u_b-1}(nI - q_{u_b}^{BW}), f_{u_b-1}(nI))$	...	$f_{u_b}(a_b)$
	$\vdots$	$\vdots$	$\ddots$	$\vdots$	$\ddots$	$\vdots$
	$N_b$	$f_{N_b}(0)$	...	$f_{N_b}(nI)$	...	$f_{N_b}(a_b)$

Equals to maximum value up to UE  $u_b - 1$  under allocated bandwidth less than  $nI - q_{u_b}^{BW}$ :  $V[u_b - 1, nI - q_{u_b}^{BW}]$   
Equals to maximum value up to UE  $u_b - 1$  under allocated bandwidth less than  $nI$ :  $V[u_b - 1, nI]$   
 UE  $u_b$  is allocated ( $x_{u_b} = 1$ ) if   is greater than  . Otherwise, UE  $u_b$  is not allocated ( $x_{u_b} = 0$ ).

Determines evaluation value to allocated bandwidth  $a_b$  and optimal combination  $\mathbf{x}_b^{opt}$

Figure 3.4: Dynamic programming table for link allocation.

$nI$  would indicate the discrete allocated bandwidth. Table-based dynamic programming is shown in Fig. 3.4. The row indicates the UE index for beam  $b$  and the column indicates the allocated bandwidth,  $a_b$  MHz, to beam  $b$ . In accordance with Eq. (3.3), each cell in the  $u_b$ -th row and the  $n$ -th column is recursively filled with either the sum of the evaluation value  $v_{u_b}$  for UE  $u_b$  and the maximum evaluation value up to UE  $u_b - 1$  under the allocated bandwidth less than  $nI - q_{u_b}^{BW}$  or that up to UE  $u_b - 1$  under the allocated bandwidth less than  $nI$ . The larger evaluation value is selected. In other words, it is determined if assigning UE  $u_b$  increases the evaluation value. The rows of the table is filled from left to right, and the table is scanned from top to bottom. Finally, the solution for all UEs in beam  $b$ , UEs up to  $N_b$ , under the allocated bandwidth  $a_b$  to beam  $b$  is obtained from the bottom right cell in the table. To summarize, the DP technique breaks down the link allocation problem into simpler subproblems, and the solutions of the subproblems are determined recursively.

The algorithm for the DP is shown in **Algorithm 1**. The maximum

---

evaluation up to UE  $u_b$  under the allocated bandwidth  $a_b$  is represented as  $V[u_b, a_b]$ , which equals to  $f_{u_b}(a_b)$  in the table in Fig. 3.4. **Algorithm 1** provides the optimal combination  $\mathbf{x}_b^{opt}$  of the allocated UEs under the allocated bandwidth  $a_b$ .

$$\mathbf{x}_{a_b}^{opt} = \{x_1^{opt}, \dots, x_{u_b}^{opt}, \dots, x_{N_b}^{opt}\}. \quad (3.4)$$

---

**Algorithm 1** Dynamic Programming

---

- 1: Get the information of the allocated bandwidth  $a_b$  to the beam  $b$  and the request bandwidth  $q_{u_b}^{BW}$  and the allocation value  $v_{u_b}$  of each UE in the beam  $b$
  - 2:  $u_b = 1$
  - 3: **while**  $u_b \leq N_b$  **do**
  - 4:   **if**  $q_{u_b}^{BW} \geq a_b$  **then**
  - 5:      $V[u_b, a_b] = V[u_b - 1, a_b]$
  - 6:   **else**
  - 7:      $V[u_b, a_b] = \max(V[u_b - 1, a_b],$
  - 8:          $V[u_b - 1, a_b - q_{u_b-1}^{BW}] + q_{u_b}^{BW})$
  - 9:   **end if**
  - 10:    $u_b = u_b + 1$
  - 11: **end while**
- 

### 3.3.2 Resource Allocation of Beams

Equation (3.1) indicates that the frequency bandwidth allocated in the previous beam dictates the maximum frequency bandwidth in the current beam  $b$ . Consequently, the resource allocation across beams can be regarded as a Markov process. Furthermore, this Markov process can be modeled as a beam-indexes-series finite MDP, especially considering that the frequency interval of the digital channelizer is discrete. The allocated frequency band-

---

width in beam  $b$ , denoted as  $a_b$ , is defined as:

$$\begin{aligned} a_b &= nI, \\ n &\in \left\{ 0, \dots, \frac{W}{I} \right\}, \end{aligned} \quad (3.5)$$

where  $I$  represents the frequency interval of the digital channelizer. Therefore, the units of the allocated bandwidth take discrete values and the resource allocation of beams can be attributed to a finite allocation problem to make no interference in adjacent beams.

The state  $S$  and action  $A$  for beam  $b$  are defined as:

$$S : s_b \in \left\{ s^0, s^1, \dots, s^n, \dots, s^{\frac{W}{I}} \right\}, \quad (3.6)$$

$$A : a_b \in \{0, I, \dots, nI, \dots, W\}, \quad (3.7)$$

where the state  $s_b$  for beam  $b$  corresponds to the frequency bandwidth allocated in the previous beam  $b - 1$ .

To tackle this finite MDP, the Q-learning algorithm is employed. If the action  $a_b$  is selected in the beam  $b$  and the state is transitioned from  $s_b$  to  $s_{b+1}$ ,  $Q(s_b, a_b)$  is updated as follows:

$$Q(s_b, a_b) \leftarrow (1 - \alpha)Q(s_b, a_b) + \alpha (r_b + \gamma \max_{a_{b+1}} Q(s_{b+1}, a_{b+1})), \quad (3.8)$$

where  $\alpha$  is the learning rate,  $\gamma$  the discounting rate, and  $r_b$  denotes the immediate reward for the action  $a_b$  in the state  $s_b$ . The determination of immediate reward  $r_b$  is contingent on the policy of NOC. The reward that maximizes the system throughput is given by the policy  $\Phi_{TH}$  while the reward that maximizes the number of allocated UEs are given by the policy  $\Phi_{UE}$ . In

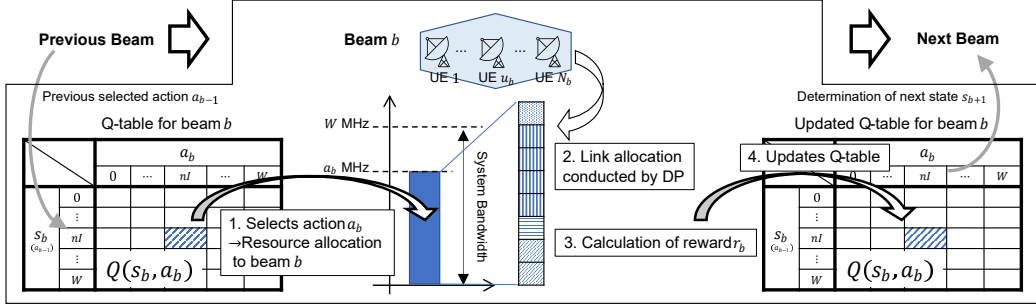


Figure 3.5: Update flow of Q-table for beam  $b$ .

each condition, the reward  $r_b$  is represented as

$$\Phi_{TH} : r_b = \begin{cases} \sum_{u_b}^{N_b} q_{u_b}^{TH} x_{u_b} - \phi \left( a_b - \sum_{u_b}^{N_b} q_{u_b}^{BW} x_{u_b} \right) & \text{if } C1 \text{ is satisfied,} \\ -1 & \text{if } C1 \text{ is **not** satisfied,} \end{cases} \quad (3.9)$$

or

$$\Phi_{UE} : r_b = \begin{cases} \sum_{u_b}^{N_b} x_{u_b} & \text{if } C1 \text{ is satisfied,} \\ -1 & \text{if } C1 \text{ is **not** satisfied,} \end{cases} \quad (3.10)$$

This chapter also aims to simultaneously optimize both functions using a combined evaluation function, resulting in a more equitable outcome. Under this policy,  $r_b$  is expressed as:

$$\Phi_{CMB} : r_b = \begin{cases} A_{TH} \left( \sum_{u_b}^{N_b} q_{u_b}^{TH} x_{u_b} \right) + A_{UE} \left( \sum_{u_b}^{N_b} x_{u_b} \right) & \text{if } C1 \text{ is satisfied,} \\ -1 & \text{if } C1 \text{ is **not** satisfied.} \end{cases} \quad (3.11)$$

where the immediate reward is -1 if the constraint by Eq. (3.1) is not satisfied.

Each beam has its own Q-table because the condition such as the number of UEs, the requested throughputs, and the MODCOD of each UE are quite different in all beams. Figure 3.5 shows the procedure to update the Q-table

---

corresponding to beam  $b$ . Initially, the present action  $a_b$  gets selected, which stems from the current state  $s_b$  influenced by the previous action  $a_{b-1}$ . This selection is subject to the restriction that frequency resources should not overlap between adjacent beams. Subsequently, using the DP algorithm, the link of each UE is allocated within the bandwidth  $a_b$  allocated to beam  $b$ . The succeeding step is to calculate the reward  $r_b$  according to the policy of NOC. Last, based on Eq. (3.8), the Q-table undergoes an update. Assuming the number of the episodes is  $E$ , the number of reward calculations is given by  $EB$ .

In addition, the proposed resource allocation is not required to be operated run in real-time. In the assumed SATCOM environment, the beam arrangement is fixed to a specific geographical location, because the transponder of the GEO satellite is controlled for frequency resource allocation and it remains stationary relative to the surface of the Earth. Therefore, the use of traffic data for a specific region as training data allows for the updating of each Q-table to match the region illuminated by each beam during the preliminary learning phase as shown in Fig. 3.5. Actions are selected based on this Q-table during real-time control. In order to apply the proposed resource allocation scheme to the non-geostationary earth orbit satellite, it is also necessary to provide geographical data, time data, or satellite orbit data as training data.

Here, we introduce three reference schemes: the immediate reward maximization, the full search, and the CCFCA algorithm in [92].

In the immediate reward maximization scheme, every feasible action within beam  $b$  is explored, subsequently selecting the action offering the

---

best immediate reward. The selected action in the beam  $b$ ,  $a'_b$  is described as

$$a'_b = \arg \max_{a_b} r_b(a_b). \quad (3.12)$$

This evaluative process persists across all beams. In the immediate reward maximization scheme, the number of reward calculations is given as  $B \left( \frac{W}{T} + 1 \right)$ .

The full search scheme explores the exhaustive combinations of actions across all beams. Here, the prime focus is on identifying the set of actions that yield the highest aggregate reward. Suppose that an action set for all the beams is represented by  $\mathbf{a} = \{a_1, \dots, a_B\}$ , the total reward  $R(\mathbf{a})$  is expressed as

$$R(\mathbf{a}) = \sum_{b=1}^B r_b(a_b). \quad (3.13)$$

Therefore, the optimum action set  $\mathbf{a}^*$  is given by

$$\mathbf{a}^* = \arg \max_{\mathbf{a}} R(\mathbf{a}). \quad (3.14)$$

In the full search, the number of reward calculations is given as  $\left( \frac{W}{T} + 1 \right)^B$ .

The study in [92], the CCFCA algorithm was proposed with objective of reducing the computational complexity and ensuring QoS of the UEs. In addition to being applied under different channel conditions of UEs, the algorithm takes the fairness among UEs into account by changing the priority of the UEs at each resource allocation phase. In this chapter, we introduce CCFCA of the frequency resource allocation algorithm in [92] as the comparison. The optimization objective function for the CCFCA algorithm is given as follows:

$$\min_{1 \leq k \leq K} (p_k^{TH} - q_k^{TH}), \quad (3.15)$$

---

where  $K$  is the number of UEs in all the beams, and denoted as  $K = \sum_{b=1}^B \sum_{u_b=1}^{N_b} 1$ . Moreover,  $p_k^{TH}$  is the actual throughput for UE  $k$  and  $q_k^{TH}$  is the requested throughput for UE  $k$ . Optimizing the objective function indicates that the UEs with the greater difference between the actual throughput and the requested throughput have higher priority to be allocated across all the beams during the current allocation phase. This allocation metric is applied iteratively in each allocation phase in order to ensure the fairness among UEs.

---

## 3.4 Numerical Results

In this section, computational simulation results are presented. First, simulation conditions are shown. Then, the computational simulation results are compared for the proposed resource allocation scheme with the Q-learning algorithm, the full search scheme, the immediate reward maximization scheme, and the resource allocation scheme with the CCFCA algorithm.

The FI is introduced to an evaluation of the fairness among UEs [74].

$$FI = \frac{(\sum_{b=1}^B \sum_{n=1}^{N_b} q_{u_b}^{TH})^2}{BN_b \sum_{b=1}^B \sum_{n=1}^{N_b} (q_{u_b}^{TH})^2}. \quad (3.16)$$

The fairness index ranges from 0 to 1, with values closer to 1 indicating greater fairness.

### 3.4.1 Simulation Conditions

Table 3.1: Simulation parameters

Parameter	value
System frequency bandwidth	500 [MHz]
Frequency interval of digital channelizer	50 [MHz]
Number of beams	5
Maximum number of UEs per beam	5
MODCOD scheme	<b>Table 3.2</b>
Number of actions	11
Number of states	11
Learning rate	0.1
Discounting rate	0.9
Number of episodes	3000
Coefficient Combinations, $(A_{TH}, A_{UE})$	$(1, 0), (0.01, 1), (0.005, 1), (0.003, 1), (0.002, 1), (0.001, 1), (0.0005, 1), (0, 1)$

The simulation conditions are presented in **Table 3.1**. The system frequency bandwidth is 500 MHz and the frequency interval of the digital channelizer is set to 50 MHz. The number of beams is five, the maximum number of the UEs per beam is five, and the MODCOD parameter sets which can be taken by the the modems of UEs are shown in **Table 3.2**. The parameters of the Q-learning algorithm, the learning rate and the discounting rate are 0.1 and 0.9, respectively, and the number of episodes is 3000. The number of coefficient combinations ( $A_{TH}, A_{UE}$ ) is eight. The NOC optimizes the system throughput and the number of allocated UEs according to the policies  $\Phi_{TH}$  and  $\Phi_{UE}$  in the coefficient combinations (1, 0) and (0, 1), respectively. When the other coefficient combinations are given, the NOC performs the frequency resource allocation to maximize the combined evaluation function.

Table 3.2: SE according to MODCOD in DVB-S2X [96]

MODCOD	SE $\eta$ [bps/Hz]	MODCOD	SE $\eta$ [bps/Hz]	MODCOD	SE $\eta$ [bps/Hz]
QPSK 2/9	0.434841	16APSK 3/5	2.370043	64APSK 32/45-L	4.206428
QPSK 13/45	0.567805	16APSK 3/5-L	2.370043	64APSK 11/15	4.338659
QPSK 9/20	0.889135	16APSK 28/45	2.458441	64APSK 7/9	4.603122
QPSK 11/20	1.088581	16APSK 23/36	2.524739	64APSK 4/5	4.735354
8APSK 5/9-L	1.647211	16APSK 2/3-L	2.635236	64APSK 5/6	4.936639
8APSK 26/45-L	1.713601	16APSK 25/36	2.745734	128APSK 3/4	5.163248
8PSK 23/36	1.896173	16APSK 13/18	2.856231	128APSK 7/9	5.355556
8PSK 25/36	2.062148	16APSK 7/9	3.077225	128APSK 29/45-L	5.065690
8PSK 13/18	2.145136	16APSK 77/90	3.386618	128APSK 2/3-L	5.241514
16APSK 1/2-L	1.972253	32APSK 2/3-L	3.291954	256APSK 31/45-L	5.417338
16APSK 8/15-L	2.104850	32APSK 32/45	3.510192	256APSK 32/45	5.593162
16APSK 5/9-L	2.193247	32APSK 11/15	3.620536	256APSK 11/15-L	5.768987
16APSK 26/45	2.281645	32APSK 7/9	3.841226	256APSK 3/4	5.900855

### 3.4.2 Performance Evaluation for No. of allocated UEs and System Throughput Maximization

Figure 3.6 shows the average system throughput versus the number of episodes for the Q-learning algorithm when the NOC adopts the policy that maximizes the system throughput. The system throughput with the full search scheme

---

is indicated by the green line in Fig. 3.6 and that with the immediate reward maximization scheme is described by the orange line. The system throughput with the Q-learning algorithm is presented by the blue line and is approaching the maximum value as the number of episodes grows. The probability of reaching the maximum throughput versus the number of episodes for the Q-learning algorithm is shown in Fig. 3.7. In the other words, this is the probability that the solution of the Q-learning algorithm and the immediate reward maximization scheme reaches that of the full search scheme. The probability of reaching the maximum throughput with the Q-learning algorithm is finally around 50% when the number of episodes is 3000, while that with the immediate reward maximization scheme is below 20%. This is because the immediate reward maximization scheme only reach the optimal solution when the sum of the requested frequency in all the adjacent beams is less than the system bandwidth 500 MHz or the immediate reward maximization accidentally corresponds with the optimal allocation results. On the other hand, the Q-learning algorithm are more inclined to find the optimal solution because it explores the entire solution space.

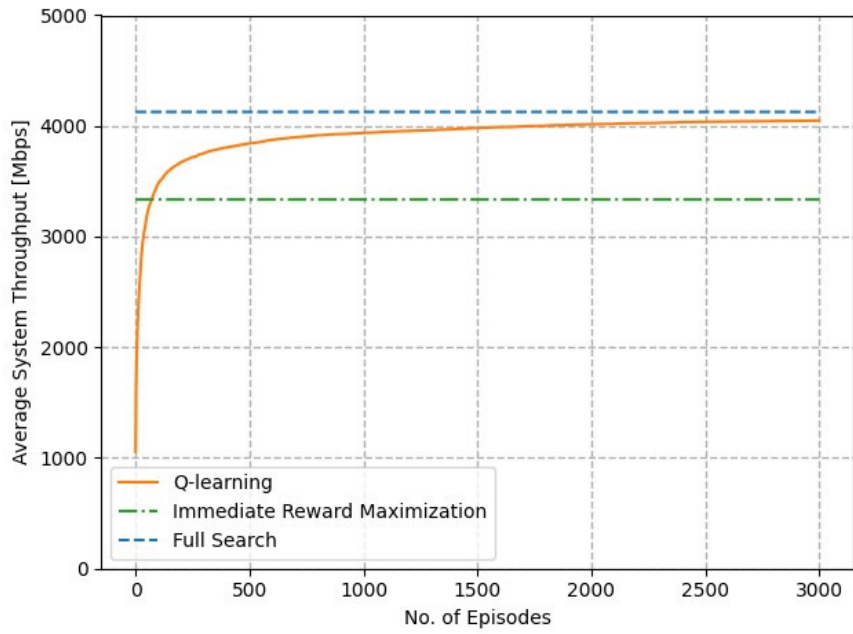


Figure 3.6: Average System throughput vs. number of episodes.

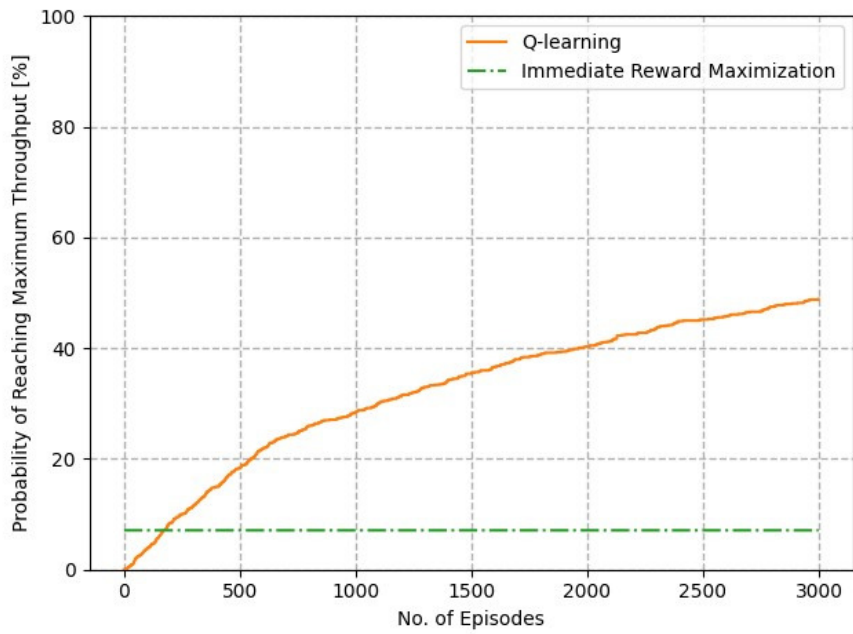


Figure 3.7: Probability of reaching maximum throughput vs. number of episodes.

---

Figures 3.8 and 3.9 respectively show the average number of allocated UEs versus the number of episodes and the probability of reaching the maximum number of allocated UEs versus the number of episodes when the NOC adopts the policy that maximizes the number of allocated UEs. The average number of allocated UEs with the Q-learning algorithm is closer to that of the full search scheme when the number of episodes is 3000. The convergence to the maximum number of allocated UEs in Fig. 3.8 is faster than that of the system throughput in Fig. 3.6. In support of that, the probability of reaching the maximum number of allocated UEs with the Q-learning algorithm is over 80% when the number of episodes is 3000. This is because the large number of MODCODs in **Table 3.2** that each UE can adopt results in a complicated allocation problem when the policy of NOC maximizes the system throughput while the number of allocated UEs calculated from Eq. (3.10) is the sum of the variables  $x_{u_i}$  represented by 0 or 1 in Eq. (3.3) when the policy of NOC maximizes the number of allocated UEs.

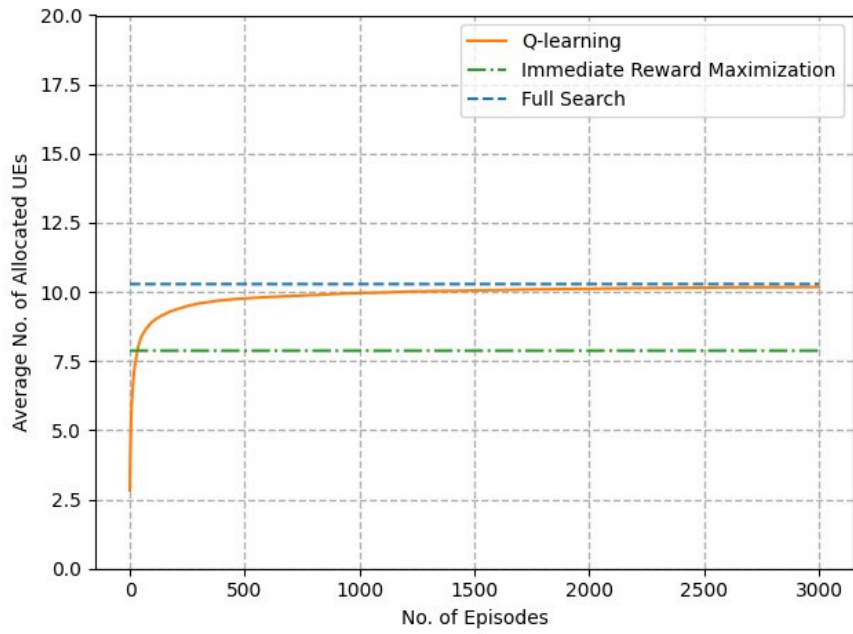


Figure 3.8: Average number of allocated UEs vs. number of episodes.

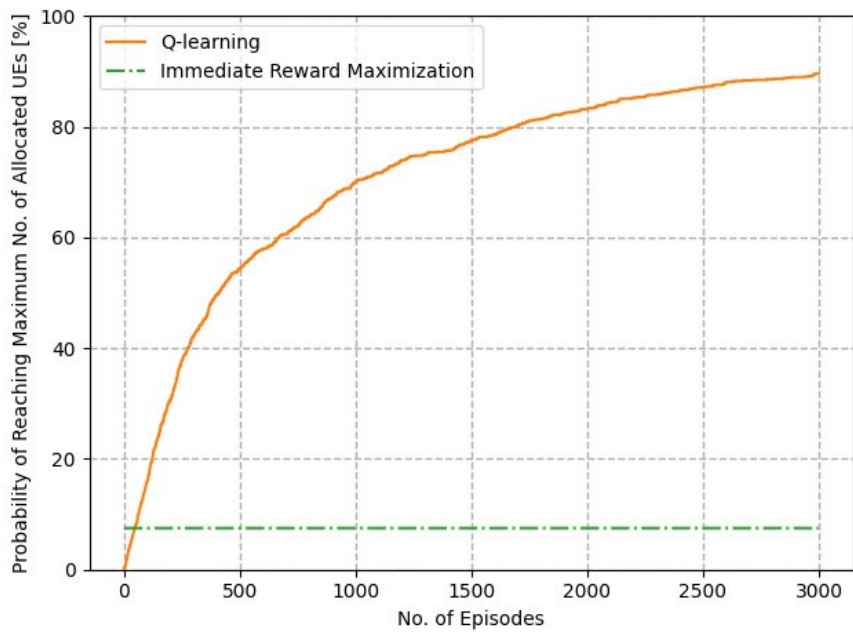


Figure 3.9: Probability of reaching maximum number of allocated UEs vs. number of episodes.

---

### 3.4.3 Performance Evaluation for Combined Evaluation Function

Figure 3.10 shows the system throughput versus the FI according to the coefficient combinations  $(A_{TH}, A_{UE})$  when the number of learning episodes is 3000. The blue and orange lines of the resource allocation schemes, which respectively employ the Q-learning algorithm and the full search, indicate a trade-off between the system throughput and the fairness that depends on the coefficient combinations  $(A_{TH}, A_{UE})$ . The resource allocation scheme with the CCFCA algorithm is shown with the black point. The value of the system throughput is more significant when the ratio of  $A_{TH}$  to  $A_{UE}$  is larger. The performance of the proposed resource allocation with the Q-learning algorithm is closer to that of the full search compared to the immediate reward maximization scheme and the resource allocation with the CCFCA algorithm. The resource allocation with the CCFCA algorithm shows greater fairness than the immediate reward maximization scheme, while the system throughput of the CCFCA algorithm is equivalent to that of the reward maximization scheme. The proposed resource allocation exhibits better performance than the allocation scheme with the CCFCA algorithm in terms of the system throughput and the fairness when the number of learning episodes for the Q-learning algorithm is 3000. In the following, the numerical analysis using the coefficient combination  $(A_{TH}, A_{UE}) = (0.003, 1)$  is performed.

Figure 3.11 shows the system throughput versus the FI according to the number of episodes. As the number of learning episodes increases, it asymptotically approaches the optimum performance obtained by the full search.

---

The system throughput of the proposed allocation scheme is consistently higher than that of the immediate reward maximization scheme and the allocation scheme with the CCFCA algorithm. This is due to the coordinated policy of the NOC to emphasize the system throughput by employing the coefficient combination  $(A_{TH}, A_{UE}) = (0.003, 1)$ . Furthermore, the fairness of the proposed allocation scheme becomes greater than that of the allocation scheme with the CCFCA algorithm when the number of the learning episodes exceeds 1700.

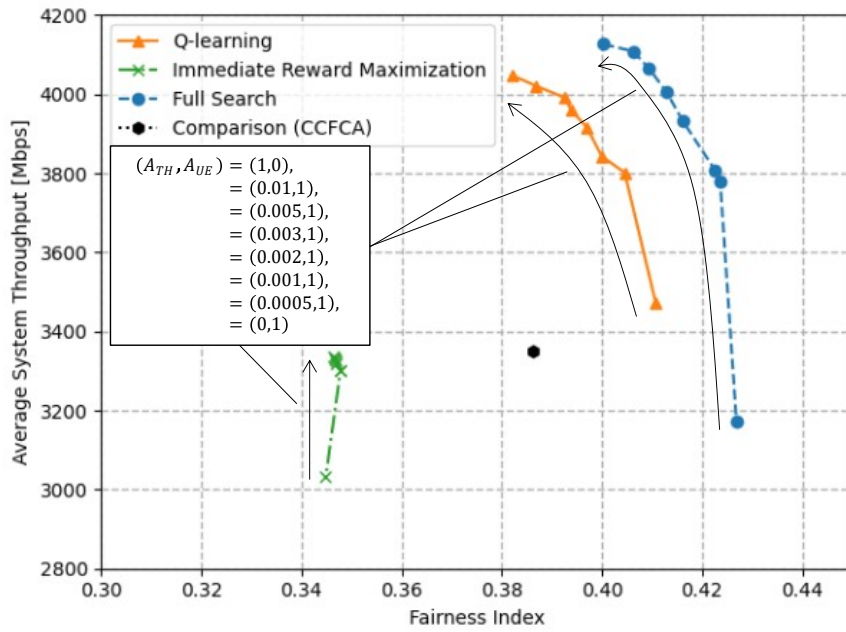


Figure 3.10: Average system throughput vs. FI.

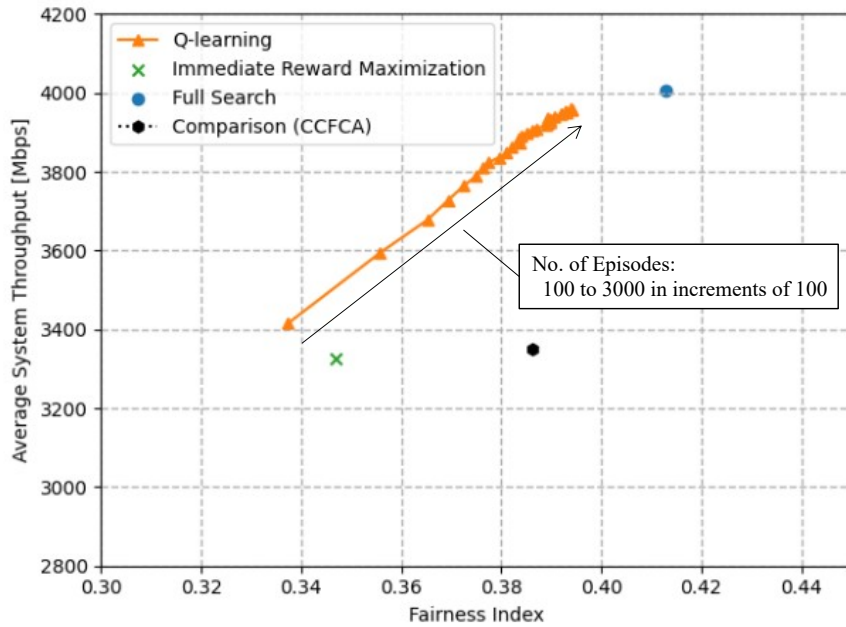


Figure 3.11: Average system throughput vs. FI  $((A_{TH}, A_{UE}) = (0.003, 1))$ .

---

A convergence performance is analysed as shown in Fig. 3.12 when the coefficient combination  $(A_{TH}, A_{UE})$  is  $(0.003, 1)$ . The evaluation function value of the proposed resource allocation scheme with the Q-learning algorithm converges at early episodes. Given sufficient episodes and training data, the Q-learning algorithm will converge to the optimal action-value function. It is important to reach a suboptimal solution with limited training data because it is difficult to search the entire vast solution space when the channelizer interval is fine or when considering the adaptation to NGSO satellites.

Figure 3.13 shows the distribution of evaluation function values of the immediate reward maximization scheme and the Q-learning scheme for the optimum solution by the full search. While the full search reaches the optimal solution every trial, the other schemes do not necessarily reach. The optimum solutions by the full search are linearly aligned and the evaluation function values with the other schemes are below the line represented by full search. The average evaluation function value with the full search is 21.91, that with the Q-learning algorithm is 20.79, and that with the immediate reward maximization scheme is 17.81: the average deterioration rate for the full search of the evaluation function value with the Q-learning algorithm is 5.15% while that with the immediate reward maximization scheme is 19.49%. The standard deviation for the deterioration rate of the Q-learning algorithm is 4.93% and that of the immediate reward maximization is 13.75%. In other words, The evaluation function values of the immediate reward maximization are widely distributed while those of the Q-learning scheme are distributed around the optimum value, which represents performance advantage of the Q-learning scheme over the immediate reward maximization scheme.

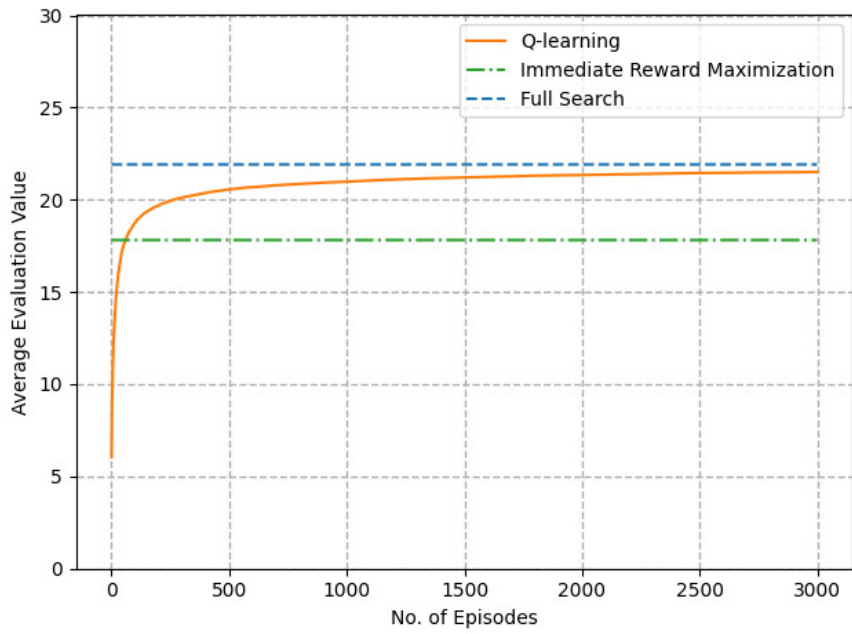


Figure 3.12: Convergence performance analysis.

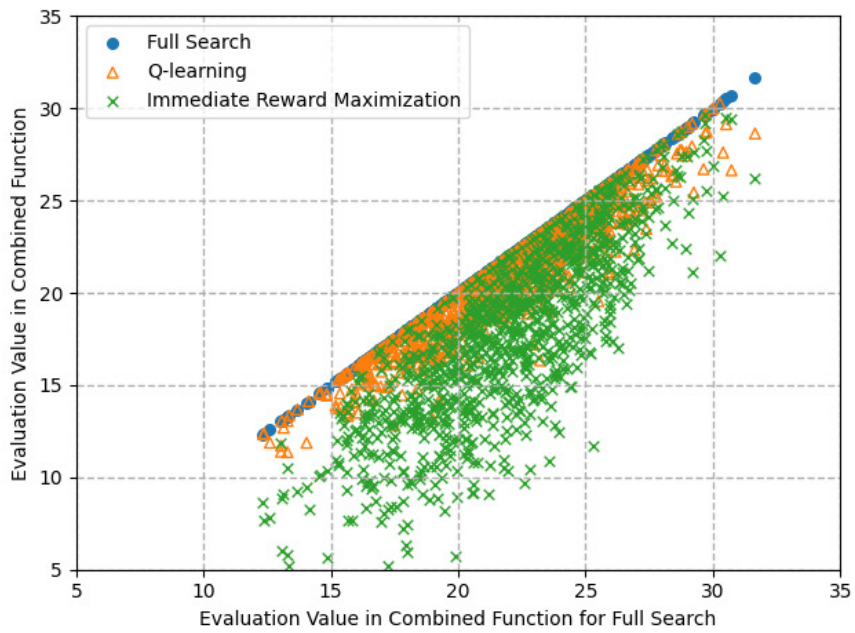


Figure 3.13: Distribution of evaluation function value to full search.

---

### 3.5 Conclusions of Chapter 3

In chapter 3, we proposed the allocation scheme of frequency resources to beams with the Q-learning algorithm in HTS communication systems. The resource allocation problem was modeled as the beam-indexes-series finite MDP. In addition, the frequency resource allocation to links was solved by the DP algorithm and the Q-table was updated based on the reward. The proposed resource allocation scheme does not need the real-time learning and has low computational complexity for the actual operation because the Q-table is preliminarily trained for the region illuminated by each beam. The combined evaluation function to the frequency resource allocation problem also has been proposed. The NOC conducts the resource allocation of beams and links with the Q-learning algorithm and the DP in the resource allocation problem. Numerical results obtained through the computer simulation show that the proposed resource allocation scheme with the Q-learning algorithm using the combined evaluation function reaches the suboptimal solution, compared to the immediate reward maximization and the resource allocation scheme with the CCFCA algorithm introduced as the comparison scheme. The proposed scheme with the coefficient combination  $(A_{TH}, A_{UE}) = (0.003, 1)$  is superior to other resource allocation schemes in terms of the system throughput and the fairness among UEs when the sufficient number of learning episodes is provided. The value distribution compared to full search show that most of the evaluation function values of the proposed scheme is distributed around the optimal solution obtained by the full search.

# Chapter 4

## Overall Conclusions

The integration of the TN and the NTN is expected in the 6G mobile communication system. The resource allocation schemes under the condition of the limited frequency resources is essential for both the TN and the NTN in order to improve the SE and decrease the bit per cost. In this dissertation, the user scheduling scheme in DAT for TN and the resource allocation scheme in next-generation HTS for NTN were investigated. The mitigation of the interference in the assumed system is the key issue of the dissertation. The inter-cell interference and the intra-cell interference were mitigated by the initial phase selection and the UE set selection, respectively, in the DAT system. The interference between the beams was mitigated by the frequency resource allocation to beams in the next generation HTS system using the digital channelizer. It is significant to operate the three-dimensional frequency resources between the different systems in order to integrate the TN and the NTN due to some overlapping frequency bands allocated to them. In [97, 98], spectrum sharing technologies for the SATCOM system and the TN are shown and can be applied to the other NTN systems. There are two major steps for the spectrum sharing, the spectrum awareness and the

---

spectrum exploitation. The spectrum awareness is to be aware of the surrounding radio environment and the spectrum exploitation is to effectively exploit the available spectrum obtained through the spectrum awareness.

The solid way of the spectrum awareness is based on a database concept, such as Licensed Shared Access [99] and Spectrum Access System [100]. There is a primary system that is prioritized in the assumed frequency and a secondary system that is not prioritized. The primary system registers the operation schedule and the secondary system obtains the information from the database. Second, a spectrum sensing technology can realize the autonomous spectrum sharing for the secondary system [98]. The secondary system has a sensing capability for the presence or the absence of the primary system and exploits vacancies in time, frequency, and spatial domains. Environmental parameters can be classified into two categories: those that do not need data from the primary system and those that do, such as waveforms and transmit power.

The spectrum exploitation can be classified into three types, “interweave”, “underlay”, and “overlay” [101]. In interweave communication, the secondary system only can exploit the spectrum in which the primary system does not use and no interference to the primary system exists. In underlay communication, the coexistence of the primary system and the secondary system is permitted only if the secondary system meets the strict interference criteria. In overlay communication, these systems coexist in the same spectrum and time and the signals of the secondary system interfere with the primary system. The mitigation of the interference is realized by advanced coding and transmission technologies at the secondary system. There is a trade-

---

off between flexible resource management and technology readiness levels. The overlay communication realizes higher spectrum efficiency and is hard to implement while the interweave communication and the underlay communication enable lower spectrum efficiency and are relatively feasible.

The resource allocation in this dissertation treats the spectrum exploitation in the single system. It is necessary to control resources such as the power, the frequency bandwidth, and the beam shape under the limited computational capability in the large-scale network. Our future task is to extend the optimization of the resources for individual networks to those over the multi-layered networks composed of the TN and the NTN and to contribute the solution of the social issue through the establishment of a fundamental technology in 6G mobile communication.

---

## 4.1 User Scheduling in DAT for TN

DAT is the promising system that can compensate the larger path loss in high frequency band in 6G for TN. Although the PF scheduling achieves higher system throughput and the fairness among UEs than the RR scheduling and the Max-C/I scheduling, there is the challenge about the computational complexity. This problem is stem from the huge feedback overhead at the CU including CSI due to the numerous TPs. Chapter 2 introduces the improved RR scheduling that requires low computational complexity.

In section 2.1, the initial phase selection for the RR scheduling has been proposed. The conventional RR scheduling allocates UEs according to the allocation sequence in order. That is why the RR scheduling hardly requires computational complexity. However, no interference is not taken into account. The proposed RR scheduling sequentially selects the initial phases of the sequence of the RR scheduling for each macro-cell to maximize the system throughput. The inter-cell interference from the other macro-cells can be estimated because the initial phase is determined in one of the seven macro-cells at each timeslots and the allocation information of the other macro-cells is centralized at the CU. Four different criteria have been proposed for the initial phase selection; the full search, the random selection, the maximum selection, and the selection with Gibbs sampling. It is shown that the maximum selection is closer to the optimum solution of the full search than the other criteria.

To achieve higher system throughput and the fairness among UEs, it is required to take intra-cell interference into account. In section 2.2, the UE

---

set selection in the sequence of the RR scheduling has been proposed. Some UE sets in the RR sequence suffer from the severe intra-cell interference due to the close arrangement of UEs allocated in the same RBs. As the CU exhaustively searches the initial phases with the maximum selection, the expected throughput for each UE set is obtained. The UE set with the highest Q-value is eliminated from the sequence. The proposed RR scheduling shows the superior performance than the weighted-PF scheduling in terms of the system throughput, the fairness, and the computational complexity if the weight for the PF scheduling is lower than 0.3 and the inter-antenna distance is larger than 50 meters.

---

## 4.2 Frequency Resource Allocation in Next-generation HTS for NTN

HTSs have the wide bandwidth using above Ka-band, provide the dense multi-beam ,and realize lower cost per bit. In addition, the next-generation HTSs are expected to be equipped with the digital channelizer that realizes flexible resource allocation. Chapter 3 introduces the resource allocation scheme for the next-generation HTS.

With the digital channelizers, the allocation bandwidth is shared with the adjacent beams. That means the allocation bandwidth to the current beam is influenced by that to the preceding beam. In this chapter, the frequency resource allocation problem is modeled as the beam-indexes-series finite MDP. The state is defined as a bandwidth allocation to the preceding beam. The action is defined as the allocation bandwidth to the current beam and the number of the actions is determined by the configurable frequency interval of the digital channelizer.

The resource allocation problem is solved with the Q-learning algorithm. In order to obtain the reward for the action, the resource allocation of the links is conducted by the DP. The evaluation function of the reward is depend on the policy of the NOC and the three policies are proposed for the proposed resource allocation scheme with the Q-learning algorithm; the system throughput maximization, the number of the allocated UEs maximization, and the combined evaluation function. The proposed allocation scheme reduces the computational complexity if the enough amount of the prior training is conducted. Also, the immediate reward maximization scheme,

---

the full search, and the resource allocation with the CCFCA algorithm are introduced for the reference schemes. Numerical results obtained through computer simulation show the proposed allocation scheme realizes the sub-optimum solution in terms of the system throughput and the fairness.

# Acknowledgements

First and foremost, I would like to express my deepest gratitude to Prof. Yukitoshi Sanada for his guidance and encouragement over the course of six and a half years. He has always been thoroughly committed to guiding his students. Despite his busy schedule, whenever I visited his office, he patiently entertained my questions until they were completely resolved. I am particularly grateful for his unwavering support during my senior year as an undergraduate, when I was hospitalized for several months and almost gave up on graduating that year. It was his dedication to teaching that enabled me to graduate on time. Furthermore, I vividly remember his compassionate support during my second year of the master's program, when I faced a recurrence of illness and significant uncertainty about my future. He took the time to personally engage with me and helped to guide me through my doubts and fears regarding my career path.

I would like to my gratitude members of the National Institute of Information and Communications Technology (NICT) for their kind help and support. Dr. Hiroyuki Tsuji and Dr. Amane Miura have provided thoughtful and witty advice that greatly enhanced my research. Dr. Tomoshige Kan introduced me to the fundamentals of satellite communication systems when I had no prior knowledge in the field. Ms. Mariko Sekiguchi taught me

---

not only logical thinking methods but also imparted valuable lessons on the attitudes towards work and research.

I would also like to express my gratitude to my friends, who supported me emotionally and kept me motivated throughout my research endeavors. Their constant encouragement were crucial to my perseverance.

Lastly, I must extend my deepest gratitude to my parents. I could not have come this far without your support, dedication, and at times, your sacrifices. Thank you very much.

# Bibliography

- [1] National Institute of Information and Communications Technology, “NICT Beyond 5G/6G White Paper (Version 3.0),” Mar. 2023.
- [2] Ministry of Internal Affairs and Communications, “Beyond 5G Promotion Strategy–Roadmap towards 6G,” Jan. 2020.
- [3] NTT DOCOMO, INC., “DOCOMO White Paper 5G Evolution and 6G (Version 5.0),” Jan. 2023.
- [4] TR 38.811, “Study on New Radio (NR) to Support Non-terrestrial Networks,” V15.4.0, Oct. 2020.
- [5] X. Lin, S. Rommer, S. Euler, E. A. Yavuz and R. S. Karlsson, “5G from Space: An Overview of 3GPP Non-Terrestrial Networks,” *IEEE Communications Standards Magazine*, vol. 5, no. 4, pp. 147-153, Dec. 2021.
- [6] TR 38.821, “Solutions for NR to Support Non-terrestrial Networks (NTN),” V16.2.0, Mar. 2023.
- [7] Y. Shiroishi, K. Uchiyama and N. Suzuki, “Society 5.0: For Human Security and Well-Being,” in *Computer*, vol. 51, no. 7, pp. 91-95, July 2018.

- 
- [8] Y. Shiroishi, K. Uchiyama and N. Suzuki, "Better Actions for Society 5.0: Using AI for Evidence-Based Policy Making That Keeps Humans in the Loop," in *Computer*, vol. 52, no. 11, pp. 73-78, Nov. 2019.
- [9] F. Tao, H. Zhang, A. Liu and A. Y. C. Nee, "Digital Twin in Industry: State-of-the-Art," *IEEE Transactions on Industrial Informatics*, vol. 15, no. 4, pp. 2405-2415, April 2019.
- [10] A. Fuller, Z. Fan, C. Day and C. Barlow, "Digital Twin: Enabling Technologies, Challenges and Open Research," *IEEE Access*, vol. 8, pp. 108952-108971, 2020.
- [11] A. F. M. Shahen Shah, "A Survey From 1G to 5G Including the Advent of 6G: Architectures, Multiple Access Techniques, and Emerging Technologies," 2022 IEEE 12th Annual Computing and Communication Workshop and Conference (CCWC), Las Vegas, USA, pp. 1117-1123, 2022.
- [12] E. Dahlman, S. Parkvall, and J. Skold, *4G:LTE/LTE-Advanced for Mobile Broadband Edition*, Academic Press, 2011.
- [13] "Specific Attenuation Model for Rain for Use in Prediction Methods," ITU-R p.838-3, 2005.
- [14] "Propagation Data and Prediction Methods Required for the Design of Earth-space Telecommunication Systems," ITU-R P.618-13, 2017.
- [15] G. Albertazzi, S. Cioni, G. E. Corazza, M. Neri, R. Pedone, P. Salmi, A. Vanelli-Coralli, and M. Villanti, "On the adaptive DVB-S2 physical

- 
- layer: design and performance,” *IEEE Wireless Communications*, vol. 12, no. 6, pp. 62-68, Dec. 2005.
- [16] A. Morello and V. Mignone, “DVB-S2: The Second Generation Standard for Satellite Broad-Band Services,” *Proceedings of the IEEE*, vol. 94, no. 1, pp. 210-227, Jan. 2006.
- [17] R. Kohno, “Spatial and Temporal Communication Theory Using Adaptive Antenna Array,” *IEEE Personal Communications*, vol. 5, no. 1, pp. 28-35, Feb. 1998.
- [18] I. Chiba, R. Miura, T. Tanaka and Y. Karasawa, “Digital Beam Forming (DBF) Antenna System for Mobile Communications,” *IEEE Aerospace and Electronic Systems Magazine*, vol. 12, no. 9, pp. 31-41, Sept. 1997.
- [19] Y. Kai-Bor and D. J. Murrow, “Adaptive Digital Beamforming for Angle Estimation in Jamming,” *IEEE Transactions on Aerospace and Electronic Systems*, vol.37, pp.508-523, April 2001.
- [20] H. Honglin and Z. Jinkang, “Performance Evaluation of Beam Hopping Communications Scheme,” *Proceedings of Personal, Indoor and Mobile Radio Communications*, Beijing, China, pp. 2470-2474 vol.3, 2003.
- [21] T. Zhang, L. Zhang and D. Shi, “Resource Allocation in Beam Hopping Communication System,” *2018 IEEE/AIAA 37th Digital Avionics Systems Conference (DASC)*, London, UK, 2018, pp. 1-5.
- [22] S. Tani, K. Motoyoshi, H. Sano, A. Okamura, H. Nishiyama and N. Kato, “Flexibility-Enhanced HTS System for Disaster Management: Re-

- 
- sponding to Communication Demand Explosion in a Disaster,” IEEE Transactions on Emerging Topics in Computing, vol. 8, no. 1, pp. 159-167, 1 Jan. 2020.
- [23] Y. Kawamoto, T. Kamei, M. Takahashi, N. Kato, A. Miura and M. Toyoshima, “Flexible Resource Allocation With Inter-Beam Interference in Satellite Communication Systems With a Digital Channelizer,” IEEE Transactions on Wireless Communications, vol. 19, no. 5, pp. 2934-2945, May 2020.
- [24] A. Miura et al. “On Critical Design of Bandwidth-on-Demand High Throughput Satellite Communications System Technology,” Proceedings of the 25th Ka and Broadband Communications Conference, Sept, 2019.
- [25] A. A. M. Saleh, A. J. Rustako Jr., and R. S. Roman, “Distributed Antennas for Indoor Radio Communications,” IEEE Transactions on Communications, vol. 35, no. 12, pp. 1245–1251, Dec. 1987.
- [26] L. Yu, J. Wu, A. Zhou, E. G. Larsson and P. Fan, “Massively Distributed Antenna Systems With Nonideal Optical Fiber Fronthauls: A Promising Technology for 6G Wireless Communication Systems,” IEEE Vehicular Technology Magazine, vol. 15, no. 4, pp. 43-51, Dec. 2020.
- [27] J. Joung, Y. K. Chia and S. Sun, “Energy-Efficient, Large-Scale Distributed-Antenna System (L-DAS) for Multiple Users,” IEEE Journal of Selected Topics in Signal Processing, vol. 8, no. 5, pp. 954-965, Oct. 2014.

- 
- [28] J. Ge, Y. -C. Liang, J. Joung and S. Sun, “Deep Reinforcement Learning for Distributed Dynamic MISO Downlink-Beamforming Coordination,” *IEEE Transactions on Communications*, vol. 68, no. 10, pp. 6070-6085, Oct. 2020.
- [29] M. V. Clark, T. M. Willes III, L. J. Greenstein, A. J. Rustako, Jr., V. Erceg, and R. S. Roman, “Distributed versus Centralized Antenna Arrays in Broadband Wireless Networks,” *IEEE 53rd Vehicular Technology Conference*, May 2001.
- [30] A. Kyrgiazos, B. G. Evans and P. Thompson, “On the Gateway Diversity for High Throughput Broadband Satellite Systems,” *IEEE Transactions on Wireless Communications*, vol. 13, no. 10, pp. 5411-5426, Oct. 2014.
- [31] A. J. Roumeliotis, C. I. Kourogiorgas and A. D. Panagopoulos, “Optimal Capacity Allocation Strategies in Smart Gateway Satellite Systems,” *IEEE Communications Letters*, vol. 23, no. 1, pp. 56-59, Jan. 2019.
- [32] Y. Abe, H. Tsuji, A. Miura and S. Adachi, “Frequency Resource Allocation for Satellite Communications System Based on Model Predictive Control and Its Application to Frequency Bandwidth Allocation for Aircraft,” *2018 IEEE Conference on Control Technology and Applications (CCTA)*, pp. 165-170, Aug. 2018.
- [33] Y. Abe, M. Okawa, A. Miura, K. Okada, M. Akioka and M. Toyoshima, “Performance Study of Frequency Flexibility in High Throughput Satellites and its Contribution to Operations Strategy,” *Proceedings of*

- 
- the 37th International Communications Satellite Systems Conference (ICSSC-2019), Okinawa, Japan, 2019.
- [34] Y. Seki and F. Adachi, “Downlink Capacity Comparison of MMSE-SVD and BD-SVD for Cooperative Distributed Antenna Transmission using Multi-user Scheduling,” IEEE 86th Vehicular Technology Conference, Sept. 2017.
- [35] F. Adachi, A. Boonkajay, T. Saito, S. Kumagai, and H. Miyazaki, “Cooperative Distributed Antenna Transmission for 5G Mobile Communications Network,” IEICE Transactions on Communications, vol. E100-B, no. 8, pp. 1190-1240, Aug. 2017.
- [36] F. Adachi, R. Takahashi, and H. Matsuo, “Enhanced Interference Coordination and Radio Resource Management for 5G Advanced Ultra-dense RAN,” IEEE 91st Vehicular Technology Conference, May 2020.
- [37] F. Adachi, R. Takahashi, H. Matsuo, S. Xia, C. Ge and Q. Chen, “On Design Concept of Cellular Distributed MU-MIMO for Ultra-dense RAN,” 2022 27th Asia Pacific Conference on Communications (APCC), Jeju Island, Korea, pp. 266-271, 2022.
- [38] M. Sawahashi, Y. Kishiyama, A. Morimoto, D. Nishikawa and M. Tanno, “Coordinated Multipoint Transmission/reception Techniques for LTE-advanced [Coordinated and Distributed MIMO],” IEEE Wireless Communications, vol. 17, no. 3, pp. 26-34, June 2010.
- [39] Y. Seki, T. Saito and F. Adachi, “A Study on Dynamic Antenna Clustering for Distributed MIMO Cooperative Transmission using Multi-user

- 
- MMSE-SVD,” 2018 21st International Symposium on Wireless Personal Multimedia Communications (WPMC), Chiang Rai, Thailand, pp. 64-68, 2018.
- [40] S. Kumagai, Y. Seki and F. Adachi, “Joint Tx/Rx Signal Processing for Distributed Antenna MU-MIMO Downlink,” 2016 IEEE 84th Vehicular Technology Conference, Montreal, Canada, 2016.
- [41] Y. Arikawa, T. Sakamoto, and S. Shigematsu, “Hierarchical Scheduling with FPGA-based Accelerator for Flexible 5G Mobile Network,” IEEE 91st Vehicular Technology Conference, May 2020.
- [42] Y. Arikawa, T. Sakamoto, and S. Kimura “User Throughput Analysis of Coordinated Radio-Resource Scheduler with Hardware Accelerator for 5G Mobile Systems,” IEICE Communications Express, 7(6), pp. 183-188, 2018.
- [43] G. Otsuru and Y. Sanada, “Phase Selection in Round-Robin Scheduling Sequence for Distributed Antenna System,” IEICE Transactions on Communications, vol. E103-B, no. 10, pp. 1155-1163, Oct. 2020.
- [44] G. Otsuru and Y. Sanada, “UE Set Selection for RR scheduling in Distributed Antenna Transmission with Reinforcement Learning,” IEICE Transactions on Communications, vol. E106-B, no. 7, pp. 586-594, July 2023.
- [45] W. Keusgen, “On Limits of Wireless Communications When Using Multiple Dual-polarized Antennas,” 10th International Conference on Telecommunications, Papeete, France, pp. 204-210, 2003.

- 
- [46] H. Matsuda, H. Tomeda, and F. Adachi, "Channel Capacity of Distributed Antenna System Using Maximal Ratio Transmission," The 5th IEEE VTS Asia Pacific Wireless Communications Symposium, Aug, 2008.
- [47] Y. Guan, J. Homer, "Review of High Throughput Satellites: Market Disruptions, Affordability-Throughput Map, and the Cost Per Bit/Second Decision Tree," IEEE Aerospace and Electronic Systems Magazine, vol. 34, no. 5, pp. 64-80, 1 May 2019.
- [48] P. Inigo O. Vidal, B. Roy, E. Albery, N. Metzger, D. Galinier, J. Anzalchi, G. Huggins, and S. Stirland, "Review of Terabit/s Satellite, the Next Generation of HTS Systems," 2014 7th Advanced Satellite Multimedia Systems Conference and the 13th Signal Processing for Space Communications Workshop (ASMS/SPSC), Livorno, Italy, pp. 318-322, 2014.
- [49] K. Kaneko, H. Nishiyama, N. Kato, A. Miura, and M. Toyoshima, "Construction of a Flexibility Analysis Model for Flexible High-throughput Satellite Communication Systems with a Digital Channelizer," IEEE Transactions on Vehicular Technology, vol. 67, no. 3, pp. 2097–2107, 2018.
- [50] D. Gupta, T. V. Filippov, A. F. Kirichenko, D. E. Kirichenko, I. V. Vernik, A. Sahu, S. Sarwana, P. Shevchenko, A. Talalaevskii, and O. A. Mukhanov, "Digital Channelizing Radio Frequency Receiver," IEEE

- 
- Transactions on Applied Superconductivity, vol. 17, no. 2, pp. 430–437, 2007.
- [51] J. Cherkaoui and V. Glavac, “Signal Frequency Channelizer/ Synthesizer,” 2008 10th International Workshop on Signal Processing for Space Communications, Oct. 2008.
- [52] H. Yang, J. Dang, Y. Pan, and Z. Li, “A digital Channelizer Design Approach for Broadband Satellite Communications Based on Frequency Domain Filter Theory,” 2013 International Conference on Mechatronic Sciences, Electric Engineering and Computer (MEC), pp. 2986-2990, Dec. 2013.
- [53] Y. He, B. Sheng, H. Yin, D. Yan and Y. Zhang, “Multi-objective Deep Reinforcement Learning Based Time-frequency Resource Allocation for Multi-beam Satellite Communications,” China Communications, vol. 19, no. 1, pp. 77-91, Jan. 2022.
- [54] D. Zhao, H. Qin, N. Xin and B. Song, “Flexible Resource Management in High-Throughput Satellite Communication Systems: A Two-Stage Machine Learning Framework,” IEEE Transactions on Communications, vol. 71, no. 5, pp. 2724-2739, May 2023.
- [55] “Assessment of the Global Mobile Broadband Deployments and Forecasts for International Mobile Telecommunications,” ITU-R M.2243, Mar. 2011.
- [56] H. Shanmuganathan and A. Mahendran, “Current Trend of IoT Market and its Security Threats,” 2021 International Conference on Innovative

---

Computing, Intelligent Communication and Smart Electrical Systems (ICSES), Chennai, India, 2021.

- [57] “IMT Vision - Framework and Overall Objectives of the Future Development of IMT for 2020 and beyond,” ITU-R M.2083-0, Sept. 2015.
- [58] Y. Arikawa, H. Uzawa, T. Sakamoto, and S. Shigematsu, “High-Speed Radio-Resource Scheduling for 5G Ultra-High-Density Distributed Antenna Systems,” 2016 8th International Conference on Wireless Communications and Signal Processing, Oct. 2016.
- [59] M. Matinmikko-Blue and M. Latva-aho, “Micro Operators Accelerating 5G Deployment,” 2017 IEEE International Conference on Industrial and Information Systems, Dec. 2017.
- [60] K. B. S. Manosha, M. Matinmikko-Blue, and M. Latva-aho, “Framework for Spectrum Authorization Elements and its Application to 5G Micro-operators,” 2017 Internet of Things Business Models, Users, and Networks, Nov. 2017.
- [61] G. Otsuru and Y. Sanada, “User Allocation with Round-Robin Scheduling Sequence for Distributed Antenna System,” IEEE 90th Vehicular Technology Conference, Sept. 2019.
- [62] G. Otsuru and Y. Sanada, “User Set Elimination in Allocation Sequences of RR Scheduling for Distributed Antenna Transmission,” IEEE 93rd Vehicular Technology Conference, Apr. 2021.

- 
- [63] S. H. R. Naqvi, A. Matera, L. Combi, and U. Spagnolini, "On the Transport Capability of LAN Cables in All-Analog MIMO-RoC Fronthaul," 2017 IEEE Wireless Communications and Networking Conference (WCNC), Mar. 2017.
- [64] M. Feng and S. Mao, "Dealing with Limited Backhaul Capacity in Millimeter-Wave Systems: A Deep Reinforcement Learning Approach," IEEE Communications Magazine, Vol. 57, pp. 50-55, Mar. 2019.
- [65] F. Tang, Y. Zhou, and N. Kato, "Deep Reinforcement Learning for Dynamic Uplink/Downlink Resource Allocation in High Mobility 5G HetNet," IEEE Journal on Selected Areas in Communications, Vol. 38, pp. 2773-2782, June 2020.
- [66] Y. Zhou, F. Tang, Y. Kawamoto, and N. Kato, "Reinforcement Learning-Based Radio Resource Control in 5G Vehicular Network," IEEE Wireless Communications Letters, Vol. 9, pp.611-614, Dec. 2019.
- [67] W. Lei, Y. Ye, and M. Xiao, "Deep Reinforcement Learning-Based Spectrum Allocation in Integrated Access and Backhaul Networks," IEEE Transactions on Cognitive Communications and Networking, Vol. 6, pp. 970-979, Sept. 2020.
- [68] M. Elsayed, M. Erol-Kantarci, and H. Yanikomeroglu, "Transfer Reinforcement Learning for 5G New Radio mmWave Networks," IEEE Transactions on Wireless Communications, Vol. 20, pp. 2838-2849, May 2021.

- 
- [69] M. Elsayed and M. Erol-Kantarci, "Radio Resource and Beam Management in 5G mmWave Using Clustering and Deep Reinforcement Learning," GLOBECOM 2020 - 2020 IEEE Global Communications Conference, Taipei, Taiwan, 2020.
- [70] Y. Liu, C. He, X. Li, C. Zhang and C. Tian, "Power Allocation Schemes Based on Machine Learning for Distributed Antenna Systems," in *IEEE Access*, vol. 7, pp. 20577-20584, 2019.
- [71] G. Qian, Z. Li, C. He, X. Li and X. Ding, "Power Allocation Schemes Based on Deep Learning for Distributed Antenna Systems," in *IEEE Access*, vol. 8, pp. 31245-31253, 2020.
- [72] Q. H. Spencer, A. L. Swindlehurst, and M. Haardt, "Zero-forcing Methods for Downlink Spatial Multiplexing in Multiuser MIMO Systems," *IEEE Transactions on Signal Processing*, vol. 52, no.2, pp.461-471, Feb. 2004.
- [73] R. Agrawal, A. Bedekar, R.J. La, and V. Subramanian, "Class and Channel Condition Based Weighted Proportional Fair Scheduler," *Proceedings of ITC2001*, Sept. 2001.
- [74] R. Jain, D. Chiu, and W. Hawe, "A Quantitative Measure of Fairness and Discrimination for Resource Allocation in Shared Computer Systems," *DEC Research Report*, TR-301, Sept. 1984.
- [75] X. Chen, A. Benjebbour, A. Li, and A. Harada, "Multi-User Proportional Fair Scheduling for Uplink Non-orthogonal Multiple Access (NOMA)," *IEEE 79th Vehicular Technology Conference*, May 2014.

- 
- [76] “Study on Channel Model for Frequencies from 0.5 to 100 GHz,” 3GPP, TR 38.901, V14.3.0, Jan. 2018.
- [77] T. Okuyama, S. Suyama, J. Mashino, and Y. Okumura, “5G Distributed Massive MIMO with Ultra-High Density Antenna Deployment in Low SHF Bands,” *IEICE Transactions on Communications*, vol. E100-B, no. 10, pp. 1921-1927, Oct. 2017.
- [78] Satellite Industry Association, “State of the Satellite Industry Report 2022.” Available: <https://sia.org/news-resources/state-of-the-satellite-industry-report/>.
- [79] Y. Guan, F. Geng and J. H. Saleh, “Review of High Throughput Satellites: Market Disruptions, Affordability-Throughput Map, and the Cost Per Bit/Second Decision Tree,” *IEEE Aerospace and Electronic Systems Magazine*, vol. 34, no. 5, pp. 64-80, 1 May 2019.
- [80] “High Throughput Satellites: On Course for New Horizons”, Euroconsult, 2014.
- [81] A. I. Perez-Neira, M. A. Vazquez, M. R. B. Shankar, S. Maleki and S. Chatzinotas, “Signal Processing for High-Throughput Satellites: Challenges in New Interference-Limited Scenarios,” *IEEE Signal Processing Magazine*, vol. 36, no. 4, pp. 112-131, July 2019.
- [82] H. Fenech, S. Amos, A. Tomatis and V. Soumholphakdy, “High throughput satellite systems: An analytical approach,” *IEEE Transactions on Aerospace and Electronic Systems*, vol. 51, no. 1, pp. 192-202, Jan. 2015.

- 
- [83] J. Lizarraga, P. Angeletti, N. Alagha and M. Aloisio, “Flexibility performance in advanced Ka-band multibeam satellites,” IEEE International Vacuum Electronics Conference, Monterey, USA, 2014.
- [84] J. Lizarraga, P. Angeletti, N. Alagha and M. Aloisio, “Multibeam satellites performance analysis in non-uniform traffic conditions,” 2013 IEEE 14th International Vacuum Electronics Conference (IVEC), Paris, France, 2013.
- [85] M. Takahashi, Y. Kawamoto, N. Kato, A. Miura and M. Toyoshima, “DBF-Based Fusion Control of Transmit Power and Beam Directivity for Flexible Resource Allocation in HTS Communication System Toward B5G,” IEEE Transactions on Wireless Communications, vol. 21, no. 1, pp. 95-105, Jan. 2022.
- [86] M. G. Kibria, H. Al-Hraishawi, E. Lagunas, S. Chatzinotas and B. Ottersten, “Joint Beam Hopping and Carrier Aggregation in High Throughput Multibeam Satellite Systems,” IEEE Access, vol. 10, pp. 122125-122135, 2022.
- [87] L. Lei, E. Lagunas, Y. Yuan, M. G. Kibria, S. Chatzinotas and B. Ottersten, “Beam Illumination Pattern Design in Satellite Networks: Learning and Optimization for Efficient Beam Hopping,” IEEE Access, vol. 8, pp. 136655-136667, 2020.
- [88] F. G. Ortiz-Gomez, D. Tarchi, R. Martinez, A. Vanelli-Coralli, M. A. Salas-Natera and S. Landeros-Ayala, “Cooperative Multi-Agent Deep Reinforcement Learning for Resource Management in Full Flexible

- 
- VHTS Systems,” *IEEE Transactions on Cognitive Communications and Networking*, vol. 8, no. 1, pp. 335-349, March 2022.
- [89] T. S. Abdu, E. Lagunas, S. Kisseleff and S. Chatzinotas, “Carrier and Power Assignment for Flexible Broadband GEO Satellite Communications System,” 2020 IEEE 31st Annual International Symposium on Personal, Indoor and Mobile Radio Communications, London, UK, 2020.
- [90] G. Cocco, T. de Cola, M. Angelone, Z. Katona and S. Erl, “Radio Resource Management Optimization of Flexible Satellite Payloads for DVB-S2 Systems,” *IEEE Transactions on Broadcasting*, vol. 64, no. 2, pp. 266-280, June 2018.
- [91] G. Cocco, T. De Cola, M. Angelone and Z. Katona, “Radio resource management strategies for DVB-S2 systems operated with flexible satellite payloads,” 2016 8th Advanced Satellite Multimedia Systems Conference and the 14th Signal Processing for Space Communications Workshop (ASMS/SPSC), Palma de Mallorca, Spain, 2016.
- [92] X. Liu, K. Xu, F. Wu and J. Wu, “A beam-dominating frequency resource allocation and scheduling scheme for multi-beam satellite system,” 2021 IEEE International Conference on Power Electronics, Computer Applications (ICPECA), Shenyang, China, pp. 532-535, 2021.
- [93] “Technical Specification Group Radio Access Network; Solutions for NR to support non-terrestrial networks (NTN),” 3GPP, TR 38.821, V16.20.0, March 2023.

- 
- [94] R. Bellman, “On the Theory of Dynamic Programming,” Proceedings of the National Academy of Sciences of the United States of America, pp.716-719, 1952.
- [95] S. T. Thant Sin, “The Parallel Processing Approach to the Dynamic Programming Algorithm of Knapsack Problem,” 2021 IEEE Conference of Russian Young Researchers in Electrical and Electronic Engineering, St. Petersburg, Moscow, Russia, pp. 2252-2256, 2021.
- [96] “Digital Video Broadcasting (DVB); Implementation Guidelines for the Second Generation System for Broadcasting, Interactive Services, News Gathering and Other Broadband Satellite Applications; Part 2: S2 Extensions (DVB-S2X)”, ETSI TR 102 376-2 V1.2.1.
- [97] M. Höyhty et al., “Database-Assisted Spectrum Sharing in Satellite Communications: A Survey,” IEEE Access, vol. 5, pp. 25322-25341, 2017.
- [98] S. K. Sharma, T. E. Bogale, S. Chatzinotas, B. Ottersten, L. B. Le and X. Wang, “Cognitive Radio Techniques Under Practical Imperfections: A Survey,” IEEE Communications Surveys & Tutorials, vol. 17, no. 4, pp. 1858-1884, 2015.
- [99] M. D. Mueck, V. Frascolla and B. Badic, “Licensed shared access — State-of-the-art and current challenges,” 2014 1st International Workshop on Cognitive Cellular Systems (CCS), Germany, 2014.

- 
- [100] M. M. Sohal, M. Yao, T. Yang and J. H. Reed, "Spectrum access system for the citizen broadband radio service," *IEEE Communications Magazine*, vol. 53, no. 7, pp. 18-25, July 2015.
- [101] A. Goldsmith, S. A. Jafar, I. Maric and S. Srinivasa, "Breaking Spectrum Gridlock With Cognitive Radios: An Information Theoretic Perspective," *Proceedings of the IEEE*, vol. 97, no. 5, pp. 894-914, May 2009.

# List of Achievements

## Journal Publications

1. G. Otsuru, and Y. Sanada, “Phase Selection in Round-Robin Scheduling Sequence for Distributed Antenna System,” IEICE Transactions on Communications, Vol.E103-B, No.10, pp. 1155-1163, 2019.
2. G. Otsuru, and Y. Sanada, “UE Set Selection for RR Scheduling in Distributed Antenna Transmission with Reinforcement Learning,” IEICE Transactions on Communications, Vol.E106-B, No.7, pp. 586-594, 2023.
3. G. Otsuru, Y. Sanada, H. Tsuji, and A. Miura, “Frequency Resource Allocation Using Combined Evaluation Function in High Throughput Satellite Communication System,” IEICE Transactions on Communications [Accepted for Publication].

## Other Journal Publications

1. M. Yata, G. Otsuru, and Y. Sanada, “User Scheduling with Beam Selection for Full Digital Massive MIMO Base Station,” IEICE TRANSACTIONS on Communications, Vol.E104-B, No.4, pp. 428-435, 2021.

- 
2. T. Tsukamoto, G. Otsuru, and Y. Sanada, “Macro Cell Switching of Transmit Antennas in Distributed Antenna Transmission,” *IEICE Transactions on Communications*, Vol.E105-B, No.3, pp. 302-308, 2022.

### **Conference Publications**

1. G. Otsuru and Y. Sanada, “User Allocation with Round-Robin Scheduling Sequence for Distributed Antenna System,” 2019 IEEE 90th Vehicular Technology Conference, 2019.
2. G. Otsuru, H. Tsuji, R. Miura, J. Suzuki and Y. Kishiyama, “Efficient Antenna Tracking Algorithm for HAPS Ground Station in Millimeter-Wave,” 2022 25th International Symposium on Wireless Personal Multimedia Communications (WPMC), Herning, Denmark, 2022, pp. 261-266.
3. G. Otsuru, Y. Sanada, H. Tsuji, and A. Miura, “Frequency Resource Allocation Using Q-learning for User Link in High Throughput Satellite Communication,” 2023 26th International Symposium on Wireless Personal Multimedia Communications (WPMC), Tampa, FL, USA, 2023.

### **Other Conference Publications**

1. M. Sekiguchi, A. Miura, Y. Abe, G. Otsuru, E. Morikawa, N. Yoshimura, T. Takahashi, T. Kubo-Oka, T. Fuse, H. Tsuji, and M. Toyoshima, “A Study on Satellite-Terrestrial Cooperation System as a Part of Research and Development of Ka-band Satellite Communication Control

- 
- for Various Use Cases,” 2021 24th International Symposium on Wireless Personal Multimedia Communications (WPMP), Okayama, Japan, 2021.
  2. T. Tsukamoto, G. Otsuru and Y. Sanada, “Attribution Macro Cell Switching in Distributed Antenna Transmission,” 2021 IEEE 94th Vehicular Technology Conference (VTC2021-Fall), Norman, OK, USA, 2021.
  3. T. Tsukamoto, G. Otsuru and Y. Sanada, “Attribution Macro Cell Switching for CoMP in Distributed Antenna Transmission,” 2023 IEEE 97th Vehicular Technology Conference (VTC2023-Spring), Florence, Italy, 2023.

### **Technical Reports**

1. G. Otsuru and Y. Sanada, “User Allocation with Round-Robin Scheduling Sequence for Distributed Antenna System,” Technical Reports of IEICE, RCS2019-74, June 2019.
2. G. Otsuru and Y. Sanada, “User Set Elimination in Allocation Sequence for RR Scheduling in Distributed Antenna Systems,” Technical Reports of IEICE, RCS2020-155, Jan. 2021.
3. G. Otsuru, H. Tsuji, Y. Abe, M. Sekiguchi, R. Miura, T. Okura, T. Kan, J. Suzuki, and Y. Kishiyama, “Development of 38GHz-band Wireless Communication System Using High Altitude Platform Station (HAPS) for 5G Network,” Technical Reports of IEICE, SAT2022-9, May 2022.

- 
4. G. Otsuru, H. Tsuji, R. Miura, J. Suzuki and Y. Kishiyama, “[Invited Lecture] Research and Development of Antenna Device for HAPS Ground Station Composed of 2-Axis Mechanically Driven Gimbal and Lens Antenna,” AP2022-201, Feb. 2023.

### **Other Technical Reports**

1. T. Tsukamoto, G. Otsuru, and Y. Sanada, “Macro Cell Switching of Transmit Antennas in Distributed Antenna Transmission,” Technical Reports of IEICE, RCS2021-48, June 2021.
2. T. Tsukamoto, G. Otsuru, and Y. Sanada, “Coordinated Multi-Point Transmission with Attribution Macro Cell Switching in Distributed Antenna Transmission,” Technical Reports of IEICE, RCS2022-255, Mar. 2023.
3. H. Kotake, Y. Abe, Y. Takahashi, G. Otsuru, T. Kan, D. Kolev, Y. Saito, Y. Sato, T. Itahashi, S. Yamakawa, H. Tsuji, and M. Toyoshima, “[Encouragement Talk] Seasonal Performance Comparison of Ground-to-Satellite Optical Communication Using LUCAS Onboard the Optical Data Relay Satellite,” Technical Reports of IEICE, SAT2023-41, Aug. 2023.